The effect of high linear energy transfer ionizing radiation on mutation and reversion events at the hypoxanthin-guanin-phosphoribosyltransferase locus

Inaugural-Dissertation

zur

Erlangung des Doktorgrades

Dr. rer. nat.

der Fakultät für Biologie

an der

Universität Duisburg-Essen

vorgelegt von

Mathias Sebastian Kallies

aus Mülheim an der Ruhr

Januar 2016

Die der vorliegenden Arbeit zugrunde liegenden Experimente wurden am Institut für Medizinische Strahlenbiologie der Universität Duisburg-Essen durchgeführt.

1. Gutachter: Prof. Dr. G. Iliakis

2. Gutachter: Prof. Dr. S. Knauer

Vorsitzender des Prüfungsausschusses: Prof. Dr. C. Johannes

Tag der mündlichen Prüfung: 11.05.2016

Table of contents

List of figures

List of tables

1 Introduction

1.1 Physical properties of ionizing radiation (IR)

1.1.1 Interaction of photons with matter

Radiation is the emission and propagation of energy through space or matter in form of photons of the electromagnetic spectra, or of particles. A radiation form is termed ionizing radiation (IR) when the transmitted energy is sufficient to eject an electron from the atom's shell of the irradiated matter. To remove an electron from the atom's shell the transferred photon or particle energy must be higher than the binding energy of the electron in the atom. The property to ionize and excite molecules of the absorbed matter is found in the electromagnetic spectra for photons of high energy like X-rays or ɣ-rays. One characteristic of IR is the distribution of energy into deposition events along the tracks of the generated particles. The interaction of photons with matter occurs by primary and secondary effects. Primary effects are for example the direct interaction of a photon with the electron of the atom's shell. The term secondary effect describes the situation when a primary interaction results in the ejection of an electron from the shell that in the next step leads to further ionization events. These ejected electrons are also termed δ-rays (Hall 2006). The ionization potential of a photon depends on the photon energy that can either get transferred completely or partly to the electron during its interaction with matter. In the case of partial transfer of photon's energy, the photon is also scattered at the atom's shell. As a result the photon energy decreases continuously in repeated interactions (figure 2). The interaction of photons with the electrons of the atom's shell is described by the photoelectric and the Compton effects (figure 1).

In the photoelectric effect a photon ejects an electron from the atom's inner shell by transferring all its energy. The so released energetic electron is then able to ionize and excite other atoms. Electrons that are removed from the inner shell get refilled from the outer electron shell by emitting the photons of energy equal to the difference between the shell energy levels.

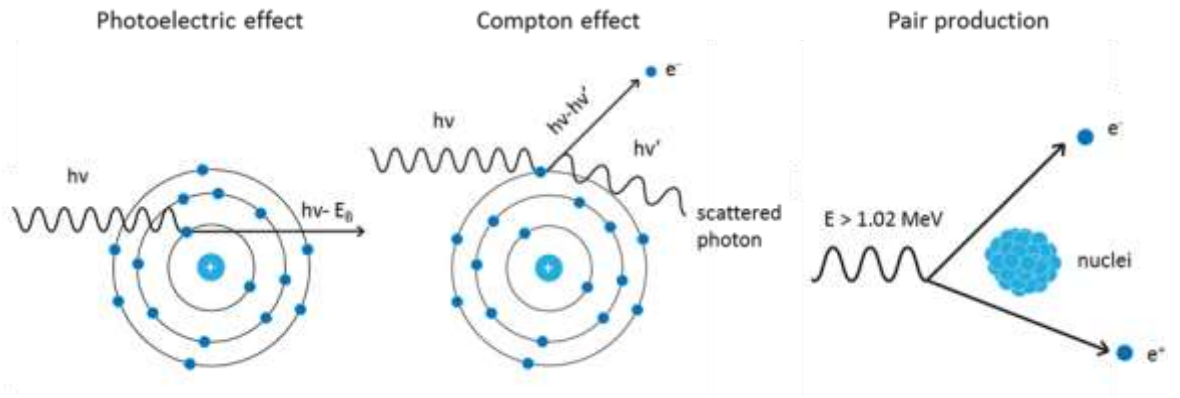

Figure 1: Interaction of photons with material

In the photoelectric effect the photon transfers its entire energy to the electron that becomes ejected from the atom. In the Compton effect a portion of the photon energy is transferred, resulting in an ejected electron and a scattered photon. The pair production is the formation of one electron and positron (positive charged electron), when at higher energies the photon gets in proximity to the nucleus. hv = energy of the photon, E_B = bound energy of the electron, e = electron with the indicated charge. Modified from (Sherer 2011).

In the Compton effect, the photon transfers a portion of its energy to an electron of the material, resulting in a recoiled electron and a scattered photon. The photoelectric effect dominates the interaction at energies up to 60 keV in water, while at higher energies up to about 10 MeV the Compton effect dominates (Gunderson 2015). The type of photon interaction with matter depends also on the material that is irradiated. The photoelectric effect for example increases with the atomic number of the irradiated molecule (Z^3 dependency) while the Compton effect is almost independent on the material (Gunderson 2015).

The characteristic of photons to generate secondary electrons (δ-rays) that cause most of the ionization events leads to their classification as indirectly ionizing radiation modality (Hall 2006). This is different from particle irradiation that is described in the next section.

1.1.2 Interaction of charged particles with matter

Particle radiation includes electrons, protons, α-particles, neutrons and heavy charged ions and is either generated in an accelerator or ejected from the decay of a radioactive nucleus. In contrast to photons that mainly ionize indirectly, particles have sufficient energy to ionize atoms and break bonds along their track directly (directly ionizing) (Hall 2006). Particles that are set in motion interact with the electrons of the atoms, or with the nuclei, but the latter is not further discussed here (Gunderson 2015). The interactions of particles with matter depend on their energy, which also determines their penetration depth (Khan 2009). The kinetic energy of a charged particle decreases after every ionization event and the slower the charged particle gets the more ionization events occur per unit of track length. This results in a maximum in energy deposition (termed Bragg peak) that determines the penetration depth. The Bragg peak is characterized by the highest number of ionization events per unit of track length. After the Bragg peak the energy of the particle is not sufficient for further ionization events and the particle stops completely. More energetic particles transfer more energy and penetrate deeper the irradiated material (figure 2). The change in particle energy occurring along its track affects the distribution of the ionization events. Associated biological effects are described in the next section and are compared to those generated by photon irradiation.

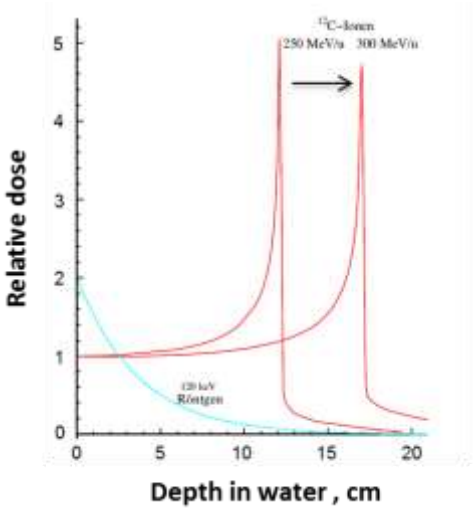

Figure 2: Depth dose distribution of X-rays and particle radiation with different energy

Photons decrease with depth of absorbing material exponentially, while particles have their maximum of energy deposition events in the end of their track. Difference in particle energy results in modulation of the penetration depth that is used in cancer therapy for targeting the tumor tissue. Modified from (Kraft 2005).

1.2 Linear energy transfer (LET) and the effect of IR on biological tissue

Particle and photon IR transfer their energy when passing through matter. The amount of energy that matter absorbs per unit of mass is described as the radiation dose. The dose is measured in units of Gray (Gy) and one Gy is equivalent to 1 J/kg.

$$D = \frac{\mathrm{E}}{\mathrm{m}}$$

With D = dose [Gy], E = energy [Joule], m = mass [kg]

Radiation modalities differ in their spatial distribution of ionization events along the tracks of the ionizing particles. High energy photons like X-rays and ɣ-rays generate through their secondary electrons mainly well separated ionization events and are therefore termed sparsely ionizing. Particle radiations like α-particles, proton or neutron, on the other hand, generate mainly ionization events in close proximity along their tracks and are therefore classified as densely ionizing (Hall 2006). The distribution of ionization events along the particle track is described by the linear energy transfer (LET). LET is defined as the energy that is transferred by ionization and excitation events per unit track length (keV/µm).

$$LET = \frac{\mathrm{dE}}{\mathrm{dx}}$$

With LET = linear energy transfer [keV/µm], E = energy of the ion/photon [keV], x = length of the ion track [µm]

LET indicates an energy deposition average and is often used to compare the quality of radiation types with each other. Depending on the energy of the radiation modality, radiation forms can be classified as low-LET (in general less than 3 keV/µm) and high-LET (>10 keV/µm). Low-LET are sparsely ionizing radiation forms such as X-rays or ɣ-rays, while high-LET are considered particle radiation modalities with densely ionizing characteristics (figure 3).

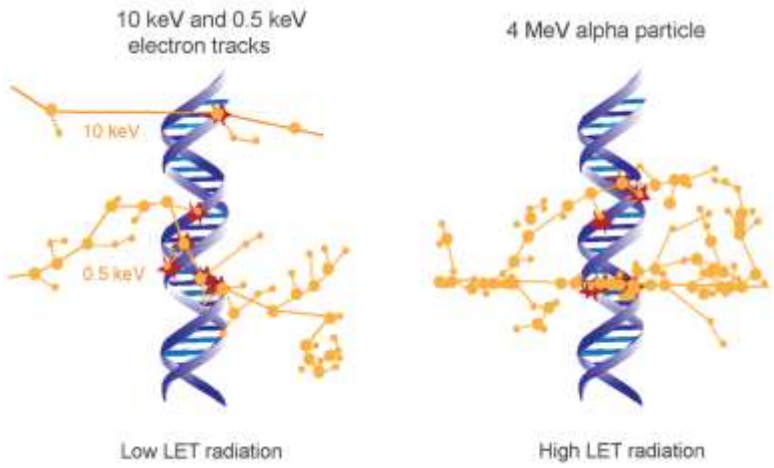

Figure 3: Low and high-LET irradiation tracks and their effect on DNA damage induction

Energy deposition events are localized along of tracks. The generation of ionization events in close proximity along the track is more pronounced at high-LET radiation. The large and small dots represent ionization and excitation events along the track, respectively. The tracks are simulated by the Monte Carlo model and drawn on the same scale as the DNA. Modified from (Schipler 2013).

According to the LET definition, the LET value of a radiation type depends on the energy of the photon or particle. An increase in the energy of the particle reduces the density of ionization events along the track, and therefore also its LET. The consequence is that the exposure to different radiation modalities with the same dose may result in different biological outcome. To compare the effects of different radiation quality on biological tissue, the relative biological effectiveness (RBE) is used. The RBE is defined with reference to X-rays or ɣ-rays, based on which the effects of other radiation types are compared.

$$RBE = \frac{Dose_{(ref)}}{Dose_{(test)}}$$

RBE, relative biological effectiveness, $Dose_{(ref)}$ of reference radiation (X-rays or ɣ-rays) and $Dose_{(test)}$ dose of test radiation required to produce the same biological effect

RBE therefore reflects differences in the biological responses generated by radiations of different LET. Figure 4 illustrates that high-LET radiations result in higher biological effectiveness. The RBE correlates with LET and typically increases with LET.

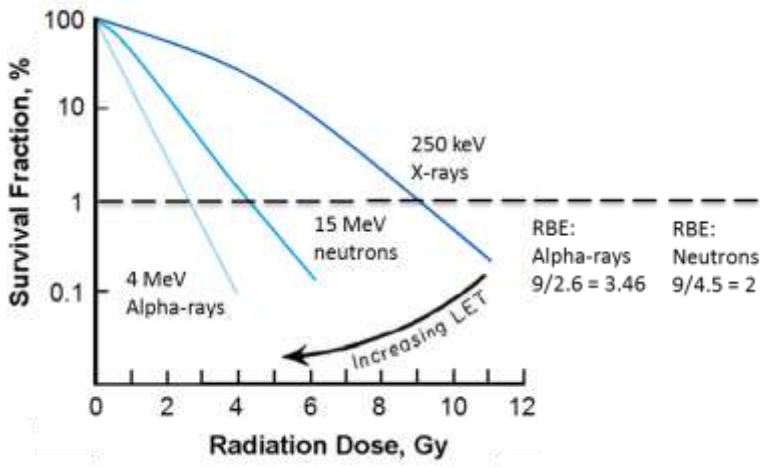

Figure 4: Survival curves for cultured cells after exposure to radiation modalities with increasing LET

Irradiation of cells with neutrons or α-particles leads to steeper cell survival curves than after exposure to X-rays. Increase in LET results in a reduction of the surviving fraction for the same dose of radiation. Neutron and α-particles have an RBE larger than one when compared to the reference radiation (X-rays), which indicates that these radiation modalities generate biological effects 2 and 3.46 times stronger, respectively. The comparison here is made at a survival level of 1%. Modified from (Hall 2006).

1.3 Chemistry of ionizing radiation absorption

Energy deposition on molecules by IR leads to the ejection of an electron and to radical formation. In principle, all molecules in a cell are the target of IR, but damages on the DNA are the most severe form since it affects the genomic stability and integrity. The DNA is damaged by IR either by direct or indirect action (figure 5) (Hall 2006). Considering that cells consist 70% of water molecules, irradiation leads mainly to radiolysis of water. The radiolysis of water or other molecules, damages the DNA indirectly through radical generation (Kelley 2012). The physical interaction that ejects an electron from water occurs within 10^{-15} seconds. The so formed primary ion radical has a life time of 10^{-10} seconds and produces a hydroxyl radical with a life time of 10^{-9} seconds (Friedberg 2006, Hall 2006). The ejected electron on the other hand reacts quickly with oxygen; together with protons they

produce the less reactive H_2O_2. Another primary interaction with water is the homolysis of excited water molecules.

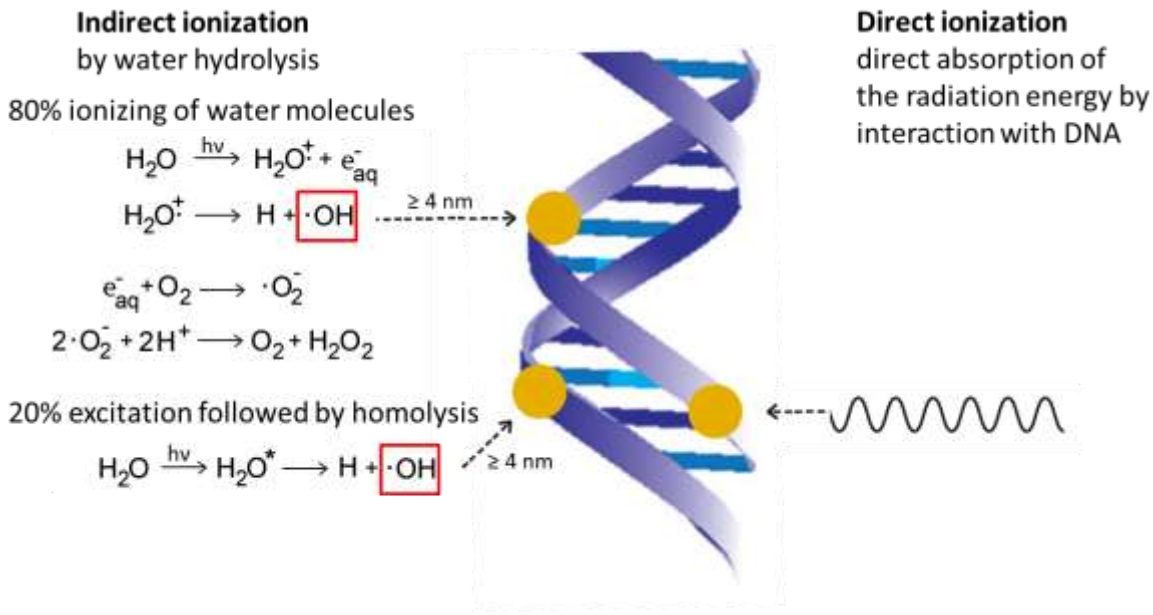

Figure 5: IR induces DNA damage by indirect and direct ionization events

IR ionizes by direct interaction with DNA or by indirect interaction through the ionization of water molecules in close proximity to the DNA. A small part of water molecules are excited and also contribute to DNA damages. The ionization of water molecules results in hydroxyl-radicals that are highly reactive. In the presence of oxygen the electron get incorporated to form less harmful hydrogen peroxide. Modified from (Friedberg 2006) and from (Hall 2006).

Hydroxyl radicals damage the DNA only when they are formed in close proximity to the DNA due to the short life time. 80% of the indirectly ionizing events are from the removal of electron and 20% from excitation reactions.

The direct ionization of DNA by IR leads to the release of an electron from the sugar, phosphate or base components. Modification of bases is highly diverse. Figure 6 illustrates the oxidation possibilities on DNA upon IR.

The modification of nucleotides by IR may also lead to an interruption and formation of a single strand break (SSB). Two SSBs that are formed at opposite DNA strands with a distance of a few nucleotides leads to the disruption of the

hydrogen bonds between the bases and therefore also to the disruption of the DNA molecule. This lesion is then termed DNA double strand break (DSB).

High-LET irradiation generates with higher probability ionization clusters that result in cluster damage sites (CDS). CDSs are regions on the DNA that are composed of two or more lesions in close proximity within one or two helical turns (Ward 1985, Ward 1987). Therefore CDSs have a higher probability of SSBs formation and with that also for the development of DSBs (Friedberg 2006). A DSB arises in various forms. These are described in more detail in the next section.

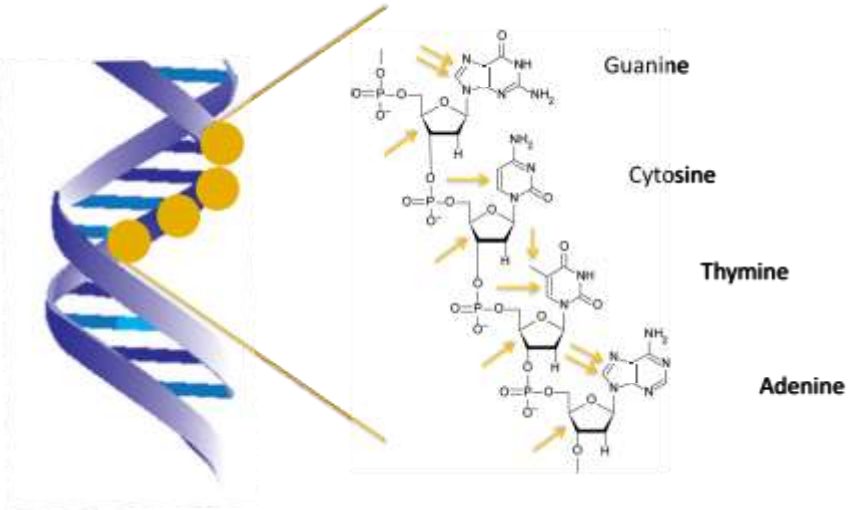

Figure 6: Major sites of oxidative damage by IR

The orange dot illustrates an ionization event on the DNA. On the right side the DNA strand is shown with four DNA bases. The arrows indicate possible sites of oxidative damage. Modified from (Lindahl 1993).

1.4 Types of DNA DSBs and damage complexity induced by IR

The types of DSBs are classified on the basis of DSB complexity into T1-T7 categories (Schipler 2013). The simplest form of DSB is the T1 DSB type that is only generated enzymatically by nucleases, forming ligatable 5'-phosphate and 3'-OH-groups (figure 7, A). These ends are termed 'clean' as they are directly ligatable. The ends of DSBs that arise after IR contain various modifications of base or sugar components of the nucleotides in the DNA. This DSB type is termed

T2 and is illustrated in figure 7,B by the presence of 5'OH and 3'phosphoglycolate groups at the break site (Schipler 2013). These lesions cannot be directly ligated and require additional DNA end processing steps. Exposure to higher doses of sparsely ionizing radiation, or exposure to densely ionizing radiation generates DSBs that are accompanied by additional lesions close to their ends (figure 7, C). DSBs accompanied by such additional modifications (DSBs of the type T3) are termed complex DSBs and may also arise from CDSs.

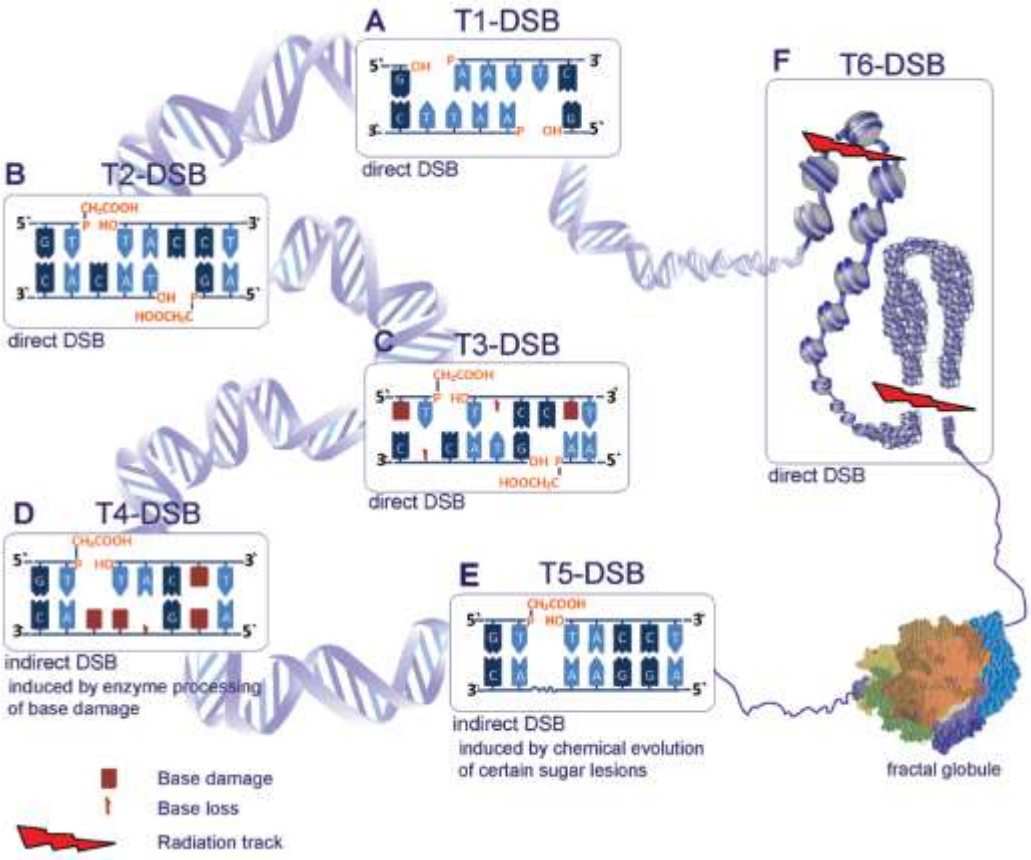

Figure 7: DSB types with increasing levels of complexity

A) DSBs generated by restriction endonucleases exhibit a 5'posphate and 3'OH group. B) DSBs that arise from IR often show chemically modified ends, indicated here with a 3'phosphoglycolate and 5'OH group. C) DSBs that arise after irradiation in clustered DNA damages display the next level complexity. D) DSBs are formed indirectly after enzymatically processing or E) after chemical evolution. F) DSBs that occur in clusters may lead to the loss of nucleosomes and chromatin loops. As an example for the loss of a nucleosome two DSBs are formed in F) in the linker regions of the nucleosome. Modified from (Schipler 2013).

The level of complexity is further increased with increasing LET of radiation. Densely ionizing radiation for example generates with higher probability DSB clusters that are distributed over a large range of the DNA (figure 7, F). DSB clusters (T6 DSB) represents the highest level of DSB complexity as they lead to destabilization of chromatin and may result in the loss of whole nucleosomes or DNA fragments. There is evidence that also simple DNA lesions can convert to DSB if generated in close proximity, by enzymatic processing (T4 DSB), or chemical processing (T5 DSB) in a temperature depended manner (figure 7, D and E) (Singh 2013).

The occurrence of DSBs may result in diverse patterns of complexity at the DNA. Theoretical DNA damage models enhance our understanding of the effect of radiation and the role of DSBs. Radiation induced DNA damage sites can for example be predicted by simulation of the track structure and by overlay of the track on DNA or chromatin. To model indirect effects, water radical diffusion reactions are simulated and used to adapt it on DNA. This modelling of DNA damage induction reveals stochastic aspects of the radiation action. Studies using modelling by Monte Carlo calculations showed that clustered damages are generated more likely than DSBs in a ratio of 4 to 1. Furthermore, the formation of more complex damages seemed largely to depend on the ionization density. Goodhead for example showed that 30% of all induced DSBs after low-LET ɣ-rays, but about 70% of all induced DSBs after high-LET α-particles are complex DSBs (Nikjoo 1999).

Taking modelling and experimental studies together we see that high-LET radiation increases the DSB complexity as compared to low-LET irradiation. The increase in complexity may result in different selection of repair pathways. In the present thesis the repair of DSBs of different complexities are investigated by the administration of low-LET (X-rays) and high-LET (^{241}Am α and ^{56}Fe ions) radiation. We also use enzymatic induction of single and complex DNA DSBs. DSBs are recognized and processed by different repair pathways, and these are described in the next section.

1.5 Biological response to DSBs generated by IR

1.5.1 The DNA damage response (DDR)

DSBs generated by ionizing radiation initiate a cascade of events in the cell, termed the DNA damage response (DDR). DDR promotes the repair, or triggers the cell to undergo apoptosis. There are diverse cellular responses to DSBs, such as transient cell cycle arrests that facilitate repair, chromatin modifications or altered gene expression that also facilitate repair. To ensure repair of all types of DSBs different repair pathways have evolved that benefit from four common components of DDR: DNA damage sensors, transducers, mediators and effectors (figure 8) (Harper 2007). DNA sensor proteins that recognize and bind DSBs include the Mre11-Rad50-Nbs1 (MRN) complex (Lee 2005), the Poly(ADP-ribose)polymerases1 (PARP-1) (D'Silva 1999, Kim 2005) and the heterodimer Ku70/80 (KU).

One of the DNA sensor proteins is the MRN complex. The core enzyme of this complex is the meiotic recombination 11 (Mre11) that binds to DNA by two DNA binding motifs. Mre11 shows DNA endonuclease and 3'-5' exonuclease activities that may not be directly associated with DSB repair but in other processes, e.g. telomere homeostasis. In the MRN complex Mre11 is associated to Rad50, a protein composed of a hook domain that connects a globular region (Walker A and B) on each subunit via coiled coil polypeptide dimers. The coiled coil structures are required for intramolecular interactions and the globular regions to bind the DNA. Mre11 and Rad50 have been shown to bridge and stabilize broken DNA ends and are involved in replication fork stability (van den Bosch 2003). The third component is the Nijmegen breakage syndrome 1 (NBS1) protein that interacts with Mre11 independently of Rad50 and recruits as component of the MRN complex to DSBs the ataxia-telangiectasia mutated (ATM) protein (Williams 2008).

The other DNA sensor protein is PARP-1. PARP-1 binds to interruptions in DNA continuity via its two zinc finger motifs and starts to poly(ADP)ribosylate proteins (Wang 2006). PARP-1 was shown to bind also to other DNA damages (e.g. abasic sites, strand breaks) (Kedar 2012) and to have a role in the repair of SSBs (Dantzer 2000). However, the affinity of PARP-1 to bind DNA is higher for DSBs than for

SSBs (Audebert 2004). The role of PARP-1 in DSB repair is described in more detail in the alternative non-homologous end-joining pathway (alt-EJ).

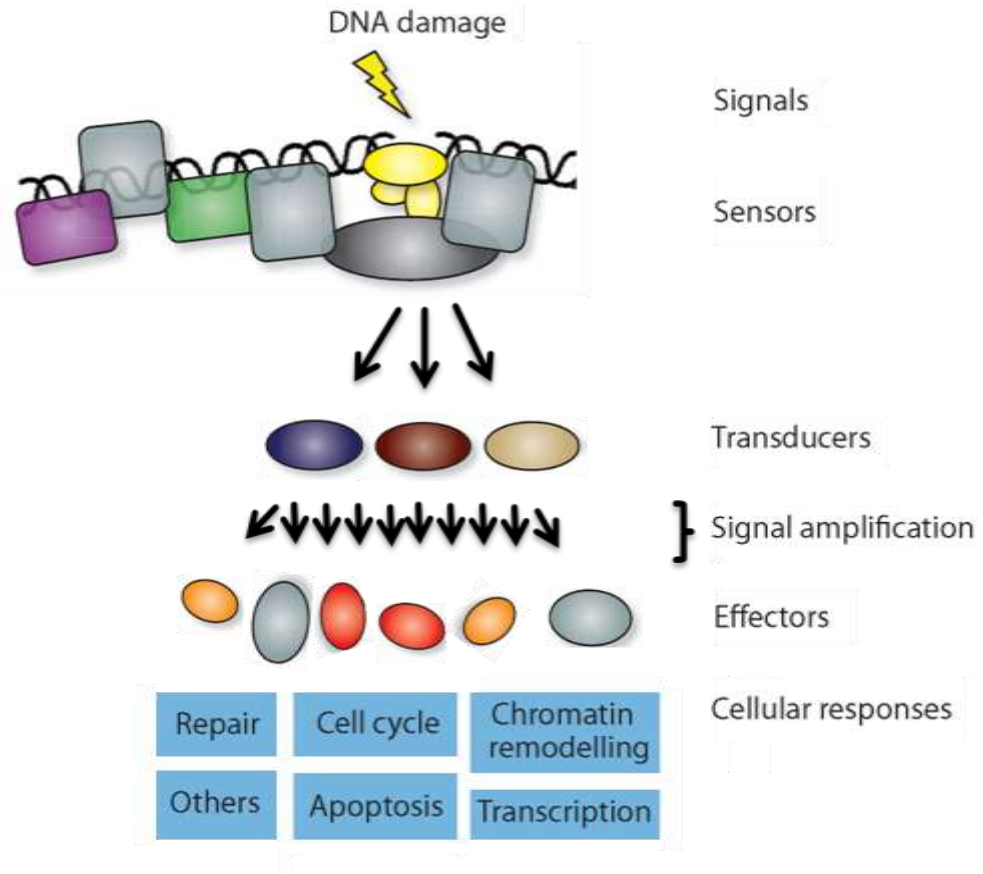

Figure 8: Simplified scheme of the DNA damage response (DDR)

DDR is composed of a complex network of interacting pathways. For simplicity only the linear pathways from sensing of a DSB via transducers and effectors are shown. The cellular response to DSBs is highly regulated within the cell and leads to diverse cellular responses. This indicates that the cell takes each DSB seriously. Modified from (Jackson 2009).

The third DNA sensor protein is the heterodimer Ku70/80 that binds to the DSB and is described in more detail together with the DNA-PK dependent non-homologous end-joining (D-NHEJ) repair pathway.

These sensor proteins may compete with each other for DNA binding at DSBs, or may cooperate following a certain hierarchy of recruitment according to their DSB affinity. The Ku70/80 heterodimer shows a higher affinity than PARP-1 for DSB binding. PARP-1 on the other hand was found to modulate MRN recruitment (Wang

2006, Haince 2008). The affinities of recruitment of these sensor proteins may also vary depending on the type of DSB induced. So is the affinity in vitro for blunt and nick ends higher for PARP-1, while 3' single-base overhangs are attracted more by Ku70/80 bound to DNA-PK (D'Silva 1999). It is likely that the binding of DNA sensor proteins contributes to the activation of specific downstream signaling repair pathways.

Sensor proteins are not restricted to work only through transducers. Instead, they may also get involved in diverse repair pathways. The DSB repair pathways that engage these DNA sensor proteins are described in more detail in a separate section.

The binding of damage sensor proteins to DNA leads to the recruitment of transducers that amplify and diversify the signal. The role of transducers is taken by the protein kinases ataxia-telangiectasia mutated (ATM), ATM and Rad3-related (ATR), and the catalytic subunit of DNA-dependent protein kinase (DNA PKcs). The ATM, ATR and DNA PKcs protein kinases belong to the phosphatidylinositol-3 (PI3) kinase-like kinase family (PIKK) and are recruited to DSBs by different mechanisms. While ATM is mainly recruited by MRN and DNA PKcs by Ku70/80, ATR is activated mainly by replication protein A (RPA) coated single stranded DNA in conjunction with ATR-interacting protein (ATRIP). PARP, on the other hand, poly-(ADP)-ribosylates various proteins and leads to a DNA damage response. However, the role of DNA PKcs in the DDR is still under debate. The activated protein kinases are key response regulators propagating DSB signals by interacting with downstream mediators (Polo 2011). This cascade of events eventually targets the downstream effector checkpoint kinases 1 and 2 (CHK1, CHK2). ATM-CHK2 and the ATR-CHK1 are two signaling cascades that coordinate the checkpoint activation during the cell cycle. The cell cycle arrest allows repair to take place and prevents damage potentiation that can occur as the cell progress with unrepaired or miss-repaired damages through the replication phase. In the case of too severe DNA damages prolonged checkpoint activation also may induce apoptosis (Jackson 2002, Saha 2013).

1.5.2 Interplay between ATM and ATR in HRR

The protein kinases ATM and ATR are involved in DDR signaling and signal amplification. Furthermore, they are involved through distinct mechanisms in homologous recombination repair (HRR) and will be described briefly here. As consequence of DSB induction, MRN activates ATM at DSB sites that in turn regulates the generation of 3'-ended ssDNA overhangs. This is achieved by liberating the nucleolytic activity of C-terminal binding protein interacting protein (CtIP) and Mre11. ATR on the other hand primarily responds to ssDNA overhangs and is therefore indirectly activated by IR-induced DSBs and mostly found active at stalled or collapsed replication forks. In the classical view, ATM and ATR were therefore considered to operate in separate pathways like ATM at DSBs and ATR after DNA replication stress. However, ATM and ATR signaling have also overlapping substrates, like the MRN complex, implying a possible crosstalk between these proteins in DDR. After DSB induction, a sequential activation of ATM and ATR was found that indicates a biphasic DSB response pathway. In vitro studies reveal that they are regulated oppositely depending on the length of single-strand overhangs (SSOs) at the break and on the junction of single/double stranded DNA (Shiotani 2009). The presence of increasing length of SSOs attenuates the ATM activation while enhancing ATR activation. Furthermore, ATM was shown to be required for an efficient resection during HRR by ATR. A study showed that this sequential switch from ATM to ATR activity after irradiation varies depending on LET. After exposure to high-LET radiation the sequential activation is delayed and shows sustained and prolonged end resection as compared to cells that are exposed to low-LET radiation (Saha 2013). The two key proteins ATM and ATR are investigated in the present thesis in an effort to examine how HRR is coordinated after exposure to low and high-LET irradiation.

1.5.3 DDR signal amplification at the DSB

ATM is present in the cell as an inactive dimer or multimer. The kinase domain of the ATM molecule in the inactive form is bound to an internal domain of another

ATM molecule. Upon DSB induced DDR signaling, ATM gets activated and dissociates into its active monomer by autophosphorylation at serine 1981 (Bakkenist 2003). Thus, the kinase domain of ATM is no longer hidden, and phosphorylates in one of the first responses the histone H2A variant H2AX at serine 139 residue, resulting in γH2AX. Inhibitor studies with human cells deficient in distinct PIKK kinases reveal that besides ATM, also DNA PKcs and possibly ATR are candidate H2AX kinases (Wang 2005). The mediator of DNA damage checkpoint protein 1 (MDC1) binds to γH2AX and promotes further recruitment of MRN and ATM that leads to amplification of the DNA damage signal by spreading the γH2AX signal over a few megabases at both DSB sides. This provides a binding platform for other factors like 53BP1 and breast cancer susceptibility 1 (BRCA1) proteins (Rogakou 1999, Polo 2011). These factors are implicated in the accumulation of the E3 Ubiquitin ligases RNF8 and RNF168, which then ubiquitylate the histone H2A and its variant H2AX.

1.6 Repair of DNA DSBs

DSBs are generated either spontaneously by endogenous factors like oxidative metabolic byproducts and replication fork accidents, or by exogenous cytotoxic agents and IR. However, DSBs are also generated by the cell during V(D)J recombination and class switch recombination (CSR), processes that are required for the development of T and B cell lymphocytes, as well as in meiotic recombination. Recently, a group showed that cells use DSBs as a means for regulating gene expression and neuronal activities in postmitotic cells (Madabhushi 2015).

DSBs are thought to be repaired by three major pathways: homologous recombination repair (HRR), DNA-PK dependent non-homologous end-joining (D-NHEJ) and particularly when D-NHEJ is compromised, by the as backup functioning alternative end-joining (alt-EJ).

1.6.1 Homologous recombination repair (HRR)

Homologous recombination repair is an error free DSB repair pathway and contributes to genomic stability. HRR is characterized by the ability to rejoin broken ends correctly without altering DNA sequence at the break sites. This is achieved by using the homologous template of the sister chromatid, and much more rarely the homologous chromosome. The presence of repetitive sequences in the genome may present a basis for miss-repair events during HRR. Therefore, cells predominantly use the sister chromatid as template to restore the sequence at the break site (Iliakis et al. 2015). This restricts the HRR to the late S and G_2 phases of the cell cycle during which a sister chromatid is available.

As described in the previous section, the induction of a DSB recruits DNA sensor proteins to the break site. In HRR, MRN binds in the first step to the DSB and initiates resection generating an extended 3' ssDNA overhang (figure 9). This resection involves CtIP, the exonuclease Exo1, Dna2 and the bloom helicase (BLM) (Tomimatsu 2012). To prevent degradation or formation of secondary structures at the ssDNA, replication protein A (RPA) proteins bind and coat the single strand DNA segments generated (Sleeth 2007). However, this RPA coated ssDNA blocks kinetically the next step: RAD51 filament formation. Therefore RAD51 requires for its assembly on these single stranded segments the help of proteins that mediate its function (Heyer 2010). One of the mediators is the breast cancer susceptibility protein 2 (BRCA2) that has binding motifs for single and double stranded DNA, as well as for Rad51 and facilitates thus the process. Other factors that act as mediators are the Rad51 paralogs (RAD51B, RAD51C, RAD51D, XRCC2, XRCC3), members of the RAD52 epistasis group (RAD50, 52, 54, Mre11) and CtIP (Heyer 2010).

After resection RAD51 binding, the generated RAD51 filament searches for homology and invades the DNA strand in a process termed synapsis. Strand invasion generates a displacement loop (D-loop) in the heteroduplex DNA between the substrate and the homologous template. The homologous template is then used by the 3'-end of the invading end to prime a leading DNA strand in the DNA synthesis step. Rad54 promotes the transition from invasion to the priming of DNA synthesis and branch migration by detaching Rad51 from the heteroduplex DNA

(Heyer 2006, Iliakis et al. 2015). The last step of HRR is the junction resolution that can result in crossover or non-crossover products. Several subpathways like break-induced replication (BIR), synthesis dependent strand annealing (SDSA) and double Holliday junction (dHJ) formation and resolution exist and lead to different products but this is not discussed further here.

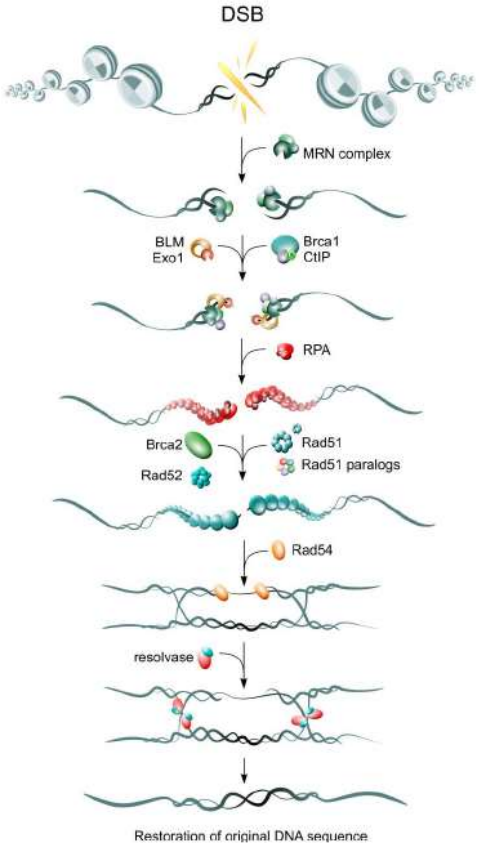

Figure 9: Schematic overview of HRR steps

HRR recognizes the appropriate ends of the DSBs and rejoins them while ensuring sequence restoration. The HRR steps can be distinguished in the DSB recognition, the synapsis formation and the resolution of the junction. In this figure ATM and ATR are not shown. Figure adapted from Dr. Mladenov

1.6.2 DNA-PK dependent non-homologous end-joining (D-NHEJ)

D-NHEJ is a fast operating repair pathway that rejoins DSB ends throughout the cell cycle without a DNA template requirement. The absence of a DNA template increases the risk to repair a DSB in an error prone manner. However, based on its fast kinetic D-NHEJ is considered to contribute to genomic stability.

The first step in the repair of DSBs by D-NHEJ is the binding of the DNA damage sensor protein Ku70/80 to both sides of the interrupted DNA strand (figure 10). Ku70/80 then encircles two helical DNA turns with its ring structure and slides in a sequence-independent manner along the DNA end. There it serves as a scaffold protein for the recruitment of other D-NHEJ factors (e.g. DNA PKcs, XRCC4, DNA ligase IV, XLF). However, the major known function of Ku70/80 is the initiation of the second step of D-NHEJ (figure 10). In this step Ku70/80 recruits at the DNA terminus DNA PKcs and translocates inward of the DNA, allowing DNA PKcs to bind at that place, approximately 10 bps proximal to the end of the DNA (Yoo 1999, Walker 2001, Davis 2014). After binding of the catalytic subunit of DNA PKcs to the regulatory component Ku70/80, a DNA PK complex is formed that is termed holoenzyme. DNA PKcs, a component of the DNA-PK holoenzyme complex (Ku70/80/DNA PKcs) then starts to stabilize the broken DNA ends through the formation of a synaptic complex (DeFazio 2002). With the complex formation, DNA PKcs undergoes a change in its conformation that liberates its full kinase activity leading to phosphorylation of many mediator proteins (e.g. Ku70/80, XRCC4, DNA ligase IV, XLF, Artemis, polynucleotide kinase/phosphatase (PNKP)) as well as itself (figure 10, step 2) (Davis 2014). A study reported that X-ray repair cross complementing protein 4 (XRCC4) in Chinese hamster cells and DNA ligase IV are also recruited in the absence of DNA PKcs to DSBs and showed that this occurs through direct interactions between Ku70/80 and XRCC4 (Mari 2006). Another study proposed that an increase in DSB complexity may also lead to differential substrate recognition of D-NHEJ factors. In this study the authors followed fluorescence-labelled DNA PKcs and Ku70/80 in real time after generation of simple and complex DSBs. They reported that Ku70/80, XRCC4, Ligase IV and XLF but not DNA PKcs are recruited to simple DSBs, while DNA PKcs was found more at complex DSBs (Reynolds 2012).

Furthermore, NHEJ factors like XRCC4 and XLF may form a helical filament structure that may tether and bridge DNA ends together, similar to DNA-PK (Davis 2013). This suggests that D-NHEJ may repair a DSB in different ways in order to maintain genomic integrity.

The next step after the stabilization of the DNA ends by DNA PK is end processing to generate ligatable ends (figure 10, step 3). Only clean DSB ends do not require further processing and can be directly ligated. However, the ends of IR induced DSBs exhibit mainly non-ligatable ends with 5'hydroxyls or 3'phosphates.

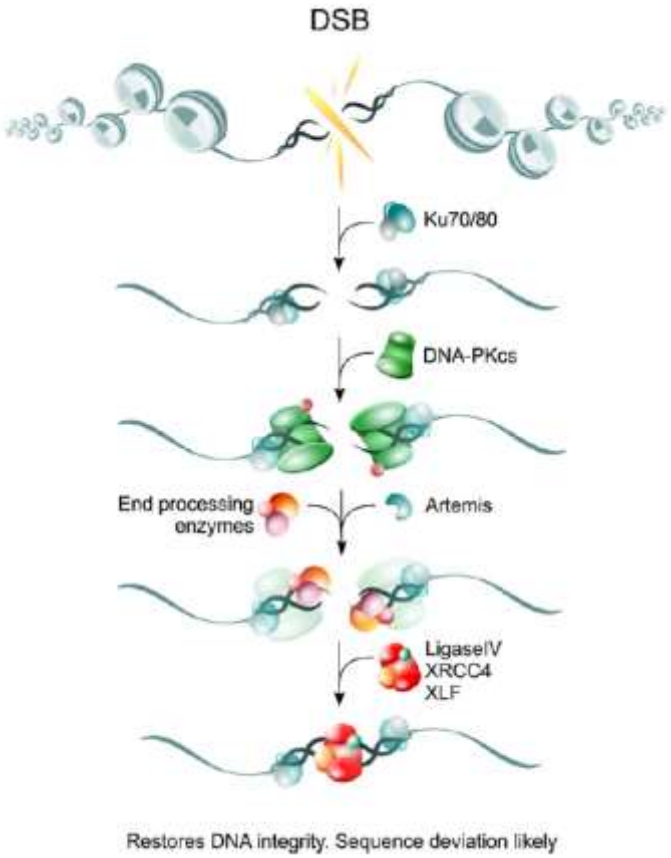

Figure 10: Schematic overview of steps of DNA PKcs dependent non-homologous end-joining (D-NHEJ)

During D-NHEJ the broken ends are rejoined without ensuring restoration of DNA sequence around the break. After DSB induction the Ku70/80 heterodimer binds to the DSB and stabilizes, in conjunction with DNA PKcs, the DSB ends. The ends are then processed by nucleases and ligated by the Ligase IV/XRCC4/XLF complex. Modified from (Mladenov 2011).

To allow repair and ligation, the DNA ends can either be resected or fill the gap by polymerizing single stranded and non-compatible overhangs. The nucleases that are implicated in resecting DNA ends are Artemis, Werner (WRN) and upon complex damages members of the family of X polymerases μ and λ that are able in

conjunction with Ku, XRCC4/DNA LigaseIV to polymerase independently of a strand template in order to fill-in the gap (Davis 2013).

The DNA Ligase IV, stabilized by XRCC4, ligates in the last step (figure 10, step 4) the DSB. This enzyme was shown to operate even across gaps of 1 nucleotide and to ligate incompatible overhangs in order to repair DNA ends (Gu 2007). These mechanisms of NHEJ result in limited deletions or insertions and do not faithfully restore the original sequence information. However, this process restores rapidly upon DSB induction DNA integrity and therefore contributes to maintain genomic stability.

1.6.3 Alternative non homologous end-joining (alt-EJ)

The alternative non-homologous end-joining pathway (alt-EJ) operates as a backup, when D-NHEJ or HRR are compromised. One of the first hints for the presence of alt-EJ was the observation that DNA PKcs deficient cells show significantly slower DSB rejoining kinetics but similar residual unrejoined DSBs as compared to their DNA PKcs proficient counterpart (DiBiase 2000). This was also observed in the absence of other D-NHEJ factors like Ku70, Ku80 and Ligase IV (Wang 2001a). Cells deficient in HRR, on the other hand, showed fast kinetics similar to wild-type cells and an unchanged slow component of rejoining. This slow component that was even observed in HRR and D-NHEJ defective cells implied that another pathway was most likely present and operating, the alt-EJ (Wang 2001b). Therefore alt-EJ is considered as a slow operating pathway that is active when other repair pathways are compromised.

It is assumed that alt-EJ substitutes for other DSB repair pathways when they fail (Dueva 2013). This suggests that more than one alt-EJ pathway exists in the absence of HRR or D-NHEJ. Plasmid rejoining studies further show that in Ku deficient cells microhomologies (5-25 nucleotides) are used to repair some DSBs, suggesting the involvement of microhomology in alt-EJ (Guirouilh-Barbat 2004, McVey 2008). Another study demonstrates that overlapping nucleotides (0-5 nucleotides) facilitate alt-EJ, but that repair does rely on 5-25 nucleotides long microhomologies (Mansour 2010). The observation that microhomology mediated

end-joining (MMEJ) is more frequent in the absence of D-NHEJ factors, has pointed to this parameter as part of alt-EJ.

In the development of the immune system DSBs are generated at specific genomic locations and are recombined by D-NHEJ. CSR produces different classes of antibodies in B lymphocytes and V(D)J recombination increases diversity of the assembly of the gene segments V, D and J in immunoglobulins and T-cell antigen receptors. Defects in factors of D-NHEJ (Ku, DNA PKcs, XRCC4, Ligase IV) show in both processes activation of a microhomology associated alt-EJ pathway, resulting in the production of T and B cells, but with defects in nucleotide sequence (Brown 2002, McVey 2008). Studies of V(D)J recombination reveal Mre11 as a factor of alt-EJ (Brown 2002). Other components associated with alt-EJ are histone H1 (Rosidi 2008), CtIP (Zhang 2011) and PARP-1 (Audebert 2004). One study showed that the ligation activity of the XRCC1/DNA ligase III complex, operating with PARP-1 is involved in alt-EJ (Audebert 2004). Further experiments indicate that XRCC1 is not required but reinforces the activity of DNA ligase III in alt-EJ and that another ligase, DNA ligase I may also operate in the ligation step (Wang 2005b, Boboila 2012, Paul 2013, Soni 2014).

Alt-EJ not only shares components with other DSB repair pathways, but also interacts with them. Examples are D-NHEJ (PARP-1-KU, CtIP-KU), HRR (Mre11, CtIP) and SSB (PARP-1) repair pathways. This unscores the ability of alt-EJ to operate as a backup whenever one of the other repair pathways is compromised. As a backup alt-EJ operates throughout the cell cycle, but is enhanced in G_2 phase. However, depending on DNA ends and the status of the other DSB repair pathways, multiple subpathways of alt-EJ are possible that operate throughout the cell cycle to rejoin DNA ends together. This way, chromosome stability is maintained at the price of increased risk for chromosomal translocations (Wu 2008, Iliakis et al. 2015).

To sum up, the presence of a DSB, as the most severe DNA lesion, induces a cascade of cellular events in order to repair and if possible to restore the sequence information at the break site. However, when one of the available repair pathways is abrogated, the error prone alt-EJ pathway takes over to eventually rejoin the open ends and to prevent the complete loss of genome integrity.

1.7 Gene editing by nuclease-based systems

Nuclease based systems allow the targeted modification of specific sequences in a genome. Recently methods have been devised that use zinc finger nucleases (ZFNs), the transcription activator-like effector nucleases (TALENs) and the clustered regularly interspaced short palindromic repeat Cas-based RNA guided DNA endonucleases (CRISPR/Cas). In ZFNs and TALENs the target sequence recognition is mediated by a sequence-specific DNA binding domain that fused to a nonspecific DNA nuclease domain (FokI). Both gene editing methods have the disadvantage that for each target recognition sequence a new set of ZFNs or TALENs has to be engineered. Therefore these techniques are not appropriate for multiple step mutagenesis experiments (Barrangou 2012).

The CRISPR/Cas system is a very recently employed genetic editing tool. It is based on the adaptive immune response strategy of archaea (90%) and bacteria (40%) to recognize invading viruses and plasmids. These organisms counteract viruses and plasmids by binding of small RNA molecules termed CRISPR RNAs (crRNAs), followed by enzymatic DNA cleavage (Cas) and degradation of invading DNA (Marraffini 2010, Gasiunas 2012, Xu 2014). Cas proteins vary in their composition and are classified into three types, of which only type II does not require additional components to operate. Among other Cas genes, Cas9 doesn't affect crRNA biogenesis when the gene is disrupted. Studies in *Streptococcus* and *Neisseria* reveal that Cas9 type II is guided to the target by a crRNA (Gasiunas 2012) and by a partially trans-acting crRNA (tracrRNA) (Deltcheva 2011). Furthermore, Gasiunas and colleagues showed that crRNA binds specifically the complementary invading sequence, and therefore are termed protospacers. The cleavage of Cas9 is executed 3 bp upstream of the recognized foreign DNA sequence, the protospacer adjacent motif (PAM) by its enzymatic active sites RuvC and HNH, generating a cut at the non-complementary and at the complementary DNA strand, respectively (Gasiunas 2012, Jinek 2012). The maturation of precrRNA is processed by RNaseIII and directed by the tracrRNA and Cas9 in *Streptococcus* (Deltcheva 2011).

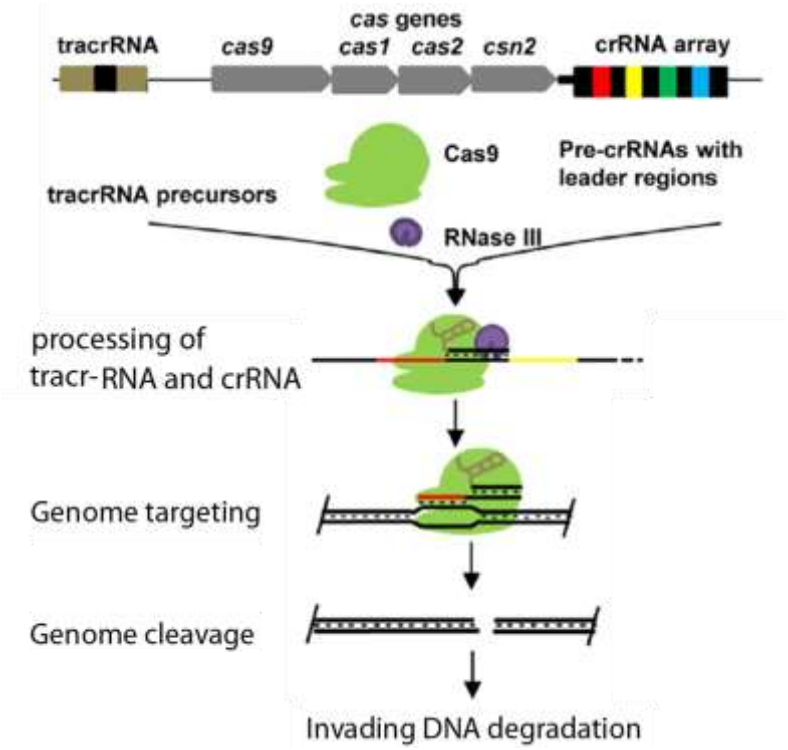

Figure 11: Scheme of type II CRISPR/Cas system in bacteria

The tracrRNA and crRNA precursors are processed by RNase III in the presence of Cas9. This complex is directed in the next step to the invading genome and induces DSBs. Modified from (Xu 2014).

This nucleotide directed target recognition mechanism that was discovered in microorganisms has been transferred into a plasmid based CRISPR/Cas9 system, in which the tracrRNA and the crRNA are fused together, termed guideRNA (gRNA). As a result of this development, genome editing in any organism has become possible, by simply transfecting customized gRNAs together with Cas9. The type II CRISPR/Cas9 system can be used either to generate (blunt) DSBs, nicks or to inhibit gene regulation/transcriptional/replication processes of a specific gene by either use the native Cas9, a one-site mutated, or both-sites mutated Cas9 nuclease, respectively (Xu 2014). In this thesis the native Cas9 was used in a CRISPR type II system.

1.8 Hypoxanthine guanine phosphoribosyl transferase (*hprt*) locus as a target for mutation analysis

1.8.1 *hprt* locus and the function of HPRT

The hypoxanthine guanine phosphoribosyl-transferase (*hprt*) gene consists of nine exons and is located on the X-chromosome at the distal Xp short arm in hamster (Farrel 1977), at the Xcen-CD region in mouse and at Xq26-Xq27 in human (Howard 1970, Chinault 1984, Stout 1985). The sequence composition of the coding region of the *hprt* gene is highly conserved (>95%), while homology in the non-translated region is reduced (~80%) (Chinault 1984, Keebaugh 2007). The *hprt* gene varies in length, ranging from 36 kb in Chinese hamster cells, 34 kb in mouse (Melton 1984, Rossiter 1991) and about 42 kb in humans (Cariello 1993, Rossiter 1991, Jinnah 2000, Kim 1986, Melton 1984, Sculley 1992). Figure 12 shows the comparison of the *hprt* gene in these three species.

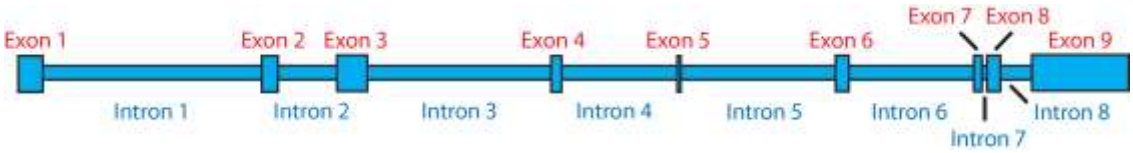

	Region	1	2	3	4	5	6	7	8	9	sum	HPRT:
Human	Exon (bp)	=145	106	184	66	18	82	46	76	637	1.36	42.83 kb
	Intron (kb)	13.8	1.6	13.4	3.9	3.0	4.0	0.17	1.6		41.47	
Mouse	Exon (bp)	145	106	184	66	18	82	46	76	593	1.316	33.72 kb
	Intron (kb)	10.8	2.9	6.5	3.6	3.9	3.9	0.2	0.6		32.4	
Hamster	Exon (bp)	N.N.	106	184	66	18	83	46	77	N.N	0.63	~35 kb
	Intron (kb)	~10	2.5	6.6	4.3	5.6	4.3	0.17	0.9		34.37	

Figure 12: Schematic structure of the *hprt* gene in human, mouse and the Chinese hamster

The organization of *hprt* locus is similar in all three species. The exon sequences and exon/intron junctions are highly conserved and differences are mainly found in the intron regions, especially in the first introns. The *hprt* gene consists of 9 exons and an overall length of 42 kb in human, 34 kb in mouse and 36 kb in hamster (Rossiter 1991). Modified from (Stout 1985).

The *hprt* gene encodes for a multimeric HPRT enzyme that is composed of identical subunits with a molecular weight of 25-26 kDa in hamster, 27 kDa in mouse and 24-26 kDa in human (Caskey 1979). The HPRT together with adenine

phosphoribosyltransferase (APRT) are the key enzymes of the purine salvage pathway and are expressed ubiquitously in all cells. However, the activity varies within tissues and HPRT seems to relate inversely to the amount of 5-phosphoribosyl-1-pyrophosphate (PRPP)-amidotransferase activity, the initial enzyme in the *de novo* purines biosynthesis (Howard 1970, Stout 1985).

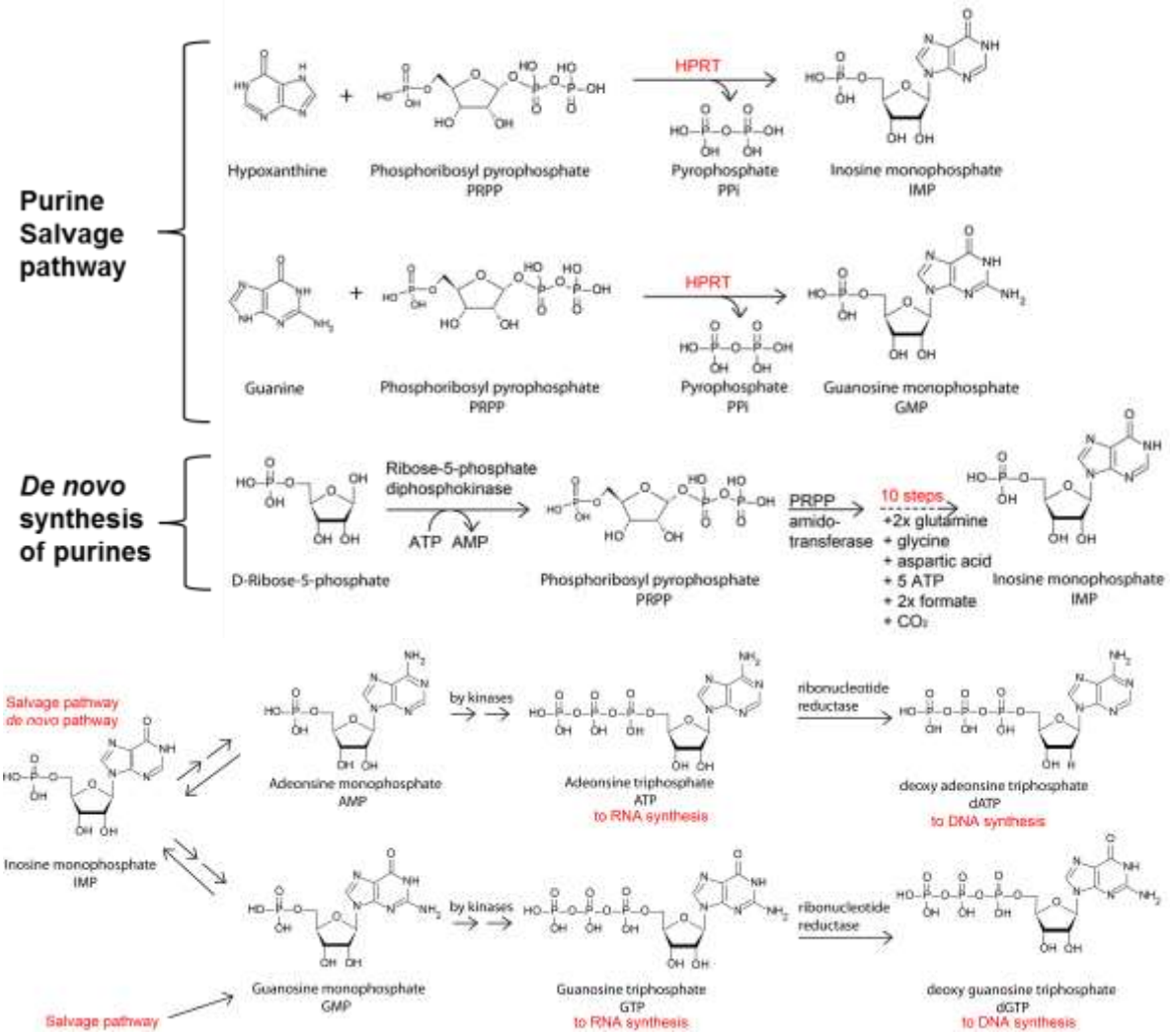

Figure 13: Overview of the function of HPRT in the purine nucleotide pathway

Purines are either synthesized *de novo* or recycled by the salvage pathway. The biochemical steps implicated in the production of purine nucleotides for RNA and DNA synthesis are shown. HPRT as a key enzyme of the purine salvage pathway is involved in the formation of the ATP and GTP precursors. Modified from (Berg 2002)

The *de novo* synthesis use D-ribose 5 phosphate as backbone on which purines are assembled (figure 13). After a phosphorylation step to form 5-phosphoribosyl-1-

pyrophosphate (PRPP), the committed step takes place; an ammonia group from glutamine is transferred on this backbone in a reaction catalyzed by the PRPP-amidotransferase. A complex series of reaction is followed to yield IMP.

The purine salvage pathway on the other hand reuses intact purine rings and involves the condensation reaction of PRPP with hypoxanthine and guanine catalyzed by HPRT (figure 13) and with adenine catalyzed by APRT to produce pyrophosphate and the nucleotide precursors IMP, GMP and AMP. The IMP substrate from the *de novo* synthesis can also be converted to GMP (Sculley 1992, Linder 2005).

1.8.2 The *hprt* gene as a mutation selection system to study mutagenesis

As mentioned above the *hprt* gene is located and encoded by a single gene on the X-chromosome. Furthermore, a loss in its function in the salvage pathway as illustrated in the previous section can be compensated by the *de novo* pathway. Therefore, malfunction or deficiencies of HPRT do not affect cell growth in culture. Based on these properties the *hprt* gene is used as an assay to analyze mutations, and offered one of the first opportunities in the last decades to investigate the mechanism of mutation generation in cultured animal cells (Caskey 1979). The *hprt* gene is also used for gene transfer techniques and cell hybridization.

To analyze mutations, selection procedures were developed that allow the analysis of forward and reverse mutation events by mimicking the substrate of HPRT and by inhibiting the *de novo* pathway respectively (Caskey 1979).

In the forward mutation selection technique, a purine analogue like 6-thioguanine (6TG) or 8-azaguanine mimics the guanine purine substrate for HPRT. Cells that express a functional HPRT converts the 6TG guanine analogue into 6-thioguanyl monophosphate 6-TGMP followed by the same subsequent steps as guanine and get it incorporated into the DNA (figure 14). There, it gets methylated by S-adenosylmethionine to 6meTG (Waters 1997) and is then recognized by MMR proteins that are recruited to the DNA damage and signal a G_2-M arrest. The prolonged G_2-M arrest eventually leads to cell death. In one model the 6TG

induced DNA lesions are believed to be repaired incompletely by MMR resulting in SSBs that may cause the cell cycle arrest (Yan 2003). The exact mechanism how MMR mediates the 6TG induced cytotoxicity remains unknown. More recently, Brem and Karran showed that 6TG liberates its toxicity also in an MMR independent pathway by oxidation reactions (Brem 2012). 6TG depletes endogenous antioxidant factors and is target of oxidizing substrates too. The administration of oxidizing agents and UVA radiation showed that the oxidization of 6TG blocks DNA replication and eventually leads to cell death. Figure 14 shows the oxidation products of 6TG.

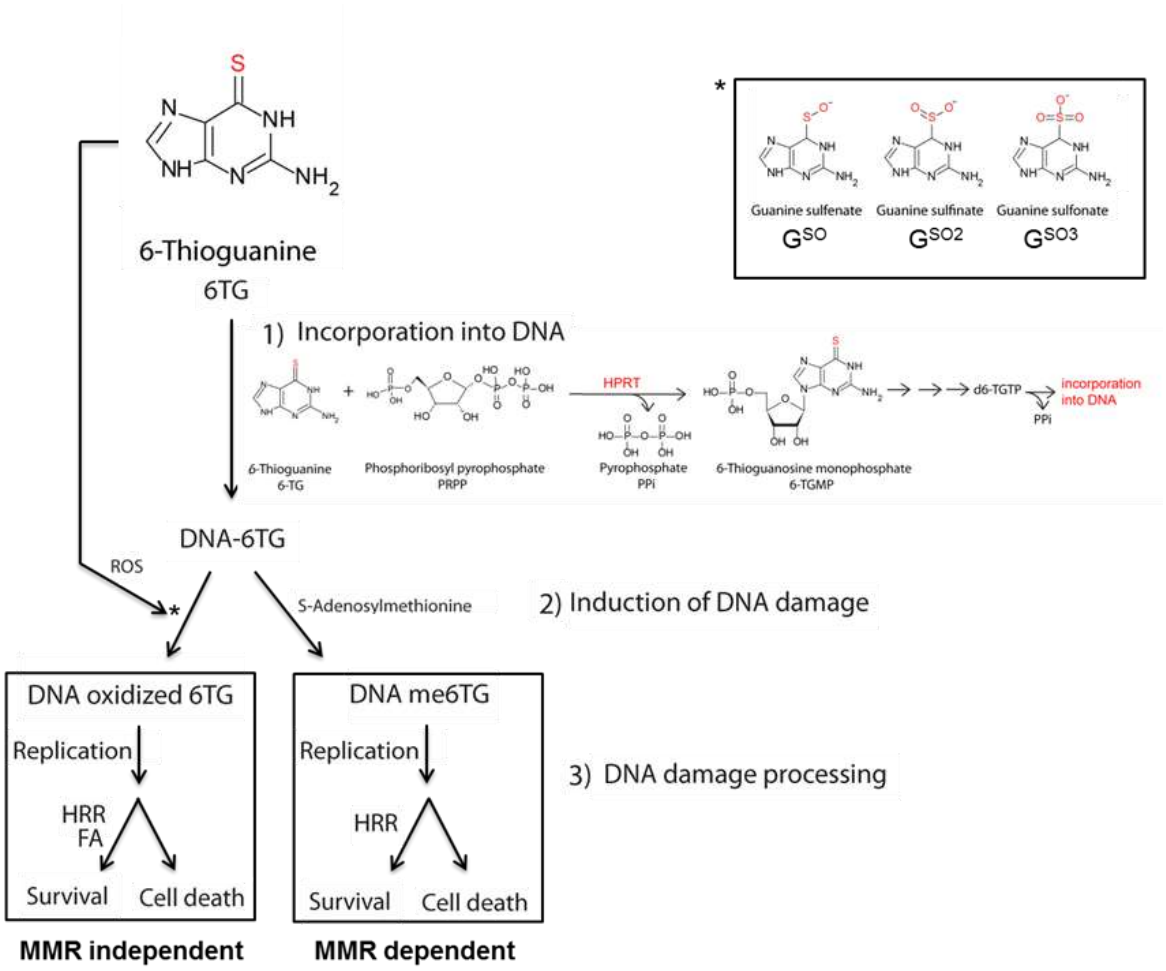

Figure 14: Overview of the cytotoxic mechanism of 6-thioguanine

6TG gets converted by HPRT and is incorporated into the DNA. The cytotoxic effect is mediated by methylation or oxidation reactions and leads eventually to replication block and cell death. The 6TG structure is drawn according to (Bugg 1970), the oxidation products according to (Ren 2010) and the 6TG metabolism according to (Sahasranaman 2008).

This forward selection technique with 6TG allows to separate *hprt* mutants from proficient cells and therefore enables the identification of sequence alterations and deletions in these mutants by screening. In this thesis the 6TG is used to select mutations and also to maintain two *hprt* mutant cell lines that are described later.

The isolation of mutants generated by the forward selection technique was used in several studies to analyze type of mutation and mutagenesis risk at the *hprt* gene after treatment with carcinogens, mutagens, clastogens (e.g., inorganic arsen, Cobalt(II)), recombinogenic agents (e.g., Cd(II)) and ionizing radiation (Bradly 1981, Thacker 1990). IR induces at the *hprt* gene primarily deletions ranging from partial to entire loss of the gene depending on the dose administrated (Hsie 1993). The same could be seen for α-particles. In addition to total and partial gene deletions, insertions are also found at the *hprt* gene after X-ray irradiation, but to a lower extend (Fuscoe 1992).

Some of the generated mutants are able to reverse their mutation spontaneously and to re-express functional HPRT protein (Zhang 1992a). These ‘reverse mutation’ events are analyzed by inhibition of the *de novo* pathway with inhibitors like azaserine or aminopterin (Szybalski 1962). Azaserine inhibits the glutamine amidotransferase that is involved in the committed step of the *de novo* synthesis as mentioned before (figure13). Aminopterin inhibits the 7,8-dihydrofolate reductase (DHFR) that blocks the *de novo* synthesis of purines by affecting the required folic acids components (figure 15).

The block of the folic acid pool eventually affects the thymidine monophosphate (TMP) production as well. Therefore these inhibitors are administrated to the media of the cell in conjunction with exogenous sources of hypoxanthine and thymidine. Hypoxanthine provides substrate for the purine salvage pathway and thymidine restores the depletion of these nucleosides as a result of the aminopterin treatment. This HAT selection medium (hypoxanthine aminopterin thymidine) results in the death of those cells that rely on the *de novo* pathway like *hprt* mutants and is used to detect reversion events in mutants.

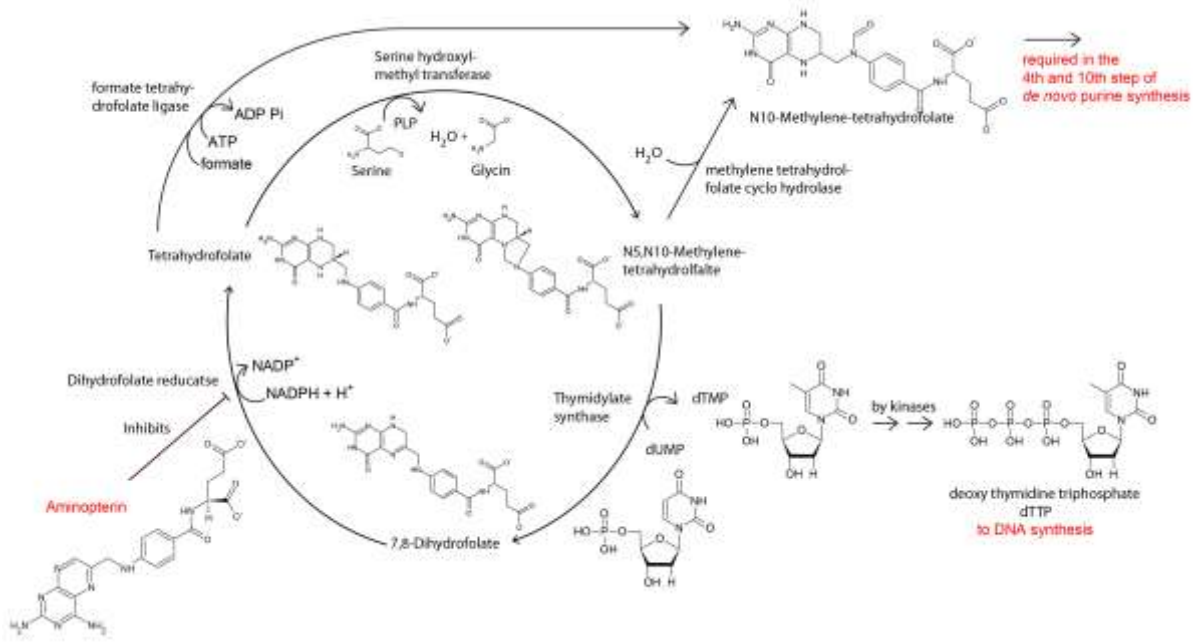

Figure 15: Overview of the cytotoxic mechanism of aminopterin

Folic acid components are required for the *de novo* pathway of purine synthesis. The administration of aminopterin leads to inhibition of the dihydrofolate reductase and affects thus the folate pool cycle. This results in the block of the *de novo* synthesis of purine nucleotides and also in an interference with the deoxy thymidine monophosphate (dTMP) conversion.

One study shows that mutants that are generated by ɣ-rays or α-particles seldom revert to HPRT proficient cells. In contrast, agents that mostly inducing point mutations, and not large deletions, like ethyl methanesulphonate (EMS) are more likely to revert (Thacker 1986). Two isolated duplication mutants that revert spontaneously from HPRT deficient to HPRT proficient phenotype are the SP5 and SPD8 mutants. They derive from the V79 Chinese hamster cell line and differ from each other in the location, the length of the duplication and the reversion mechanism (figure 16).

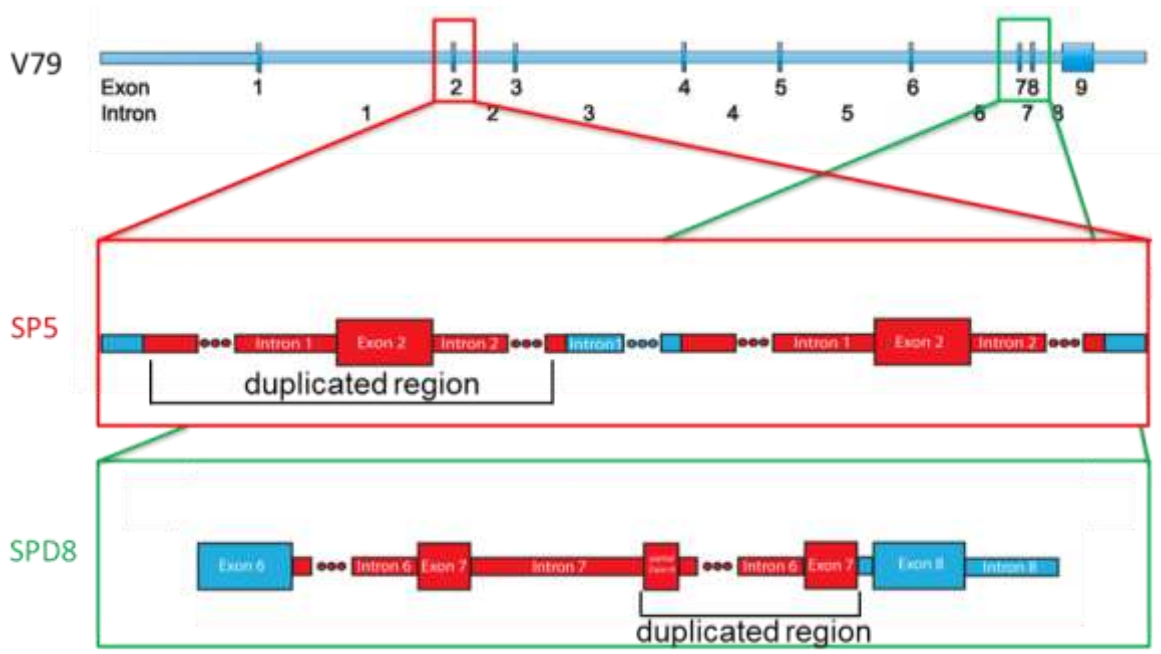

Figure 16: Schematic overview of the *hprt* gene in the Chinese hamster cell lines SP5 and SPD8

The *hprt* gene consists of 9 exons and covers a length of about 36 kb on the X-Chromosome in the Chinese hamster genome. The SP5 and SPD8 cell lines differ from their V79 wild type counterpart by duplicated regions, indicated here in red. Modified from (Helleday 1998b).

The characterization of the sequence alteration in the SP5 mutant reveals a 2.1 kb displaced duplication of exon 2 and flanking intron regions 3.7 kb downstream within intron1 (figure 17).

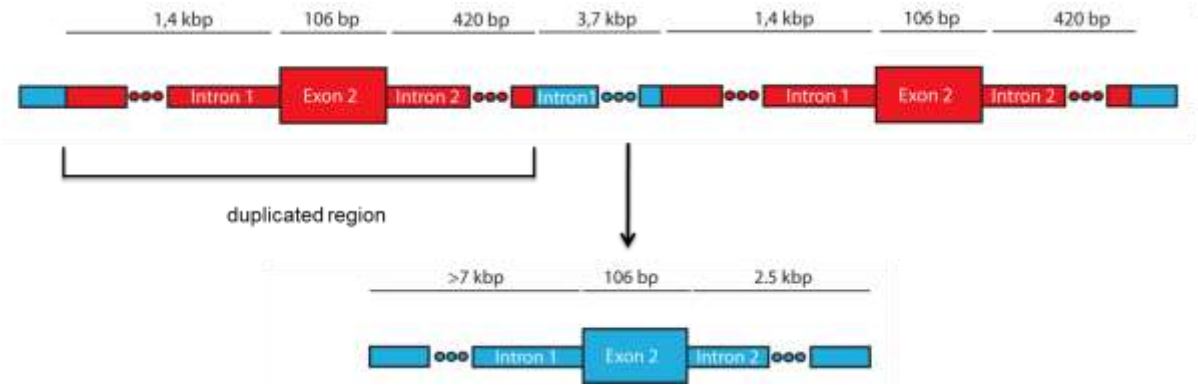

Figure 17: Schematic overview of the reversion event at the *hprt* gene in the SP5 mutant

The SP5 mutant precisely removes the duplicated region in a non-homologous recombination dependent manner. The starting and end point of this reversion event is known, but the mechanism is still under investigation.

The SPD8 mutant, on the other hand, displays duplications of intron 7, exon 7 and flanking regions of exon 6 that are arranged as tandem repeats (figure 18).

Sequence analysis of the SP5 mutant before and after reversion showed that the sequence between the duplicated regions was preserved. Therefore the SP5 cells were postulated to revert via a non-homologous recombination event (Zhang 1992a, Dare 1996, Helleday 1998b). The sequences before and after reversion are known, however the understanding of the exact mechanism as to how the SP5 reversion occurs remains unknown.

The SPD8 cell line is postulated to restore the wild type phenotype by a homologous recombination event. Different mechanisms for homologous recombination are possible. Intrachromatid exchange, single strand annealing, unequal sister chromatid exchange or sister chromatid conversion are in theory possible mechanisms (Arnaudeau 2001). The SPD8 mutant is used in many studies to examine different mechanisms for homologous recombination events (Arnaudeau 1999, Matsuoka 2004). The group of Helleday showed that homologous recombination events are enhanced after treatment with carcinogenic agents in a different manner in the SP5 and SPD8 mutants (Zhang 1994, Helleday 1998b). Furthermore, the same group showed that homologous recombination in the SPD8 mutant involves replication fork associated DSBs (Arnaudeau 2001). Based on these properties and findings, the SP5 and SPD8 mutants are used in this thesis to investigate the contribution of non-homologous and homologous recombination events in DSB repair.

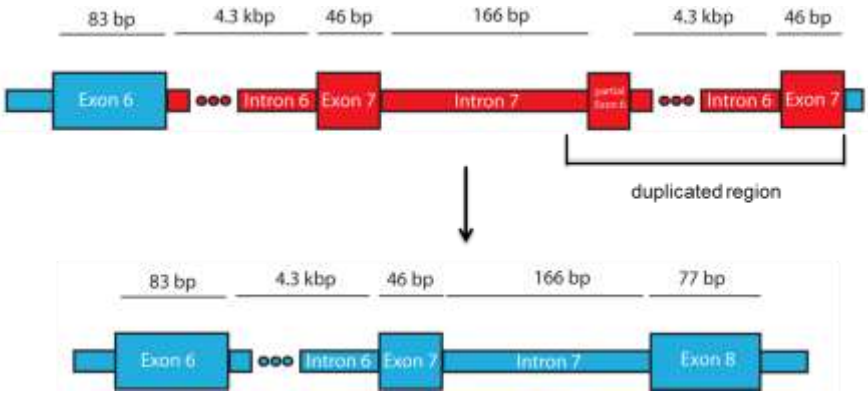

Figure 18: Schematic overview of the reversion event at the *hprt* gene in the SPD8 cells

The SPD8 mutant cell line restores the *hprt* gene by a homologous recombination event. The exact mechanism of the recombination is not known.

1.9 Aim of the project

The major aim of this study was to characterize the role of DSB repair pathways in the repair of lesions with increased complexity, as induced by different radiation modalities (low-, high-LET) and by RNA guided nucleases, in Chinese hamster cells.

To achieve this, we focused on the following specific aims:

1. Investigate how the generation of DSBs by different radiation modalities influences the reversion frequency at the *hprt* gene of male Chinese hamster mutants SPD8 and SP5.
2. Investigate the role of DSB repair pathways in the reversion of mutated *hprt* gene to functional HPRT protein.
3. Elucidate possible connections between reversion events at the *hprt* locus and DSB repair pathways.
4. Characterize the biological consequences of DSB formation and DSB clustering on reversion frequency.
5. Design guide RNAs (gRNA) recruiting Cas9 to specific sites in the *hprt* gene in order to characterize how DSBs with increased complexity (in terms of clustering) and location within the *hprt* gene influence the reversion frequency in the SPD8 and SP5 mutants.
6. Investigate the role of PI-3-kinase like family of protein kinases (PIKK) in *hprt* gene reversion by DSBs induced by Cas9 cleavage. Selective small molecule inhibitors will be used to determine the coordination of DNA repair pathways during reversion after induction of simple or complex DSBs (DSB clustering).
7. Investigate the contribution of DSB repair pathways to the increased mutation frequency in the V79 cell line after induction of DSBs with different levels of complexity (simple DSBs and DSB clusters).
8. Assess the role of error prone pathways like D-NHEJ or alt-EJ in the process of DSB related mutagenesis.

2 Materials and Methods

2.1 Materials

Laboratory apparatus	Model	Manufacturer
^{241}Am α radiation device	Am-241 Alpha Strahler	Amersham Buchler, Germany
Cell counter	Multisizer™ 3	Beckman Coulter, Germany
Cell counter	Z2 Coulter particle count and size analyzer	Beckmann Coulter, Germany
Cell culture dish scanner	GS-800 Calibrated Densitometer	Bio-Rad, Germany
Cell culture incubator	HERA cell 240	Heraeus, Germany
Centrifuge	Multifuge 3 S-R	Heraeus, Germany
Centrifuge	Rotanta 460 R	Hettich Zentrifugen
Dry block heater/cooler	HLC PROGR	HLC, Oehmen, Germany
Electroporation device	Amaxa Nucleofector®	Amaxa Biosystems, Germany
Eppendorf Shaker	Thermo Forma Orbital Shaker	Thermo scientific, Germany
Flow Cytometer	Gallios	Beckmann Coulter, Germany
Laminar Flow Hood	MSC-Advantage	Thermo Scientific, Germany
Laminar Flow Hood	Hera safe	Heraeus, Germany
Light microscope	Inverted phase contrast	Olympus, Germany
Pipet Aid	Falcon Express Pipet-Aid	BD Biosciences, Germany
Microtiter Pipettes	Pipet lite Rainin	Mettler Toledo, Germany
Mini centrifuge	Biofuge fresco	Heraeus, Germany
Photometer	Nano Drop 2000	Thermo Scientific, Germany
Refrigerator	gastro line	Liebherr, Germany
Thermo mixer	Thermo mixer comfort	Eppendorf, Germany
Vacuum pump	vacuum gas pump	VWR, Germany
Vortexer	Reax 2000	Heidolph, Germany
Weighing balance	572 DKD-Calibration	Kern, Germany
Weighing balance	VWR-124 Sartorius	VWR, Germany
Water bath		Memmert, Germany
X-ray tube	Seifert Isovolt 320HS	Seifert, GE Measurement & Control, USA

2.1.1 Chemicals

Chemical	Provider
6-Thioguanine	Sigma Aldrich, Germany
Agarose	Lonza VWR, Germany
Ampicillin	Roth, Germany
Crystal violet	Merck, Germany
Dimethyl sulfoxide (DMSO)	Sigma Aldrich, Germany
Ethanol (EtOH)	VWR, Germany
Ethylenediaminetetraacetic acid (EDTA)	Roth, Germany
Fetal calf serum FCS 14	Sigma, F7524, Charge 090M3397
Fetal calf serum FCS 17	Sigma, F0804, Charge 012M3398
Gibson Assembly® Master Mix	NEBiolabs, USA
HAT Supplement (50x) liquid	Life Technologies, Germany
Isoton II	Beckman Coulter, Germany
Kanamycin	Roth, Germany
KU55933	Merck Millipore, Germany
LB agar	USB Affymetrix, USA
LB medium	USB Affymetrix, USA
Minimum Essential Medium (MEM)	Gibco, Life technologies, Germany
NU7441	Tocris Bioscience, USA
PJ34	Calbiochem, Germany
Poly-L-lysine	Biochrom, Germany
Propidium Iodide (PI)	Sigma Aldrich, Germany
RBS	Roth, Germany
RNase A	Sigma Aldrich, Germany
Streptomycin	Calbiochem, Germany
Trypsin	Biochrom, Germany
VE821	Merck Millipore, Germany

2.1.2 Consumable materials

Consumable materials		Provider
Bacteria dishes	100 mm	Greiner, Germany
Beakers	250, 500 ml	Fisherbrand, VWR, Germany
Bottles	50, 100, 250, 500, 1000 ml	Schott Duran, VWR Borosulicate, Germany
Cell culture dishes	60, 100 mm	Cellstar, USA
Cell culture dishes	35 mm	Thermo scientific, Germany
Cell culture flasks	75 cm^2	Sarstedt, Germany
cell culture pipette	2, 5, 10, 25 ml	Cell Star, USA
Cover slips	30 mm	Neolab, Germany
Cuvettes		Ratiolab, Germany
Erlemeyer flasks	500 ml	Simax, USA
Erlemeyer flasks	1000 ml	Schott Duran, Germany
Graduated cylinders	100, 250, 500 ml	Schott Duran, Germany
Mini reaction cups	0.5, 1.5 und 2 ml	Greiner, Germany
Pipette tip	white, yellow, blue	TipOne Starlab, Germany
Plastic tubes	15 ml, 50 ml	Cell Star, USA
Sterile filter	0.22 µm Rotilabo	Roth, Germany

2.1.3 Buffer and solutions

The compositions of the buffers and solutions used follow. If not otherwise indicated, all buffers and solutions are prepared in double distilled water.

Notation	Composition	Preparation
PBS 10x	2 g/L KCl 2 g/L KH_2PO_4 80 g/L NaCl 21.6 g/L Na_2HPO_4 $7H_2O$ or 10.5 g/L Na_2HPO_4	bring up to a pH of 7.4
6TG supplement	5 - 10 mg/ml 6TG 0.1 N NaOH	5 - 10 mg/ml of 6TG powder (Sigma) in fresh 0.1N NaOH, then diluted up to final volume with sterile water. Filter sterilize through a 0.22 µm filter and aliquots were stored at -20°C
PLL		For the working solution the PLL was diluted in ddH_2O (5 ml lysine with 20 ml ddH_2O).
Crystall violett	Crystall violett, Ethanol	dissolve 1% crystal violet in 70% ethanol
HAT supplement (50x), liquid	5 mM Hypoxanthine, 20 µM Aminopterin, 0.8 mM Thymidine	liquid mixture was provided from ThermoFisher Scientific
LB-Medium	10 gm/L Casein Peptone 5 gm/L Yeast extract 10 gm/L Sodium chloride	Luria broth mixture was provided from USB products Affymetrix Used in fermentation at 25 gm/L
LB agar plates	10 gm/L Casein Peptone 5 gm/L Yeast extract 10 gm/L Sodium chloride 15 gm/L Agar	Luria Agar mixture was provided from USB Used at 40 gm/L

2.1.4 Chemical competent cells

Strain	Genotype
E.coli XL-1 Blue	supE44 hsdR17 recA1 endA1 gyrA46 thi relA1 lac F'[proAB^{+}, lacl^{q} lacZΔM15 Tn10 (tet^{r})]; Bullock et al., 1987, BioTechniques, 5, 376

2.1.5 Cell lines

The cell biological experiments in this thesis were performed with the following cell lines:

Cell line name	Species type	Cell type
V79	Chinese hamster	lung fibroblast
SP5	Chinese hamster	HPRT deficient lung fibroblast, duplication mutation in exon 2
SPD8	Chinese hamster	HPRT deficient lung fibroblast, duplication mutation in exon 7

2.1.6 Cell culture medium

To grow Chinese hamster cells the following cell culture medium was used. All growth and selection media contained 10% of fetal bovine serum (lots 14 or 17).

Medium	
500 ml MEM medium	In addition to MEM media from Sigma the following components were added: 10% FBS (14 or 17) 100 µg/ml Penicilin G 100 µg/ml Streptomycin
6TG-supplemented	5 µg/ml 6TG was added into the MEM media
HAT-supplemented	HAT 50x stock solution was diluted to 1x in MEM media (working solution)

2.1.7 gRNA sequences

The following sequences were used.

No.	Sequenze 5‘-3‘
#2	TATTCCTAATCACTATGTCG AGG
#8	GACTGTAAGTAGATGCCCTT TGG
#9	ACTTGTGACCTGAAGGAAG AGG
#11	TCTCCATTTGTCTTCCTAT GGG
#12	CGTCATTTGACCAGACTGA TGG
#13	CTCTCGAAGTGTTGGATAT AGG

2.1.8 Plasmids

The following table lists all plasmids used in this thesis. Vector maps are provided as an Appendix.

No.	Name	Description
eGFP	GFP	GFP transfection control vector
Cas9WT	hCas9	human codon-optimized Cas9 expressing vector
#2	gRNA-E2-cgHPRT-1	gRNA2 expressing vector, recognizing exon 2 in the *hprt* gene
#8	gRNA-E7-cgHPRT-1	gRNA8 expressing vector, recognizing exon 7/intron 7 junction in the *hprt* gene
#9	gRNA-F5E2-cgHPRT-1	gRNA9 expressing vector, recognizing intron 1 in the *hprt* gene
#11	gRNA-F5E7-cgHPRT-1	gRNA11 expressing vector, recognizing intron 6 in the *hprt* gene
#12	gRNA-F3E7-cgHPRT-1	gRNA12 expressing vector, recognizing intron 8 in the *hprt* gene
#13	gRNA-E7-cgHPRT-1	gRNA13 expressing vector, recognizing exon 7 in the *hprt* gene

2.1.9 Software

Software	**Provider**	**Use**
CellCounter Version 0.2.1	Nghia Ho	Colony analysis
ChemSketch C10E41	ACD/Labs	Graphic presentation of chemical reactions
SigmaPlot® 11.0	Systat Software, USA	Graphic presentation
Microsoft Excel 2010®	Microsoft Corp., USA	Data analysis and calculations
Kaluza 1.2	Beckman Coulter Inc., USA	Flow Cytometry analysis (Gallios)
Adobe Creative Suite® 5.5	Adobe Systems Inc., USA	Illustrations, presentation, cropping
UGENE 1.13.3	Unipro	*hprt* locus sequence analysis
EndNote X4	Thomson Reuters	Literature Bibliography

2.2 Methods

2.2.1 Cell culture and growth conditions

To establish and cultivate the Chinese hamster cell lines, frozen vials were taken and prewarmed shortly in a water bath at 37°C. Cells were then directly transferred into 60 mm or 100 mm dishes with MEM media containing 10% of FBS serum and placed in an incubator at 37°C with 5% CO_2. The Chinese hamster cells are adherent cells. Therefore, a prolonged incubation time leads to a confluent culture and cells enter a plateau phase; prolonged incubation leads to cell death. To maintain cells in a proliferating stage cells were passaged regularly.

For passaging, the medium was aspirated and cells were washed with 1 x PBS. In the next step cells were incubated with 0.5 ml trypsin (0.05% in EDTA) for 3 minutes at 37°C. Trypsin is an alkali pancreatic protease that cleaves the cell-junctions. This detaches cells from the substrate. To prevent irreversible injury of the cells by trypsin, cells were monitored on the light microscope and the reaction was stopped immediately after cells detached by administration of growth media supplemented with fetal bovine serum.

The cell number in the resulting cell suspension was measured using a Cell Counter from Beckman Coulter Counter and was used to seed a defined number of cells in petri dishes for experiments. For cell number determination, 500 µl of the cell suspension was transferred into a counting vessel and filled up with 9.5 ml of isoton II solution. The so diluted cell suspension was measured and cell concentration, as well as mean and median cell size in the cell population was determined. To obtain the total number of cells available, the concentration per ml was multiplied by the total volume of the cell suspension. An appropriate number of cells was then plated into 60 mm or 100 mm petri dishes for further cultivation.

In this thesis exponentially growing cells were used throughout. They were prepared at 0.1 million cells were plated into 60 mm dishes and incubated at 37°C with 5% CO_2. After each day of growth, one dish was used for cell concentration determination and for flow cytometer analysis in order to monitor the cell cycle distribution.

In general cells were subcultured every 48 hours and plated into a 100 mm dish at a concentration of 0.3 million cells. This allowed the cells to continuously proliferate exponentially. All experiments were performed under sterile conditions and only cells with a passage number of ≤ 50 were used.

2.2.2 Cell cycle analysis by flow cytometry

In a flow cytometer, single cell suspensions are driven through a laser path. Detectors measure the scattering and fluorescence emission of each cell and quantify cell parameters like the size, shape and fluorescence. The fluorescence activated cell sorting (FACS) is a flow cytometry method that in addition to these properties can also sort cells according to the size of a particular signal.

To analyze cell cycle distribution, cells were harvested and cell concentration determined as described in 2.2.1 Cell culture and growth conditions. 0.8 million cells were centrifuged at 1300 rpm at 4°C for 5 minutes and supernatant was removed. After a washing and centrifugation step with 1 x PBS, cells were fixed in 1 ml 4°C cold 70% ethanol. The ethanol solution was removed by centrifugation and the cell pellet in the next step resuspended in 0.4 ml 1 x PBS containing 40 µg propidium iodide and 62 µg/ml RNase A. Cells were subsequently incubated for 30 minutes at 37°C in a water bath to allow incorporation of the propidium iodide into DNA. Propidium iodide binds to the DNA proportionally to its mass and therefore the signal generated represents the amount of DNA in each cell.

To estimate transfection efficiency, cells were transfected with a plasmid that encodes for GFP. 24 h post transfection the cells were harvested and measured directly in a flow cytometer without ethanol fixation.

For all flow cytometry analysis experiments, up to 20,000 cells were counted from each sample. The generated data were analyzed with the Kaluza software.

2.2.3 Nucleofection

To generate a CRISPR/Cas9 mediated DSB at a specific genomic location and to investigate DSB related effects on mutation events at the *hprt* gene, plasmids that encode for Cas9 and gRNAs were transfected in Chinese hamster cells.

For nucleofection exponentially growing cells were harvested and the cell concentration was determined (2.2.1 Cell culture and growth conditions). For each sample 3 million cells were transferred into 15 ml tubes and centrifuged at 1200 rpm for 5 minutes. The supernatant was aspirated, cell pellet suspended in 100 µl nucleofection buffer, mixed with plasmid DNA and transferred into the electroporation cuvette. The cuvette was placed into the Amaxa Nucleofector® and a pulse was administrated using program X-01. During the nucleofection step an electric field is formed that opens transiently the cell membrane and facilitates thus the entry of plasmid DNA into the cell. The transfected cells were then transferred into a 30 ml flask with 37°C prewarmed media and seeded into 2 x 100 mm dishes. After an incubation time of 48 hours for SP5/SPD8 cells and 84 hours for V79 cells, cells were plated for selection or survival (2.2.10 Forward mutation assay; 2.2.11 Reverse mutation assay). For all transfection experiments 1 µg plasmid DNA was used per million cells. The transfection efficiency was 57±13, 60±16 and 53±14 percent for SP5, SPD8 and V79 cell lines respectively.

2.2.4 Inhibitor treatment

The inhibitors that were used in this thesis were dissolved in dimethyl sulfoxide (DMSO) and administrated 1 h before IR into the growth media, and in case of transfection experiments immediately into the growth media post transfection after the cells had been seeded into dishes. The concentration and the target of the inhibitors used are shown in table 1. The inhibitor treated cells were plated after IR or transfection to allow for colony formation.

Inhibitor	Target	conc. for IR exp.	conc. for transf. exp.
NU7441	DNA PKcs	5 µM	2.5 µM
KU55933	ATM	10 µM	5 µM
VE821	ATR	5 µM	2.5 µM
PJ34	PARP	10 µM	5 µM

Table 1: Overview about the used DSB repair pathway inhibitors

2.2.5 Irradiation with X-rays

Exponentially growing cells were irradiated with an X-ray device that operates at 320 kV and 10 mA with a 1.65 mm aluminum filter. The mean LET of this type of X-rays is approximately 2 keV/µm. Photon of these X-rays interact mainly by the Compton effect and partly by the photoelectric effect. At these photon energies over 50% of the energy remains in the scattered photons, while the generated secondary electrons (δ-rays) carry out further ionization events in the biological material. Cells in 60 mm dishes were irradiated at a distance of 500 mm, cells in 100 mm dishes at a distance of 750 mm. The radiation table was rotated during irradiation to ensure homogenous distribution of the radiation dose. The dose rate for 500 mm was ~2.7 Gy/minute, for 750 mm ~1.3 Gy/minute. The radiation dose was confirmed regularly using a chemical dosimeter. The irradiated cells were either collected directly after exposure to X-rays or after an incubation of 6 h at 37°C with 5% CO_2.

2.2.6 Irradiation with ^{241}Am α particles

Exponentially growing cells were irradiated with α particles (4.9 MeV) generated by americium (^{241}Am) decay; the corresponding LET is approximately 88±6 keV/µm. In the irradiation chamber americium is present in the form of americium oxid (Am_2O_3) plated on a silver foil and covered with a gold layer. This material was covered with an aluminum ring with an inner ring diameter of 50 mm. The cell irradiation chamber was connected via its 50 mm window to another chamber that was used to place the cells. Both chambers were separated with a 1.5 µm thick hostaphan foil that is thin enough to allow α particles to pass through. The radiation chamber was flushed with He gas to prevent excessive energy loss of the α particles, while the other chamber contained normal air. Before use, the irradiation chamber was flushed with He gas at a flow velocity of 16 liter/hour for 1 h, while 8 liter/h were used during irradiation. The radioactive source was rotated to ensure homogenous and uniform dose rates. The dose rate was ~1.3 Gy/minute.

For irradiation, 50 mm dishes were prepared with a hostaphan foil of 1.5 µm thickness as bottom. A ring was placed inside the 50 mm dish to prevent the growth

of cells outside the irradiation field. 0.5 million cells were plated into the 50 mm dishes on the hostaphan foil 24 h before irradiation. Cells were also plated on poly-L-lysine coated cover slips (2.2.7 Coating of cover slips) that were placed for irradiation on the hostaphan foil inside the 50 mm dish.

2.2.7 Coating of cover slips

Coating enables enhanced cell adhesion on the surface of the cover slips and leads to a more equal distribution of cells on the cover slip. To coat a cover slip 500 µl of a 1/100 in 1 x PBS diluted poly-L-lysine (PLL) solution was added and after an incubation of 5 - 15 minutes at 37°C the solution was transferred back into the tube. After a washing step with 1 x PBS, the cover slips were placed in 35 mm dishes and seeded with cells. 12 hours post seeding the cover slips were transferred to the alpha irradiation dishes with cells facing the hostaphan foil and irradiated.

2.2.8 Irradiation with ^{56}Fe particles

Exponentially growing cells were irradiated with ^{56}Fe ions at the irradiation facility of the Helmholtz Center for Heavy Ion Research (GSI) in Darmstadt, Germany. In the heavy ion synchrotron facility (SIS) of the GSI ^{56}Fe ions were generated and accelerated to an energy of 1 GeV and an LET of ~144-151 keV/µm. Cells were seeded in 75 cm^2 tissue culture flasks 24 h before irradiation. After an incubation of >12 h at 37°C, cells were plated for survival and revertant frequency determinations (2.2.9 Clonogenic survival assay; 2.2.11 Reverse mutation assay).

2.2.9 Clonogenic survival assay

The clonogenic survival assay was used to determine the radiosensitivity of cells after exposure to IR. Exponentially growing cells were exposed to radiation doses up to 10 Gy depending on radiation modality (table 2). Immediately after irradiation, cells were collected and plated at low cell densities to allow colony formation. An increase in the administrated dose leads to enhanced reduction of reproductive

integrity and therefore higher numbers of cells were plated with increasing the dose. The numbers of seeded cells in these experiments are shown in table 2. Post IR, cells were incubated for 7 days at 37°C and 5% CO_2. Cells were stained with crystal violet solution, dried and scanned. Cells that have formed a colony (≥50 cells) from a single precursor cell were counted. The scanned images were analyzed using the CellCounter Software Version 0.2.1 from Nghia Ho. The plating efficiency (PE) was calculated by the percentage of the seeded cells that have grown into colonies:

$$PE = \frac{\text{Number of colonies counted}}{\text{Number of cells seeded}} \text{ x } 100$$

The fraction that survived radiation at each dose (SF) was determined as follows:

$$\text{SF} = \frac{\text{Colonies counted}}{\text{Cells seeded x (PE/100)}}$$

In the figures of this thesis the survival fraction was plotted on a logarithmic scale as a function of radiation dose plotted on a linear scale.

X-rays

Dose administrated (Gy)	Number of cells seeded
0 – 3	200
5	800
6 – 8	5,000
10	10,000

^{241}Am α particles

Dose administrated (Gy)	Number of cells seeded
0	100
0.5	150
1	300
2	1,000
3	2,000

^{56}Fe ions

Dose administrated (Gy)	Number of cells seeded
0	200
0.5	800
1	1,500
2	10,000

Table 2: Overview of the number of cells seeded for clonogenic survival

2.2.10 Forward mutation assay

Forward mutation experiments were performed to investigate the mutation frequency of V79 cells after induction of DSBs with different level of complexities. To obtain *hprt* mutants, cells were transfected with Cas9 and gRNA plasmids (see 2.2.3 Nucleofection) and plated into dishes in media with and without 6TG supplement. As transfection control, cells were transfected with a plasmid that encodes for GFP. 7 days and 10 days post transfection cells were stained with crystal violet and colonies were counted for PE and $6TG^{Res}$ mutants respectively (according to 2.2.9 Clonogenic survival assay), while the GFP transfection efficiency was determined after 24 h by flow cytometry (2.2.2 Cell cycle analysis by flow cytometry). The mutation frequency was then calculated by considering the number of colonies forming in 6TG selective media, the transfection efficiency measured by GFP and the plating efficiency:

$$6TG^{Res}\ \text{freq.} = \frac{\text{Number of } 6TG^{Res} \text{colonies counted}}{\text{Number of cells seeded in 6TG media}}\ \text{x PE x}\ \frac{\text{GFP positive cells}}{\text{Number of cells}}$$

For PE determinations, 100 cells were seeded, while for the determination of $6TG^{Res}$ mutants a higher number of cells was plated (table 3).

V79 cell line							
Mock	#2	#8	#9	#9+2	#11	#12	#11+8
1 M	0.2 M	0.5 M	0.5 M	0.5 M	0.5 M	0.5 M	0.2 M

#12+8	#11+12	#11+12 +8	#13	#11+13	#12+13	#11+12 +13	#11+12 +13+8
0.2 M	0.1 M	0.1 M	0.2 M	0.1 M	0.2 M	0.2 M	0.2 M

Table 3: Overview of the number of cells seeded (in millions) for $6TG^{Res}$ mutants after transfection

2.2.11 Reverse mutation assay

Reverse mutation experiments using the SPD8 and SP5 mutants were carried out to determine how DNA repair pathways contribute to the repair of DSBs of increased complexity. The SPD8 mutant reverts by homologous recombination events and the SP5 mutant via non-homologous recombination events. Both cell lines show high spontaneous reversion frequencies (about 10^{-5}). To reduce spontaneous reversion, these mutants were cultivated in growth media supplemented with 6TG. 6TG mimics the guanine purine substrate for HPRT and becomes incorporated into the DNA of HPRT proficient cells. This leads to cell death, while cells deficient in HPRT survive this treatment.

To obtain revertants, SPD8 and SP5 cells were plated in growth media supplemented with HAT (Hypoxanthine Aminopterine Thymidine). The presence of aminopterin inhibits the *de novo* pathway of purine nucleotide synthesis and causes death in *hprt* mutants, but not in cells that have restored their *hprt* gene and express therefore a functional HPRT protein. In addition, cells were seeded in normal growth media for PE determinations.

The colonies that have grown in the presence of HAT were scored as revertants. The revertants in the inhibitor and irradiation experiments were determined in the same way. The reversion frequency was calculated by the number of colonies forming in HAT selective media, the cell survival at that radiation dose and the plating efficiency.

$$\text{Rev frequency} = \frac{\text{Number of rev. colonies counted}}{\text{Number of cells seeded in HAT media}} \text{ x PE x SF}$$

The number of cells that were seeded for PE in the inhibitor and irradiation experiments was similar to that shown in table 2. To obtain SPD8 and SP5 revertants, cells were plated at a higher cell density of 0.7 million in HAT selection media.

The reversion frequency of the SPD8 and SP5 cells after inhibitor and transfection experiments was determined as follows:

$$\text{Rev. frequency} = \frac{\text{Number of rev. colonies counted}}{\text{Number of cells seeded in HAT media}} \text{ x PE x } \frac{\text{GFP positive cells}}{\text{Number of cells}}$$

About 100 cells were plated for PE in the inhibitor and transfection experiments. To obtain revertants the following number of cells were plated (table 4) aiming at approximately 30-150 isolated colonies per dish.

SPD8 cell line

Mock	#2	#8	#11	#12	#13	#8+13	#11+8
1 M	1 M	0.02 M	0.02 M	0.05 M	0.02 M	0.02 M	0.02 M

#12+8	#11+12	#11+12+8	#11+13	#12+13	#11+12+13	#11+12+13+8
0.02 M	0.02 M	0.02 M	0.02 M	0.02 M	0.02 M	0.02 M

SP5 cell line

Mock	#2	#8	#9	#13	#9+12
1 M	0.025 M	0.5 - 1 M	0.007 M	1 M	0.15 M

Table 4: Overview of the number of cells seeded (in millions) for revertant determination after transfection

2.2.12 The CRISPR/Cas9 system

In the CRISPR/Cas9 technique plasmids that encode for Cas9 and gRNAs were used to induce DSBs of different complexities at specific locations within the *hprt* gene. For this approach Church's gRNA cloning protocol was used.

In the first step sequences of about 20 nucleotides in length were chosen in the *hprt* gene of the Chinese hamster genome *Cricetulus griseus*. For all sequences it was considered that the target DNA in the genome was followed or preceded by a protospacer adjacent motif (PAM) sequence. The sequence was submitted to a company, which synthesized the gRNA oligos. These oligonucleotides were

incorporated into two 60mer oligonucleotides. These oligonucleotides were annealed and extended to produce a 100 bp double stranded DNA fragment. For this approach the phusion polymerase was used. The DNA insert was then amplified with overlapping ends of 15 – 20 bp by a polymerase chain reaction (PCR). In the next step the 100 bp fragment was incorporated into an AfIII linearized target vector. For this cloning step the Gibson assembly® was used.

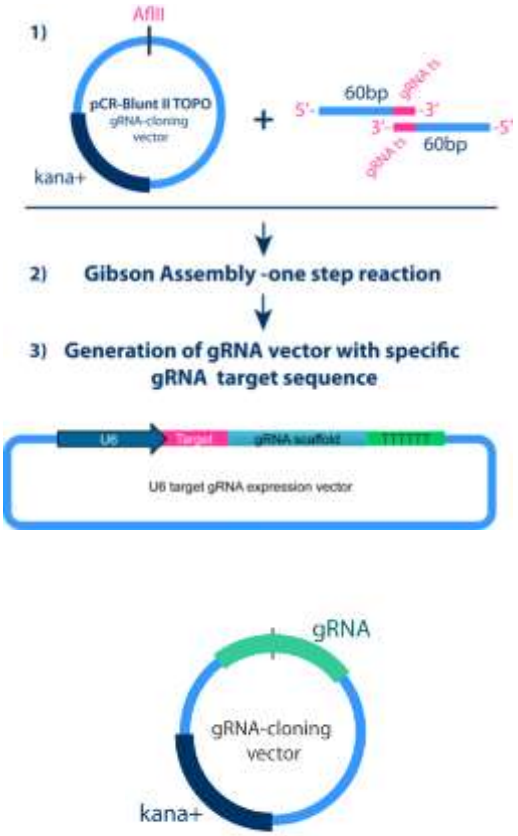

Figure 19: The gRNAs were cloned into a cloning vector via the Gibson Assembly

For cloning the DNA insert into the linearized vector, an exonuclease, DNA polymerase and DNA ligase were mixed together and incubated at 50°C for 15 minutes. The exonuclease generates single stranded 3' overhangs that facilitate the annealing of the DNA fragments. The DNA polymerase then fills the gap between insert and vector and the assembly is completed by DNA ligase that seals the nicks. Figure 19 illustrates the cloning procedure. The so generated gRNA plasmid contains all components for gRNA expression (U6 promoter, target

sequence, guide RNA scaffold and termination signal). In the CRISP/Cas9 system the gRNA directs the exonuclease Cas9 to the target DNA sequence. Therefore no modification was required and Cas9 was purchased directly as a vector. The Cas9 and generated gRNA plamids were next amplified (2.2.13 Transformation and amplification of plasmid DNA in *E.coli*).

2.2.13 Transformation and amplification of plasmid DNA in *E.coli*

To obtain a sufficient amount of the gRNA and Cas9 plasmids for transfection experiments, plasmids were transformed into the *E.coli* XL-1 strain by heat shock. For the transformation 50 µl competent XL-1 blue bacteria were mixed together with about 10 - 15 ng of the vector material and incubated for 10 minutes on ice. After a heat shock of 42°C for 30 seconds in the Eppendorf thermo-mixer, the sample was cooled for 10 minutes on ice again. Then 950 µl LB-Medium was added and incubated on a shaker for one hour at 37°C.

25 and 50 µl of the bacteria suspension was taken and plated on a LB-agar dish with ampicillin resistance for Cas9 plasmids or kanamycin resistance for gRNA plasmids and incubated overnight at 37°C. Single colonies were transferred in a 2 - 5 ml LB medium and incubated for 12 hours on the shaker at 37°C. The bacteria culture was then used to inoculate 200 ml of LB medium. The 200 ml bacteria suspension was grown overnight at 37°C. Agar dishes and LB medium were always supplemented with antibiotics according to the resistance of the plasmids (50 ng/ml for Cas9 plasmids, 100 ng/ml for gRNA plasmids). The maps of the plasmids employed in the present work are shown in the appendix.

2.2.14 Isolation and purification of plasmid DNA from *E.coli*

To isolate larger amounts of plasmid DNA, the NucleoBond® Xtra Midi EF endotoxin-free plasmid DNA purification kit from Machery-Nagel (Düren, Germany) was used. In this kit the plasmid is purified by a modified alkaline lysis.

The overnight bacteria suspension was transferred into 50 ml falcon tubes and centrifuged at 4,000 x g for 30 minutes at 4°C. The bacteria pellet was treated in

the next steps according to the manufactures protocol with the following differences: At step 14 the centrifugation was performed at 4,000 x g for 1 h at 4°C and at step 15 for 30 minutes.

2.2.15 Determination of the nucleic acid concentration by NanoDrop

The NanoDrop was used to monitor the purity of the isolated plasmid DNA and to determine the concentration of the DNA. Before the DNA concentration was determined, 1 µl TE-EF was pipetted onto the Nano-drop detector and defined as blank. In the next step 1 µl of the plasmid DNA that was dissolved in TE-EF during the DNA purification step (2.2.14 Isolation and purification of plasmid DNA from *E.coli*) was transferred on the NanoDrop and the optical density of 260 and 280 nm was measured. The bases of the nucleic acids absorb, based on their ring structure and double bonds, in the UV-range of 260 nm, while amino acids like tryptophan and phenylalanine show their maximum at 280 nm. The sample was classified as sufficiently pure when the measured ratio was in the range of 1.7 – 2.0. The concentration of the DNA was measured by the absorption at 260 nm and determined by the Beer-Lambert equation:

$$c = \frac{(A \cdot e)}{b}$$

With c = nucleid acid concentration in ng/µl; A=absorption, in absorption units; AU, e = wave length dependent extinction coefficient in ng-cm/µl; and b = the path length in cm.

The so purified gRNA and Cas9 plasmids were used for transfection experiments (2.2.3 Nucleofection).

3 Results

3.1 The SP5 and SPD8 mutants as a model system to investigate repair pathway choice in the presence of increased DSBs complexity

The aim of this thesis is, to investigate how increasing DSB complexity induced by IR and the RNA guided nucleases affect DSB repair pathway choice. For this purpose the Chinese hamster mutant cell lines SPD8 and SP5 are used. These cell lines are able to correct their *hprt* mutation via a homologous and non-homologous recombination event, respectively. To examine repair pathway choice with increasing DSB complexity, the frequency of correction events, termed reversion frequency, is scored.

3.1.1 Comparison of SPD8 and SP5 mutants to their wild type counterpart

In the first part of our investigations, the SPD8 and SP5 mutants are examined for their proliferation rate and cell cycle distribution and compared to their V79 wild-type counterpart. To measure proliferation rate, cells were seeded at a concentration of 0.1 million and proliferation was followed daily, as well as cell cycle distribution by PI staining and flow cytometry (figure 20). Figure 20 shows that there is no difference in proliferation between the V79, SPD8 and SP5 cells. The cell cycle analysis further reveals that all cell lines are in the exponential phase of growth for the first three days before entering a plateau phase. The doubling time of all cells is similar and only the SPD8 cell line seems to grow slightly slower.

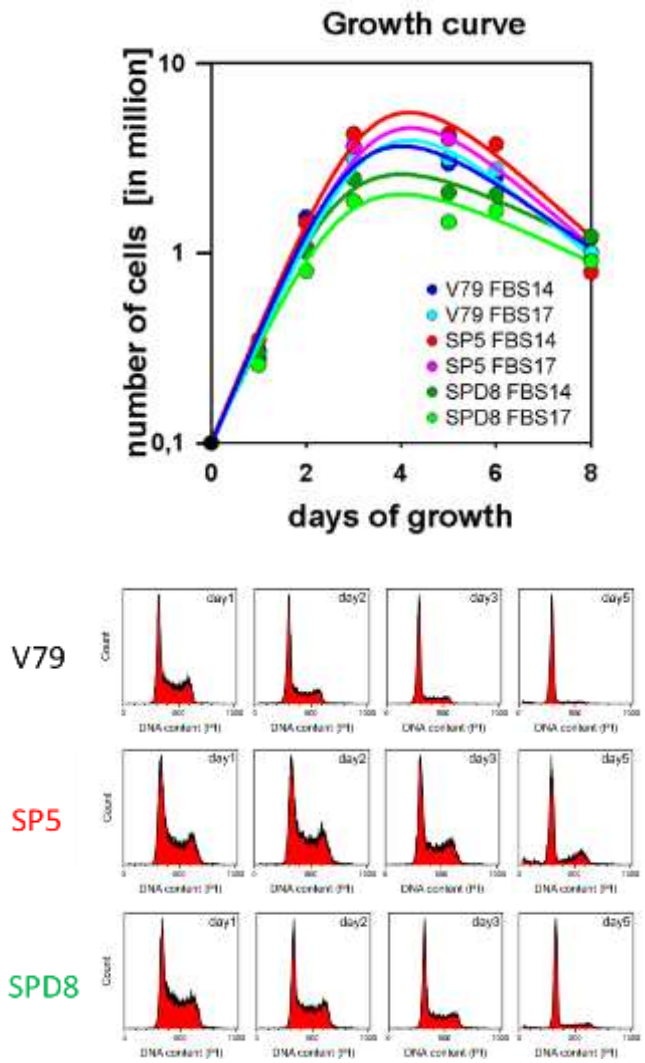

Figure 20: Growth curves of Chinese hamster cells in two different sera

0.1 million Chinese hamster cells V79, SP5 and SPD8 were seeded in 60 mm dishes. For each cell line growth media were supplemented with either 10% serum FBS14 or FBS17 (reflect different lots available in the Institute). The cell concentration was determined every day post seeding by harvesting the cells and measuring their numbers and volume using a Cell Counter. In addition, cells were fixed with 70% ethanol and stained with PI to determine their distribution through the cell cycle. In the first three days post seeding, V79, SP5 and SPD8 cells grow exponentially, reaching a plateau on day four to six; then cell number decreases because cells begin to die. There is no difference in growth for all cell lines between FBS14 and FBS17. The growth and cell cycle distribution of SP5 and SPD8 mutants are similar to V79.

To examine the radio sensitivity of the SPD8 and SP5 mutants, cells were exposed to IR and seeded for colony formation. The cells were exposed either to sparsely ionizing low-LET (250 keV X-rays, 2 keV/µm) radiation, or to densely ionizing high-LET (4.9 MeV ^{241}Am α rays, 88±6 keV/µm and 1 GeV ^{56}Fe ions, 144-151 keV/µm) radiation. In contrast to low-LET, high-LET radiation generates with higher probability ionization clusters and thus more complex DSBs. Figure 21 shows similar radiosensitivity for V79 and the SPD8 and SP5 mutants after exposure to X-rays, ^{241}Am α particles and ^{56}Fe ions. However, the shape of the survival curve depends on the radiation modality used. Sparsely ionizing X-rays results in a

survival curve with a shoulder region followed by an exponential component. A shoulder region is absent after exposure to ^{241}Am α particles and ^{56}Fe ions. The results indicate a relative biological effectiveness (RBE) of about 3 times based on slope increase (RBE for 10% survival is 2.72 for ^{241}Am α and 3 for ^{56}Fe ions).

The survival experiments reveal that the SPD8 and SP5 mutants and V79 cells repair DNA damages with similar efficiency. Before the role of DNA repair pathways can be examined in SPD8 and SP5 cells, the reversion analysis assay has to be established and validated.

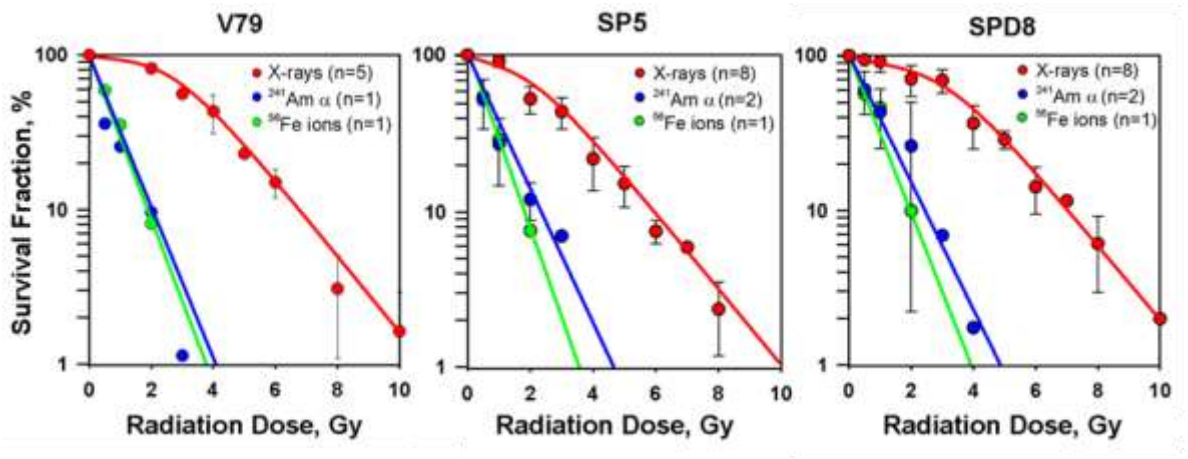

Figure 21: Survival curves of V79, SP5 and SPD8 cells after exposure to X-rays, ^{241}Am α and ^{56}Fe ions

Exponentially growing V79, SP5 and SPD8 cells were irradiated with X-rays, ^{241}Am α particles and ^{56}Fe ions and seeded for colony formation. Seven days post IR cells were stained with crystal violet and colonies counted. Unlike X-rays, exposure to ^{241}Am α particles and ^{56}Fe ion results in a steep exponential decrease in cell survival. Survival curves of SPD8 and SP5 mutants are similar to their wild-type counterpart, V79, both after exposure to low and high-LET radiation.

3.1.2 Validation of the reversion assay in the SPD8 and SP5 mutants

The SPD8 and SP5 mutants differ in the type of *hprt* mutation, its location in the gene and the mechanism required for reversion.

The SPD8 mutant is characterized by a 5 kb duplication, which includes exon 7, intron 6 and the 3' portion of exon 6. This mutation appears in tandem and is located downstream of intron 7 within the *hprt* gene (Dare 1996). The SPD8 mutant restores the function of the *hprt* gene spontaneously via a homologous recombination event. The SP5 mutant on the other hand is characterized by a displaced duplication of exon 2 that is located 3.7 kb upstream of exon 2 within intron 1 in the *hprt* gene (Dare 1996). This cell line reverts the mutation spontaneously via a non-homologous recombination event.

To prevent the generation of HPRT proficient subpopulations from spontaneous reversion events, both mutants were grown in the presence of 6TG. To determine the spontaneous reversion frequency, cells were plated in growth media supplemented with HAT and for plating efficiency in growth media with and without 6TG. Here plating efficiency results of experiments carried out in the presence of 6TG are only shown, as they are similar to those obtained in the absence of 6TG.

The spontaneous reversion frequency in the SPD8 mutant was 0.93±0.13 rev /10^5 cells (n=4). This is close to the reversion frequency described in the literature that ranges from 1.5 - 2.7 rev /10^5 cells (Dare 1996, Helleday 1998b).

The SP5 mutant showed a spontaneous reversion frequency of 2.99±0.55 rev/10^5 cells (n=4) that was within the expected range of 3.7±0.9 rev/10^5 cells found in the literature (Dare 1996).

3.1.2.1 Mitomycin C enhances the reversion frequency in the SPD8 and SP5 mutants

We validated the reversion assay described above in the SPD8 and SP5 mutants using the crosslinking agent Mitomycin C (MMC). This agent has been shown to enhance the reversion frequency in the SPD8 (Matsuoka 2004) and the SP5 mutants (Zhang 1992a, Zhang 1994). MMC reacts through the minor groove of the DNA and alkylates guanines on opposite strands to form an interstrand crosslinks (Noll 2006). This prevents the separation of DNA strands and blocks thus DNA replication and transcription processes, without generating marked structural distortions in the DNA. The blocked replication fork eventually collapses causing the formation of DSBs during repair (Al-Minawi 2009). We assume that these effects lead to the recruitment and activation of repair factors that facilitate the recombination processes causing the reversion events in the SPD8 and SP5 mutants. However, the mechanisms of MMC generated recombination are not understood and are not further discussed here.

To examine whether MMC increases the reversion frequency in the SPD8 and SP5 mutants, MMC was administrated at different concentrations. Figure 22 shows that MMC enhances the reversion frequency up to a factor of 2.87 at 100 nM (2.67 rev/10^5 cells) in SPD8 cells. For SP5 cells this effect is even more pronounced and increases the reversion frequency up to 4.2 times or 12.56 rev/10^5 cells are observed at 250 nM (figure 22). This is in agreement with results in the literature, where an increase in the reversion frequency to 12.1 - 13.6 rev/10^5 cells (Zhang 1992a, Zhang 1994) has been reported for SP5 cells. These results demonstrate that the adopted reversion system works well. Furthermore, we observed that the spontaneous reversion frequency fluctuated slightly between experiments. This was also found by Zhang and Jenssen (Zhang 1992a). Therefore, to compare reversion events measured in different experiments, reversion frequencies in this thesis were normalized to that measured in the untreated control. Both, the calculated reversion frequency (reversion events/10^5cells) and the normalized values are shown in the figures.

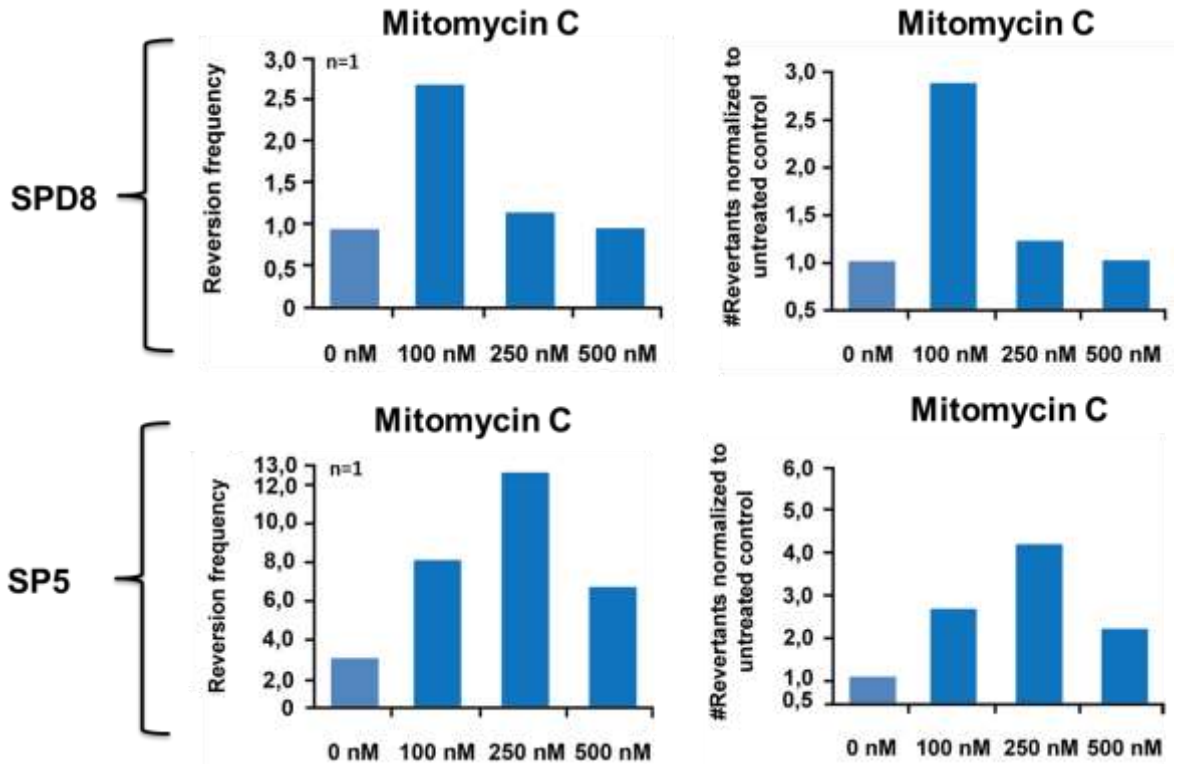

Figure 22: MMC treatment increases the reversion frequency in the SPD8 and SP5 mutants

The standard growth media of exponential growing SPD8 and SP5 cells was replaced by HAT media with different amount of the cytotoxic agent Mitomycin C and plated for survival. The measured reversion frequency is always per 10^5 cells. The measured reversion events were normalized to the untreated control. For SPD8 cells the highest reversion frequency is obtained at a concentration of 100 nM MMC with an increase by a factor of 2.87. For SP5 cells the reversion frequency increases more pronouncedly by a factor of 2.69, 4.2 and 2.22 at concentrations of 100, 250 and 500 nM MMC, respectively. Thus MMC treatment enhances reversion in the SPD8 and SP5 mutants well above their spontaneous reversion frequency.

3.1.2.2 DSBs of increased complexity enhance reversion frequency in the SPD8 and SP5 mutants

DSBs are considered the initial step in the recombination events required for reversion in the SPD8 and SP5 mutants. Therefore, we examined whether an increase in DSB complexity enhances reversion in the *hprt* gene. Cells were exposed to different radiation modalities. IR is known to generate diverse modifications in the DNA and to produce SSBs, which when in close proximity in

opposite strands generate DSBs. The number of IR related DSBs depends on the cell cycle phase. Cells that are at the end of S phase and in G_2 phase have a higher DNA content and thus a larger target for IR. This increases the number of DSBs and other lesions induced in a cell. Low-LET radiations like X-rays, are estimated to generate roughly 20 DSBs per Gray (Gy) in G_1 phase, 20 - 40 DSBs in S phase and 40 DSBs in G_2 phase of the cell cycle. High-LET radiation like ^{241}Am α and ^{56}Fe ions, on the other hand, generates more DNA damage clusters and thus also more complex DSBs. The complexity of DNA damage in general is thought to also increase with increasing radiation dose.

To examine whether increasing DSB complexity increases the reversion frequency in the SPD8 and SP5 mutants, we exposed them to X-rays, ^{241}Am α and ^{56}Fe ions and plated immediately, except for ^{56}Fe ions irradiated cells that were plated >12 h later, for determine the frequency of revertants and radiation cell survival. For all experiments cells were maintained in the exponential phase of growth. Plateau-phase cells differ in their radiosensitivity from exponentially growing cells, which may affect the outcome. To ensure that exponentially growing cells were tested in our experiments, the cell cycle distribution was recorded in all experiments by flow cytometry (figure 23, 24). For this purpose cells were collected and fixed in ethanol immediately after exposure to X-rays, ^{241}Am α particles and >12 h after ^{56}Fe ion treatment. Figures 23 and 24 show that SPD8 and SP5 cells were in the exponential growth phase during their exposure to X-rays, ^{241}Am α and ^{56}Fe ions. Changes in the cell cycle of the ^{56}Fe ions irradiated samples are due to later collection time. IR induced redistribution of cells through the cell cycle is the focus of the next section.

Exposure of the SPD8 mutant to X-rays reveals a slight increase in the reversion frequency at 1 Gy (by a factor of 1.27) and 3 Gy (by a factor of 1.32) and a stronger increase at 5 Gy (by a factor of 2.2) (figure 23). Higher doses did not further increase the reversion frequency (not shown), but increased cell killing. Exposure to ^{241}Am α and ^{56}Fe ions increased the reversion frequency by a factor of 1.96 and 2.54 for ^{241}Am α (at 2 Gy) and for ^{56}Fe ions (at 1 Gy) respectively, but also decreased at higher doses.

This experiment with low and high-LET irradiation showed an enhancement in the reversion frequency in the range of 1.96 – 2.54 times for all radiation modalities tested in the SPD8 mutant.

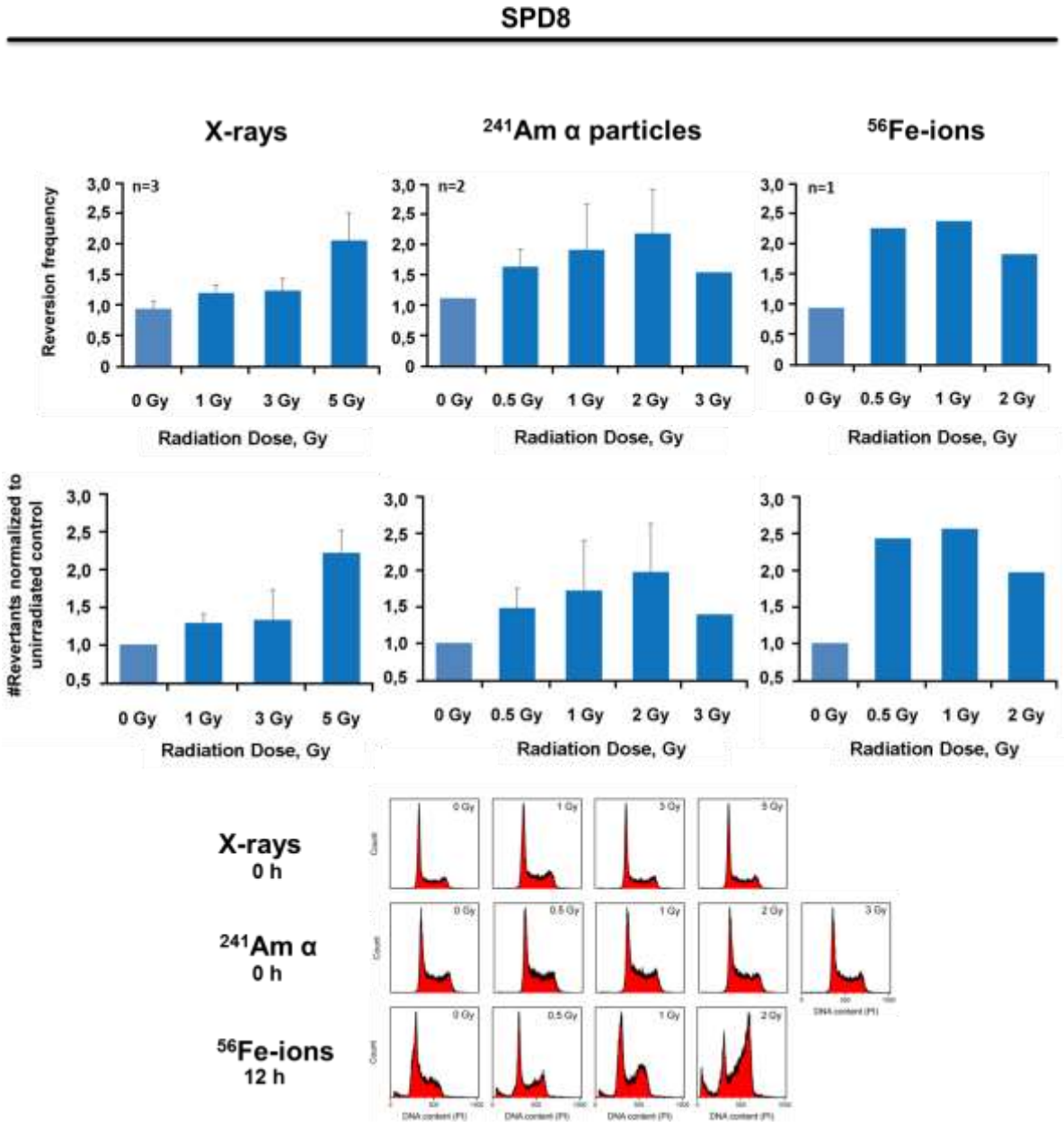

Figure 23: Exposure to IR enhances the reversion frequency in the SPD8 mutant

Exponentially growing SPD8 cells were exposed to X-rays up to 5 Gy, to ^{241}Am α particles up to 3 Gy and to ^{56}Fe ions up to 2 Gy. 6 h post irradiation cells were plated for revertant determination, and plating efficiency. In addition cells were fixed in 70% ethanol and after a centrifugation step stained in a PI solution for flow cytometry analysis. 7 – 10 d post seeding, colonies were stained with crystal violet and counted. Unlike immediate plating after exposure to X-rays and ^{241}Am α particles, ^{56}Fe ions irradiated cells were plated >12 h later. This was due to the fact that irradiation had to take

place at the GSI in Darmstadt, whereas plating took place in Essen. The reversion frequency was calculated considering the number of colonies forming in HAT selective media, the cell survival at that dose and the plating efficiency. The experiments were performed n = 8 for X-rays, n = 2 for ^{241}Am α particles and n = 1 for ^{56}Fe ions. All radiation modalities affect reversion frequency in a similar manner and show an increase with increasing dose that reaches a plateau.

Exposure of SP5 cells to low doses (1-3 Gy) of X-rays increases the reversion frequency only by a factor of 1.04 and 1.13, compared to the non-irradiated control. However, exposure to 5 Gy increases the normalized reversion frequency by 2.52 times. Irradiation with doses above 5 Gy does not cause further increase in reversion frequency, but causes excessive cell lethality (data not shown). In contrast to low-LET, high-LET irradiation increases the frequency of reversion events already at the lowest dose examined (0.5 Gy) by a factor of 1.53 for ^{241}Am α and 3.03 for ^{56}Fe ions, respectively (figure 24). This tendency is even more pronounced at higher doses where increases by 4.36 and 4.54, respectively are observed.

These experiments show that exposure to low-LET and more pronouncedly to high-LET radiation enhance the reversion frequency by up to 2.52 – 4.54 times compared to non-irradiated SP5 cells.

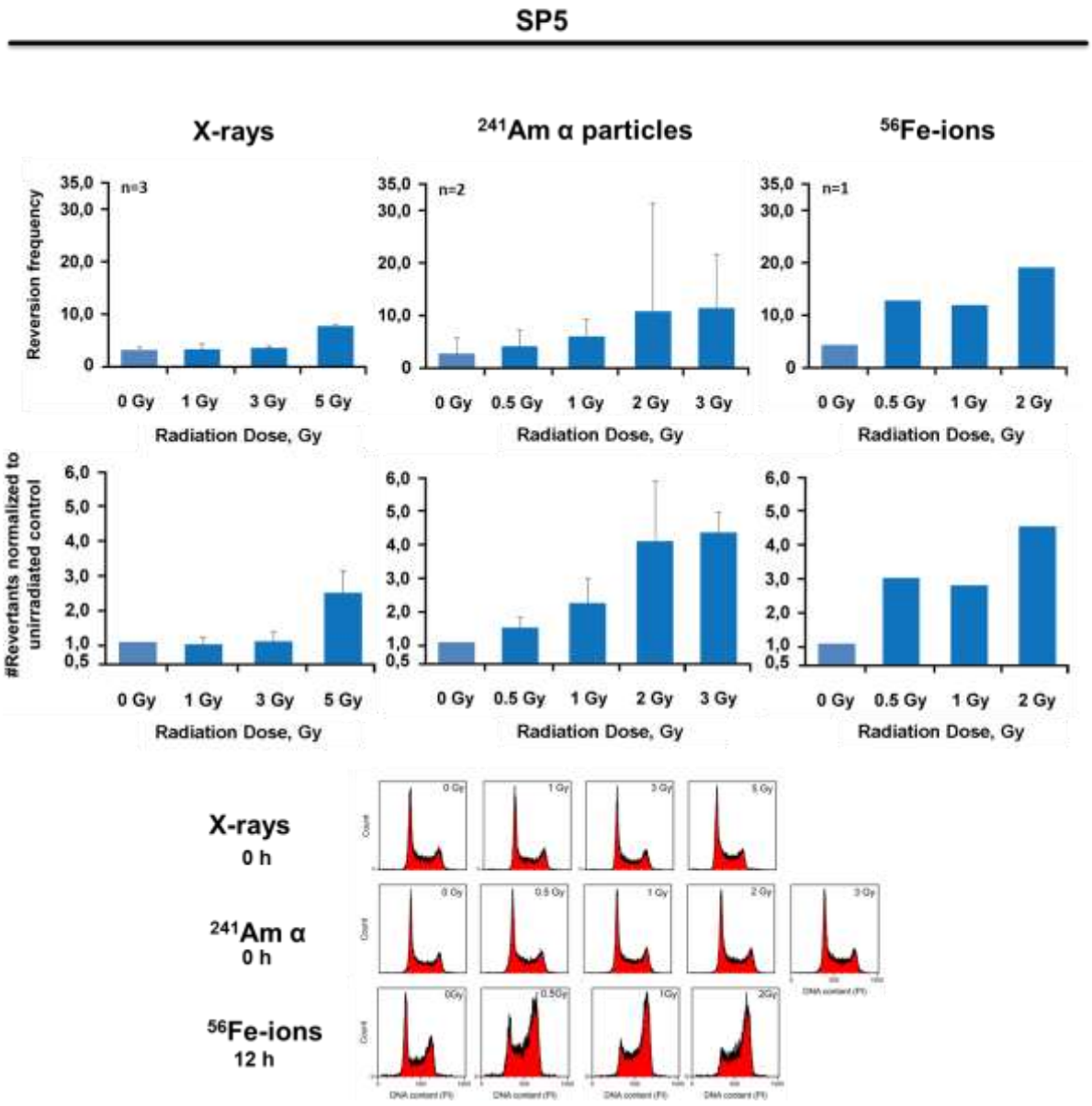

Figure 24: Exposure to X-rays, ^{241}Am α and ^{56}Fe ions enhances recombination events in the SP5 mutant

Exponentially growing SP5 cells were exposed to X-rays up to doses of 5 Gy, to ^{241}Am α particles up to 3 Gy and to ^{56}Fe ions up to 2 Gy. 6 h post irradiation cells were plated in HAT selection media for revertant determination and in regular growth media for plating efficiency determination. In addition, cells were fixed in 70% ethanol, centrifuged, resuspended and incubated in PI staining solution. The cell cycle distribution was then measured by flow cytometry. 7 – 10 days post seeding colonies were stained with crystal violet and counted. Cells were plated for survival directly after exposure to X-rays and ^{241}Am α particles, and >12 h after ^{56}Fe ion irradiation. The reversion frequency was calculated considering the number of colonies forming in HAT selective media, the cell survival at that dose and the plating efficiency. The normalized frequency of revertants measured in non-irradiated controls is also shown. The experiments were performed n = 3 for X-

rays, n = 2 for ^{241}Am α particles and n = 1 for ^{56}Fe ions. The reversion frequency increases with dose after low-LET and more pronouncedly after high-LET radiation.

Based on the above results we conclude that increase in DSB complexity enhances somewhat the reversion frequency in both, the SPD8 and in the SP5 mutant, although the effect is small. We were interested to investigate how DSB repair pathways engage with increasing levels of DSB complexity. For this purpose, we carried out experiments in which we used small molecular inhibitors that target key factors of HRR, D-NHEJ and alt-EJ.

Since the two mutants restore their *hprt* gene by different mechanisms, we describe first experiments carried out with the SPD8 mutant followed by experiments carried out with the SP5 mutant.

3.1.3 DSB repair pathway choice in the increased DSB complexity generated by IR

3.1.3.1 Role of DSB repair pathway utilization and DSB complexity in the frequency of reversion in the SPD8 mutant

The experiments described above showed that the complexity of DSBs enhances the reversion frequency in the SPD8 mutant. Since DSBs initiate homologous recombination, we examined how DSB repair pathways in general contribute to the observed effects. To address this question we used the inhibitors NU7441 (5 µM), KU55933 (10 µM), VE821 (5 µM) and PJ34 (10 µM) which were administrated 1 h prior IR. 6 hours post IR cells were plated to measure the frequency of reversion as described above.

IR induces DSBs and activates DDR arresting cells in their progression through the cell cycle. It is thought that this delay allows cells to repair DNA damage or undergo apoptosis. Cell cycle arrest is mediated by the activation of ATM and ATR protein kinases. These proteins are also implicated in DSB repair pathways and were therefore targeted with the specific inhibitors that are described in greater detail

below. Since Chinese hamster cells have a doubling time of only 12 hours, we expected noticeable cell cycle arrest 6 hours post IR. The DSB repair pathways described in the Introduction are known to operate differently in the different phases of the cell cycle (HRR predominantly in S and G_2, D-NHEJ throughout the cell cycle, alt-EJ throughout the cell cycle but enhanced in G_2). Therefore, analysis of cell cycle distribution is highly relevant as to which repair pathways contributes to reversion events in the SPD8 mutant. Furthermore, some inhibitors induce on their own cell cycle arrest. Therefore we followed cell cycle distribution in all experiments.

DNA PKcs is a major protein kinase involved in D-NHEJ and its inhibition by NU7741 has been shown to compromise this pathway. When the SPD8 mutant was treated with NU7441 strong cell cycle re-distribution was observed 6 h after exposure to low-LET radiation; this effects was less pronounced after exposure to high-LET radiation (figure 25). The reversion assay reveals no differences after NU7741 treatment after exposure to low doses of X-rays (1-3 Gy) (figure 25). At 5 Gy, however, the reversion frequency factor increases from 2.2 (DMSO) to 6.29 (NU7441).

The reversion frequency is not affected by NU7441 after exposure to low doses (0.5, 1 and 2 Gy) ^{241}Am α particles. In contrast to this, a higher dose of 3 Gy increases the reversion frequency factor 2.44 times in the treated cells compared to the normalized 3 Gy DMSO control. Exposure to ^{56}Fe ions increases already at low dose (factor of 3.43 for 0.5 Gy and 4.01 for 1 Gy) and is even more pronounced at 2 Gy with a factor of 20.89 in the reversion frequency compared to the DMSO control (2.41, 2.54 and 1.95 at 0.5, 1 and 2 Gy respectively).

These results show that inhibition of D-NHEJ enhances the reversion events at high radiation doses for all tested radiation modalities. Since HRR operates more efficiently at low doses, we examined next the contribution of HRR to the repair of DSBs of increased complexity.

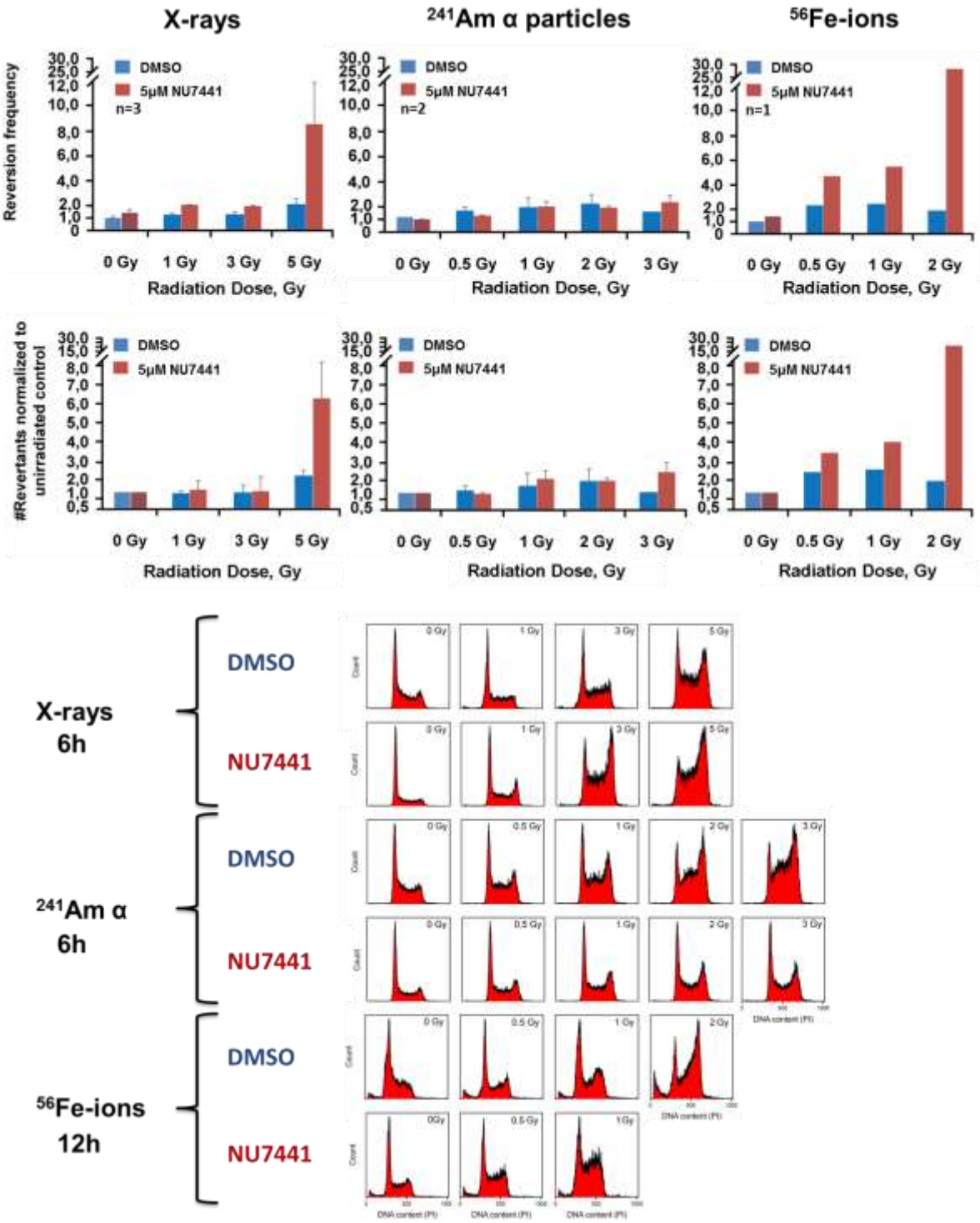

Figure 25: Effect of DNA PKcs inhibition on the reversion frequency after exposure to low and high-LET radiations

Administration of 5 μM of the DNA PKcs inhibitor NU7441, or DMSO as the solvent, to exponentially growing SPD8 cells 1 h before irradiation. Other steps were as described in figure 23. X-rays, ^{241}Am α particles and ^{56}Fe ions experiments were performed n = 3, n = 2 and n = 1 times. DNA PKcs inhibits reversion at high radiation doses.

To examine HRR in the presence of increased DSB complexity, SPD8 cells were incubated with an ATM inhibitor KU55933. ATM is not a central HRR protein, but is involved in the initiation step, the presynapsis stage of HRR and regulates there the generation of 3'-ended ssDNA overhangs by liberating the nucleolytic activity of CtIP and Mre11 (of the MRN complex) (Bakr 2015). In the absence of ATM prolonged accumulation of Rad51 foci is observed in the S-phase, suggesting incomplete HRR. (Köcher 2012). KU55933 is a specific ATM inhibitor that does not interfere with other PI3K family members (ATR, DNA PKcs) (Lossaint 2011) and was shown to affect HRR (Kass 2013).

The cell cycle analysis in figure 26 shows no difference in the KU55933 treated cells compared to the DMSO control after exposure to IR. The IR induced cell cycle arrest was similar between the KU55933 treated and DMSO controls, but more pronounced at high-LET radiation.

Treatment with KU55933 shows (figure 26) no notable affect in the reversion frequency after irradiation with X-rays, or ^{241}Am α particles at doses up to 2 Gy and for ^{56}Fe ions at low doses. Only at high doses of high-LET radiation the reversion frequency increases by a factor of 2.12 (DMSO: 1.39 at 3 Gy ^{241}Am α particles) and 11.71 times (DMSO: 1.95 at 2 Gy ^{56}Fe ions) compared to the normalized DMSO controls.

The absence of effect of KU55933 on the reversion frequency of the SPD8 mutant after low-LET radiation and at low doses of high-LET radiation suggests that ATM is mainly involved in homologous recombination events initiated by complex DSBs.

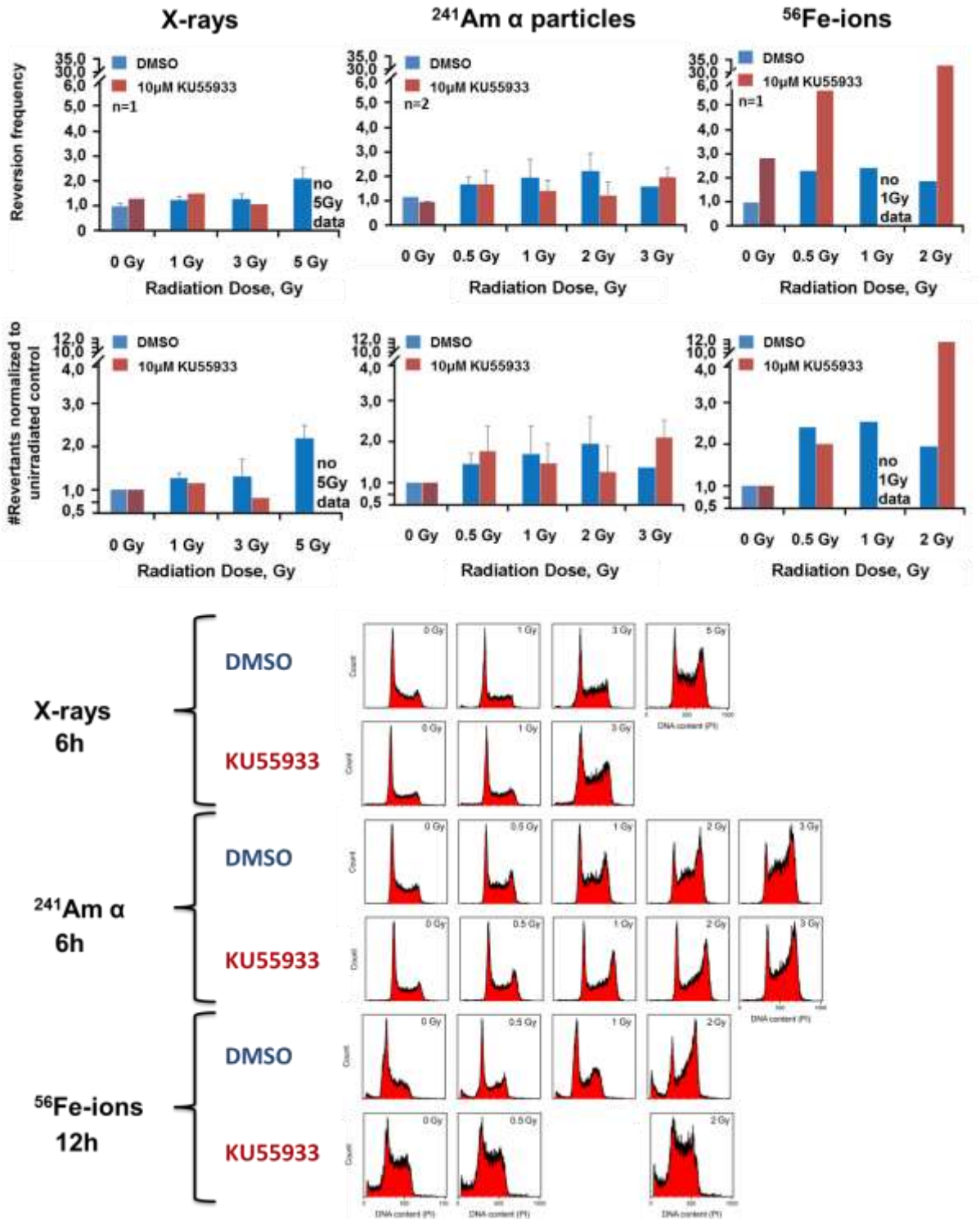

Figure 26: Effect of ATM inhibition on the reversion frequency in the SPD8 mutant after exposure to radiations of different LET

Administration of 10 µM KU55933 or DMSO only to exponentially growing SPD8 cells 1 h before irradiation. All subsequent steps were as described in figure 23. Experiments with X-rays, ^{241}Am α particles and ^{56}Fe ions were performed n = 1, n = 2 and n = 1 times. ATM inhibition does not change the reversion frequency at low and high-LET irradiation.

In the HRR pathway DSB ends are resected to form ssDNA overhangs. ssDNA regions may also derive from stalling of DNA replication forks. RPA binds with a high affinity to ssDNA. The RPA coated ssDNA is then recognized by the ATR regulator Rad17-RFC complex that recruits another ATR regulator, the Rad9-Rad1-Hus1 (9-1-1) complex to the site. Furthermore, the RPA coated ssDNA also presents a platform for the ATR-ATRIP protein that, in conjunction with the Rad17-RFC complex, 9-1-1 complex and TopBP1 then activate ATR (Flynn 2011). The activated ATR is thought to promote the recovery of stalled replication forks (Cimprich 2008). Since ssDNA are also an intermediate of HRR, ATR gets activated in response to DSBs as well. In the DDR pathways ATR coordinates the cell cycle via CHK1 phosphorylation and the ensuing arrest in the progression of cells through the cell cycle. A study with doxycycline induced ATR kinase dead cells showed a functional link of ATR and homologous recombination (Wang 2004). Furthermore studies have shown that in contrast to ATM, which operates at the early resection steps, ATR is involved in the extensive resection during HRR and that inhibition of ATR was able to block the HRR successfully (Krajewska 2015). Therefore, we investigated the involvement of HRR in the repair of DSBs of increasing complexity by inhibiting ATR using VE821. VE821 is a specific ATR inhibitor that does not interfere with other members of the PI3K family, prevents the G_2/M arrest and abrogates HRR (Prevo 2012).

Figure 27 shows that VE821 treatment does not affect cell cycle distribution after exposure to low and high-LET radiation. This observation is in line with results in the literature showing that VE821 abrogates the G_2/M checkpoint (Prevo 2012); it also validates the inhibitor for our experiments.

The VE821 treated and irradiated (X-rays) cells in figure 27 show no effect in the reversion frequency at all doses examined (factor of 1.12 and 1.53 at 1 Gy and 3 Gy). In contrast to X-rays, ^{241}Am α particles diminish the IR enhanced reversion frequency factor of the DMSO control when treated with VE821. Similar tendencies can also be observed for ^{56}Fe ion irradiation. While at low doses (0.5 Gy and 1 Gy) the factor is reduced to 0.72 (DMSO: 2.41) and 2.06 (DMSO: 2.54), at 2 Gy reversion formation is completely abolished.

This experiment showed that ATR is involved in the reversion events after high-LET irradiation, as inhibition of ATR by VE821 decreases the reversion frequency.

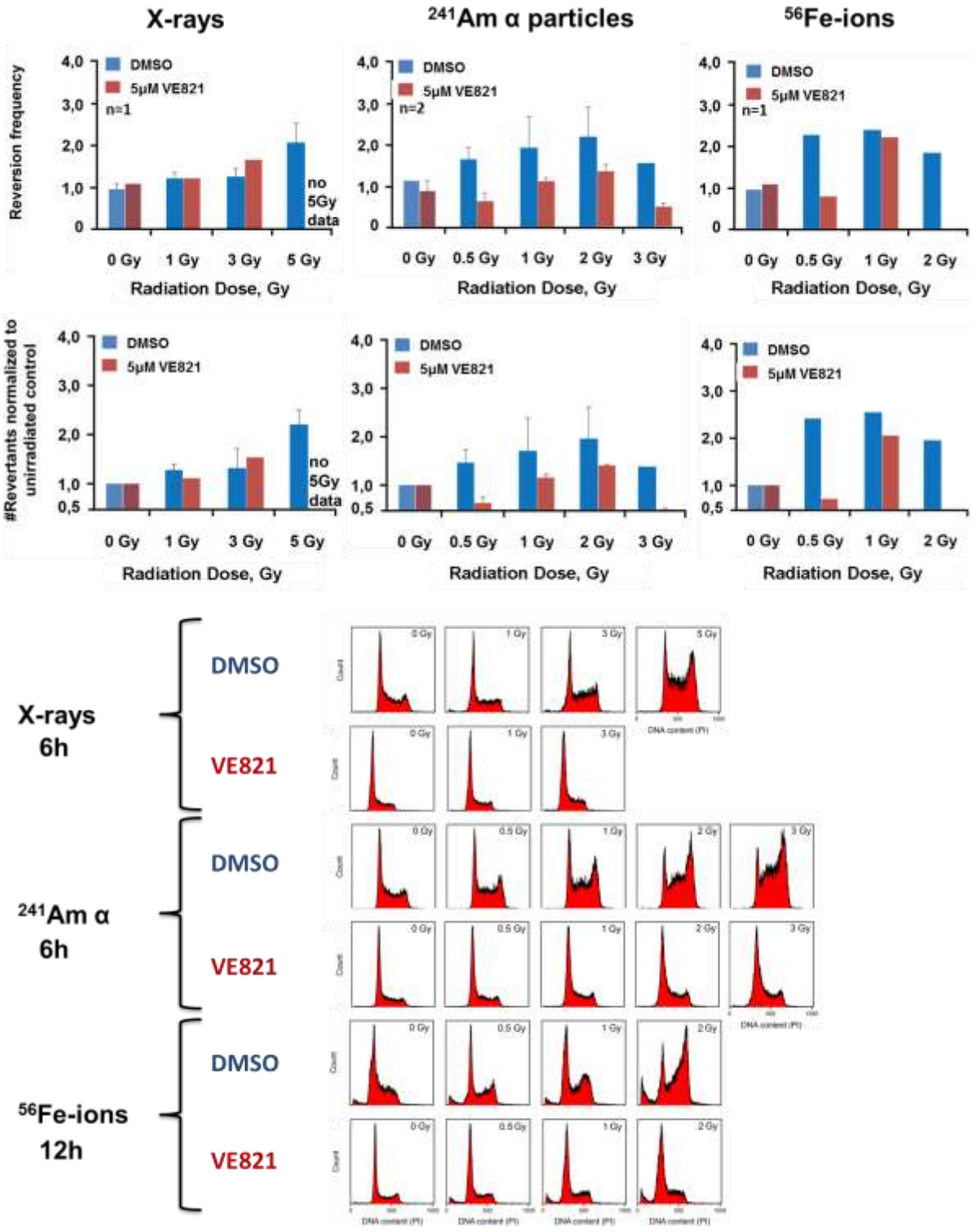

Figure 27: Effect of ATR inhibition on the reversion frequency after exposure to IR

Administration of the ATR inhibitor, VE821 (5 μM) or of solvent only (DMSO) to exponentially growing SPD8 cells 1 h before irradiation. Other details are as described in figure 23. Experiments

with X-rays, ^{241}Am α particles and ^{56}Fe ions were performed n = 1, n = 2 and n = 1 times. Inhibition of ATR reduces *hprt* reversion at high-LET irradiation.

Another DSB repair pathway is the alt-EJ that shares components with HRR and D-NHEJ and is thought to gain ground when one of these repair pathways is compromised (Iliakis 2015). While D-NHEJ operates throughout the cell cycle, HRR is restricted to the S and G_2 phase. When D-NHEJ is compromised outside the S/G_2 phase of the cell cycle, alt-EJ takes over. When a DSB forms within the S or G_2 phase of the cell cycle and HRR is compromised this lesion can be repaired in theory either by D-NHEJ or alt-EJ. However, alt-EJ but not D-NHEJ was shown to compensate when HRR was defective in the G_2 phase cells (Soni 2014). We speculate therefore that alt-EJ takes over resected ends from abrogated HRR and joins them utilizing microhomologies. This assumption is in agreement with enhanced utilization of alt-EJ in the G_2 phase of the cell cycle, a cell cycle phase in which HRR is active.

Studies showed that PARP is an important component of alt-EJ, by binding to the DNA ends in the initial steps of repair. However, access to DNA is thought to be suppressed in the presence of D-NHEJ proteins, particularly Ku (Wang 2006). We therefore speculate that the generation of DSBs with increasing complexity may enhance the activity of alt-EJ.

To examine the contribution of alt-EJ to the repair of DSBs with increasing complexity, as generated by different radiation modalities, the SPD8 cells were incubated with a PARP inhibitor PJ34 1 h before IR.

Flow cytometry analysis of PJ34 treated and irradiated cells in figure 28 shows a G_2/M arrest after low and high-LET radiation, which was expected (Madison 2011). The mechanism by which PJ34 induces this arrest is not known, but it is thought to derive from interactions with the kinases ATM and ATR that influence the cell cycle check point signaling.

PJ34 treatment has no effect on the reversion frequency after exposure to X-rays at all doses examined, and for low doses of ^{241}Am α particles (0.5 - 2 Gy) and ^{56}Fe ions (0.5 Gy). At 3 Gy ^{241}Am α particles the reversion frequency factor of 1.38 (normalized DMSO value at 3 Gy) increases in the PJ34 treated cells to 1.96. A

similar tendency was observed for ^{56}Fe ion irradiated cells that were treated with PJ34. In these cells the factor increased 3.71 times at 1 Gy and 5.21 times at 2 Gy.

The ability of PJ34 to increase the reversion frequency factor compared to the normalized DMSO control after high doses of ^{241}Am α particles and ^{56}Fe ions indicates that the homologous recombination event in SPD8 cells is not efficiently operating at complex DSBs when alt-EJ is active.

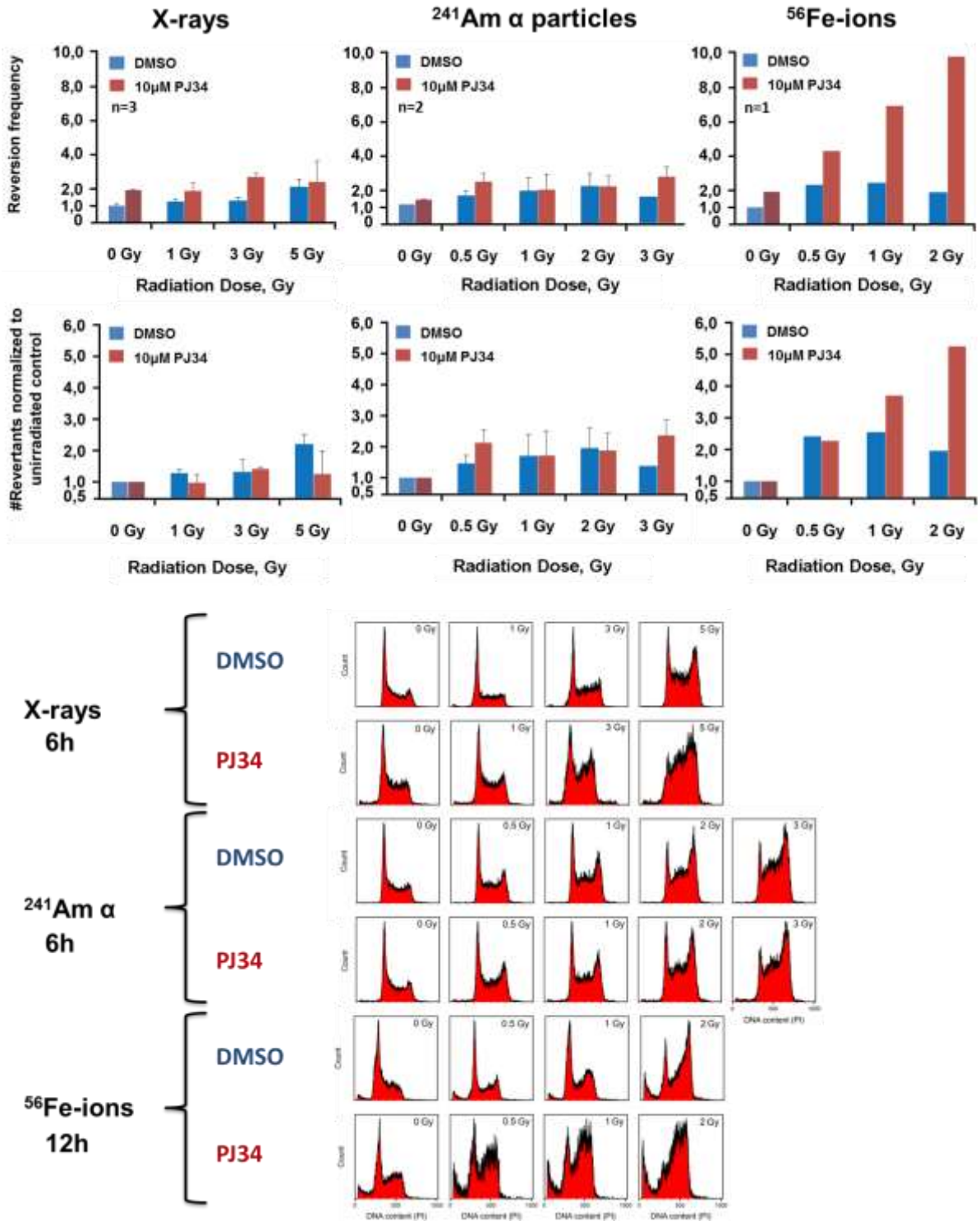

Figure 28: The effect of PARP inhibition on the reversion frequency after exposure to IR

Administration of 10 µM PARP inhibitor PJ34, or of solvent only (DMSO) to exponentially growing SPD8 cells 1 h before irradiation. Other experimental details are as in figure 23. Experiments with X-rays, ^{241}Am α particles and ^{56}Fe ions were performed n = 3, n = 2 and n = 1 times. PARP suppress the reversion frequency at high doses of high-LET radiation.

3.1.3.2 The role of DSB repair pathways in the reversion frequency mediated by DSBs of different complexity in the SP5 mutant

To examine how DSB repair pathways contribute to the repair of complex DSBs that initiate the reversion event in the SP5 mutant, we carried out experiments similar to those described for the SPD8 mutant, and utilized also the inhibitors NU7441 (5 µM), KU55933 (10 µM), VE821 (5 µM) and PJ34 (10 µM).

NU7741 was used to examine the contribution of D-NHEJ. The cell cycle distribution analysis reveals no differences in the NU7441 treated cells after exposure to X-rays and ^{56}Fe ions compared to the DMSO treated controls (figure 29). Figure 29 shows no effect of the NU7441 on reversion frequency after exposure to X-rays at low doses (up to 3 Gy). At the higher dose (5 Gy) the presence of the DNA PKcs inhibitor diminished reversion frequency factor from 2.52 (DMSO) to 1.18 (NU7441) (figure 29).

Inhibition of DNA PKcs affects reversion more pronouncedly after ^{241}Am α irradiation. Higher doses like 3 Gy ^{241}Am α particles reduced in the presence of NU7441 the reversion frequency factor from 4.36 (DMSO) to 1.68 (NU7441). When SP5 cells were treated with the same inhibitor and exposed to 2 Gy ^{56}Fe ions the reversion frequency decreased 17.56%, compared to the factor of the 2 Gy DMSO control. The tendency of NU7441 to decrease reversion frequency, as shown for X-rays and ^{241}Am α particles at higher doses, is absent for ^{56}Fe ions. For ^{56}Fe ions the reversion frequency measured at increasing doses is similar to the DMSO control.

Thus, NU7741 treatment diminishes the reversion frequency after exposure to low and high-LET radiation. The effect is stronger under conditions generating high levels of reversion. Since this effect was shown predominantly for higher radiation doses, we speculate that HRR may operate at lower doses. Therefore subsequent experiments studied the effect of HRR on this endpoint.

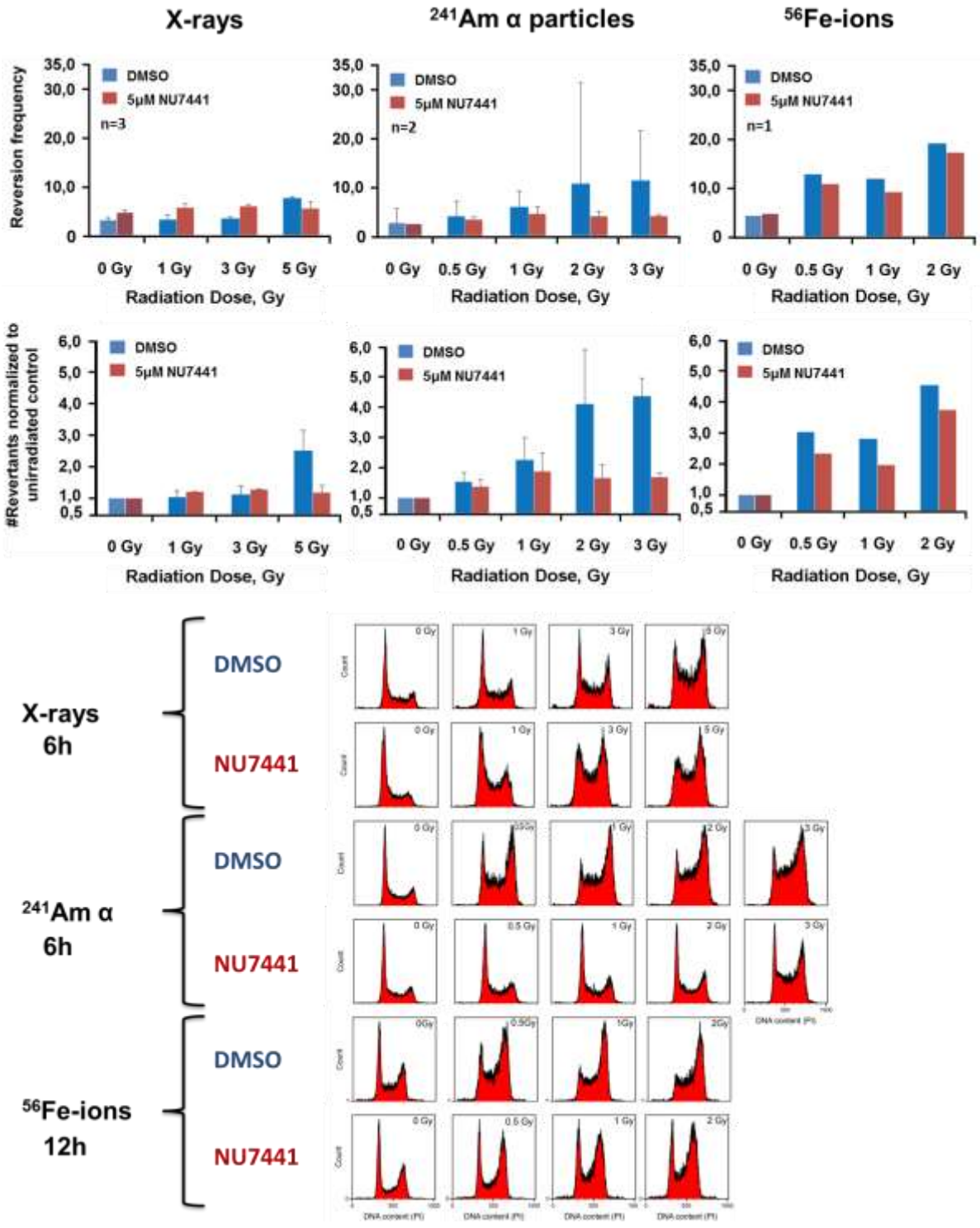

Figure 29: Effect of DNA PKcs inhibition on the reversion frequency after exposure to IR

Administration of 5 µM DNA PKcs inhibitor NU7441 and DMSO to exponentially growing SP5 cells 1h before irradiation. Other experimental details are as described in figure 23. Experiments with X-rays, ^{241}Am α particles and ^{56}Fe ions were performed n = 3, n = 2 and n = 1 times. DNA PKcs stimulates the reversion events at high doses when more DSBs are generated.

The administration of the inhibitor KU55933 shows no differences in the cell cycle distribution compared to the DMSO-only treated cells after exposure to IR. In both treatments the IR induced arrest can be observed 6 h post IR.

Furthermore, KU55933 treatment shows to diminish the radiation increase of reversion events after both, low and high-LET radiation (figure 30). This is more pronounced at 3 Gy of X-rays and ^{241}Am α particles. At this dose reversion is nearly completely abolished with a 0.87 and 0.71 times decrease compared to the normalized DMSO-only values, respectively (figure 30). Only the 5 Gy X-rays samples show a different outcome. This strong effect cannot be observed after ^{56}Fe ion radiation, although here again a tendency to reduce the reversion frequencies in the KU55933 treated cells compared to the DMSO control are noted.

The reduced reversion frequency of KU55933 treated cells in comparison to the DMSO controls after irradiation showed that HRR may take place in the presence of simple but also in the presence of complex DSBs.

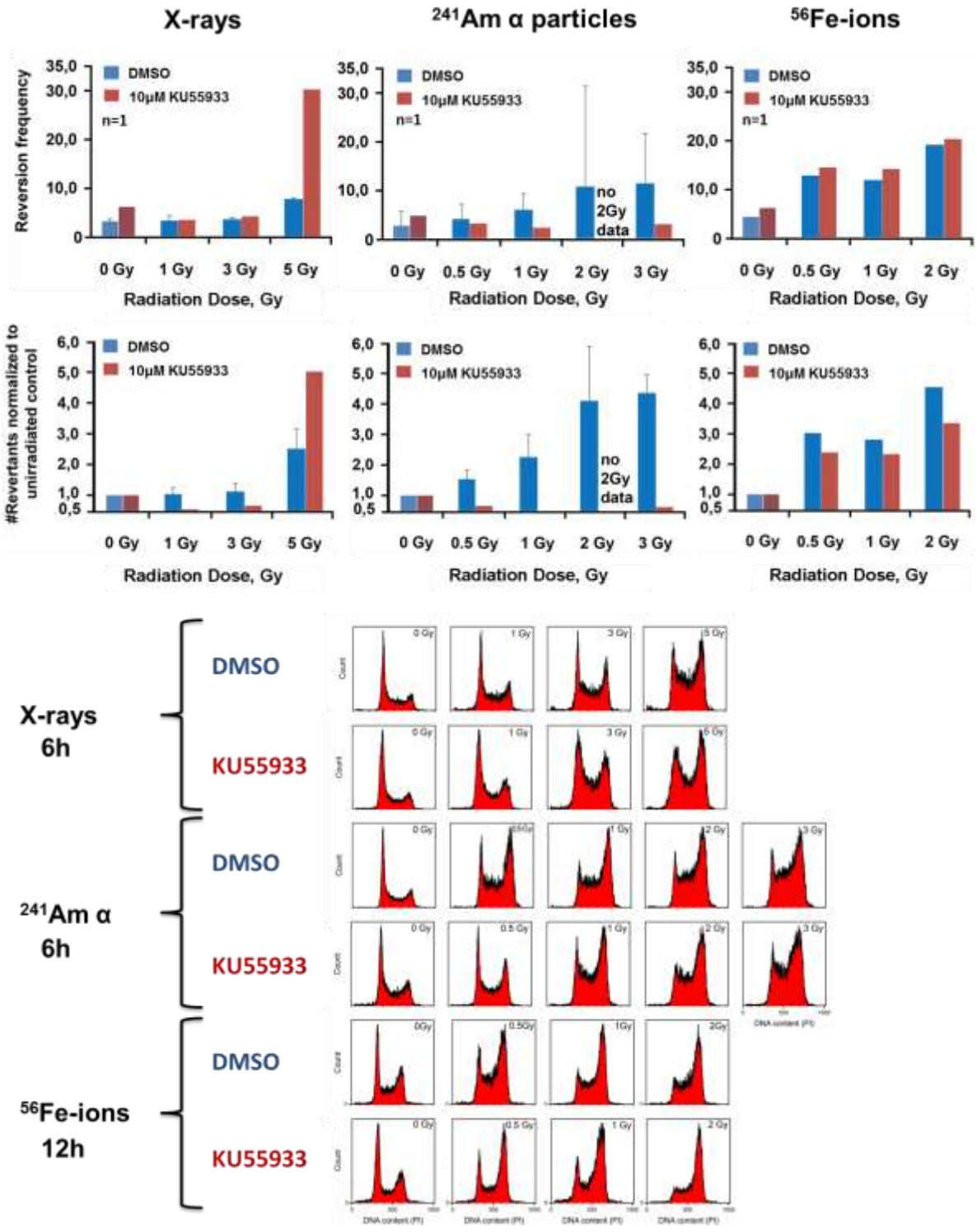

Figure 30: Effect of ATM inhibition on the reversion frequency after exposure to IR

Exponentially growing SP5 cells were treated with 10 µM of the ATM inhibitor KU55933, or with DMSO-only, 1 h before irradiation. 6 8 h post IR cells were plated to measure reversion and cell cycle distribution as described in figure 23. Experiments were performed n = 1. Inhibition of ATM reduces and almost completely diminishes the reversion events after IR.

VE821 (figure 31) induces no change in the cell cycle distribution after exposure to IR. The IR induced cell cycle arrest seen in the DMSO treated cells, cannot be observed in the presence of VE821. This indicates that VE821 abrogates, as expected, the G_2/M arrest.

Treatment with VE821 reduces reversion after exposure to IR for all doses, independently of radiation modality (figure 31). The reduction in reversion frequency is most pronounced after ^{241}Am α particles. ATR inhibition prevents the IR induced increase in the reversion frequency after exposure to X-rays and ^{241}Am α particles. However, the ^{56}Fe ion irradiation experiments are not in line with this observation and rather show enhanced reversion frequency with increasing radiation dose.

The above results of ATM and ATR inhibition implicate HRR in reversion induction by simple and complex DSBs.

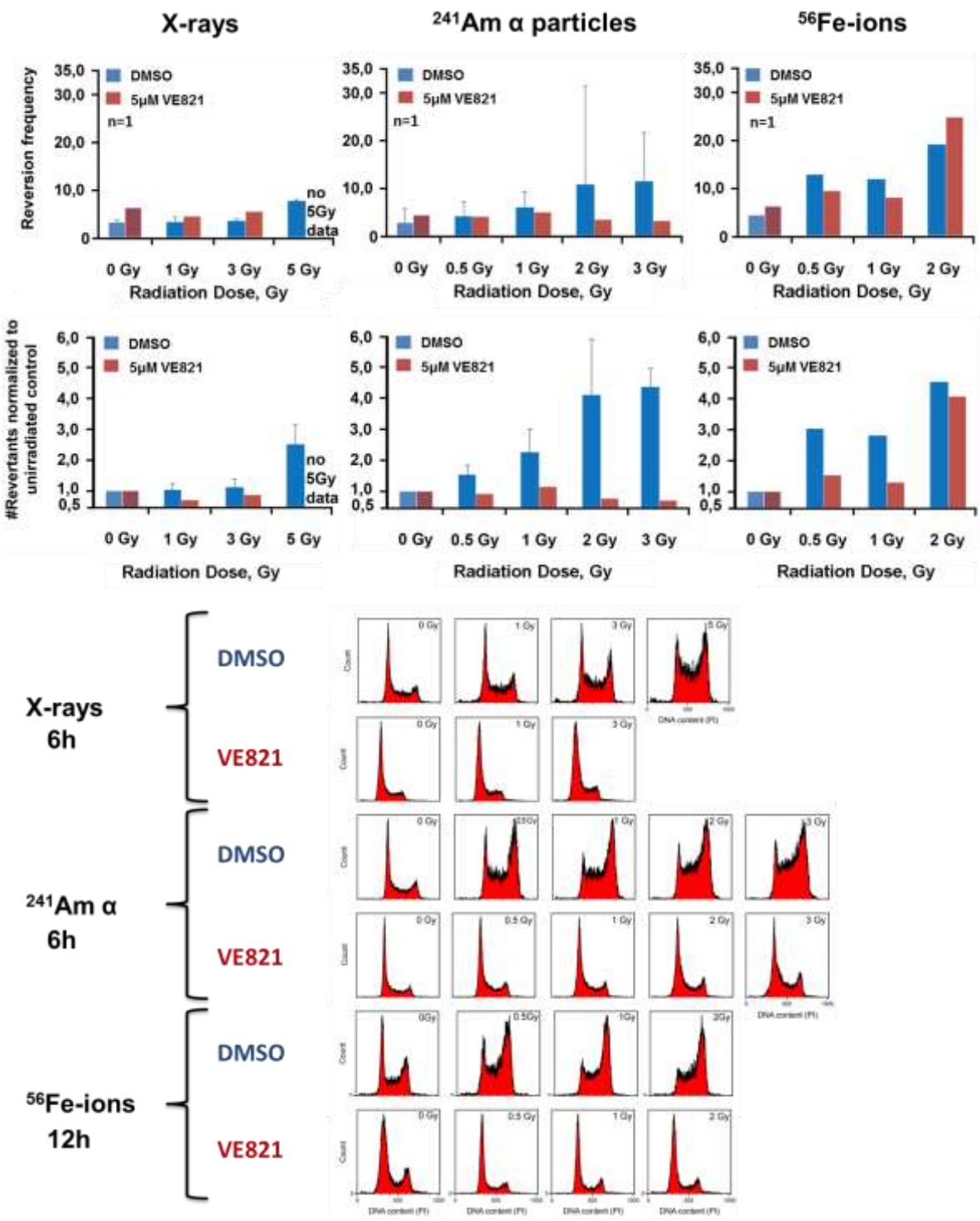

Figure 31: Effect of ATR inhibition on reversion frequency after exposure to low and high-LET radiation

Administration of 5 µM ATR inhibitor VE821, or solvent DMSO only, to exponentially growing SP5 cells 1 h before irradiation. Other experimental details are as described in figure 23. Experiments were performed n = 1. ATR affects the reversion events at low-LET and more pronouncedly after high-LET irradiation.

The administration of PJ34 generates a more pronounced accumulation of cells in G_2 phase after exposure to IR. This pronounced cell cycle arrest was expected and indicates indirectly the functionality of the inhibitor.

Furthermore, PJ34 treatment (figure 32) diminishes the IR induced reversion frequency factor from 2.52 (DMSO) to 0.87 (PJ34) after exposure to 5 Gy X-rays. A similar effect was observed after irradiation of 2 Gy ^{241}Am α particles (reduction, DMSO 4.1, PJ34 1.48). This reduction was not observed in cells exposed to ^{56}Fe ions. In fact, the reversion frequency seems to increase slightly after the ^{56}Fe ions exposure and PJ34 treatment (change by 2.42% at 2 Gy only).

The effect of PJ34 indicates IR-mediated reversion events rely not only on HRR and D-NHEJ but also on alt-EJ.

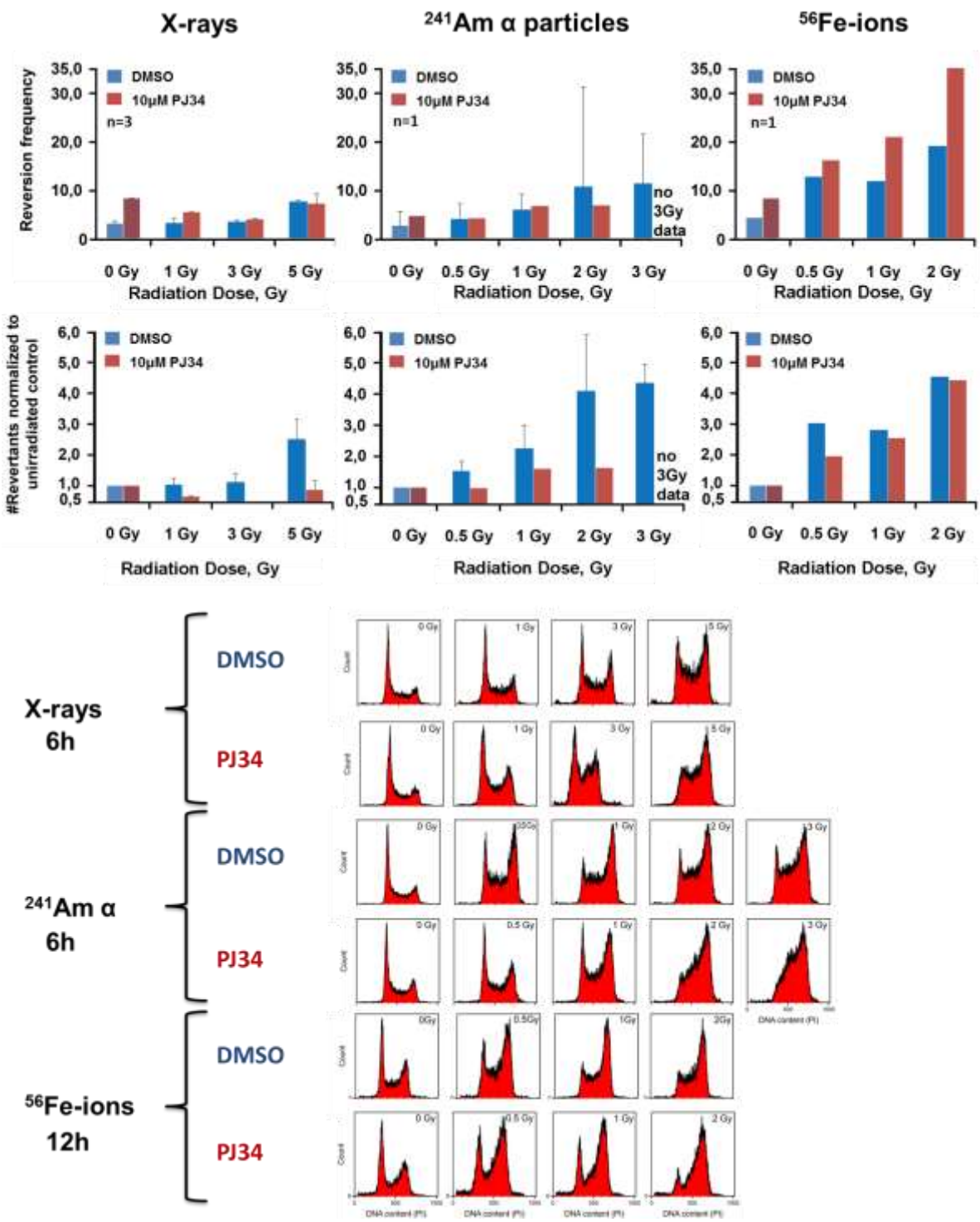

Figure 32: Effect of PARP inhibition on the reversion frequency after exposure to IR

Administration of 10 µM of the PARP inhibitor, PJ34, or of solvent only, DMSO, to exponentially growing SP5 cells 1 h before irradiation. Other experimental details are as described in figure 23. Experiments with X-rays, ^{241}Am α particles and ^{56}Fe ions were performed n = 3, n = 1 and n = 1 times. PARP stimulates the reversion frequency predominantly after exposure to low-LET radiation.

3.1.4 DSB repair pathway choice in the increased DSB complexity generated by RNA guided nucleases

The above results revealed a role for all DSB pathways in the reversion frequency at the *hprt* locus. However, these experiments were restricted to low radiation doses, as higher doses not only increase reversion frequency, but also cause cell lethality compromising analysis. Furthermore, due to the local energy deposition characteristics of IR, the probability that a DSB forms within the *hprt* gene (36 kb) in the Chinese hamster genome (2.3×10^6 kb) (Brinkrolf 2013) at the doses employed is very low (3.1 times in ten thousand after 1 Gy X-rays). For high-LET radiation, the ionization events are even less randomly distributed, as they occur mainly along the particle tracks. This distribution of ionization events, and thus of DNA damage, is expected to lower further the probability of inducing a DSB directly in the *hprt* locus. We infer therefore that the above measured reversion events do not always reflect responses to direct hits in the *hprt* gene and most likely reflect secondary effects. Such secondary effects include replication stress or oxidative damages which eventually cause the reversion events detected.

To investigate specifically the effects of DSBs within the *hprt* gene and to examine their role in reversion induction we have adopted the RNA guided nuclease technique. This method allows the generation of single DSBs of low complexity at specific genomic locations and can be used to generate lesions of increase complexity by clustering DSBs. In the following sections, we show results obtained with this approach first with the SPD8 and then with the SP5 mutant.

3.1.4.1 Role of DSB complexity and repair pathway choice in the induction of reversions in the SPD8 mutant

3.1.4.1.1 DSBs within or near the mutated region of SPD8 cells enhances the reversion frequency

We examined first, whether the induction of DSBs within the *hprt* gene affects the reversion frequency in SPD8 cells. Furthermore, we addressed the question of hot spots in the *hprt* gene that trigger enhanced reversion when DSBs incur within them.

For this approach the following guide RNAs (gRNAs) were designed: gRNA8 that targets the duplicated region (gRNA#8: exon 7), gRNA12 that targets a sequence 318 bp outside of mutated region (gRNA#12) and gRNA#2 that recognizes a sequence 25 kb upstream of the mutated region in the SPD8 cell line. The exact binding locations of the gRNAs in the *hprt* gene are shown in figure 33.

To examine the reversion frequency of RNA guided nuclease (CRISPR/Cas9) induced DSBs, exponentially growing SPD8 cells were transfected with plasmids encoding for gRNA and Cas9. For each transfection one microgram plasmid per million cells was used. After transfection and expression, the gRNA directs the Cas9 endonuclease to the sequence of interest in the *hprt* gene and induces with the nuclease activity domains RucV and HNH of Cas9 a blunt DSB. Control cells were transfected with Cas9 without gRNA. 48 h post transfection cells were plated for revertant analysis and plating efficiency determination. To measure transfection efficiency, cells were transfected with a plasmid encoding for GFP. The GFP samples were collected 24 h post transfection and were analyzed by flow cytometry. Furthermore the cell cycle distribution was determined at the time of transfection and 48 h later. The reversion events were calculated using as parameters transfection efficiency and plating efficiency.

Figure 33 shows an increase in the reversion frequency the closer the DSBs were induced to the mutated region. A DSB that is generated 25 kb upstream of the mutated region increases the reversion frequency only by a factor of 1.19

(gRNA#2) compared to the mock control. The induction of a DSB, which flanks the mutated region 318 bp increases the reversion frequency by a factor of 95.23 (gRNA#12). However, the most pronounced effect is observed when a DSB is generated within the mutated region (gRNA#8). The interruptions of the DNA strand by gRNA#8 increases the reversion frequency dramatically by a factor of 663. There is no effect on cell cycle distribution due to the experimental manipulations performed (figure 33). Thus, unlike exposure to IR, the Cas9 system generates DSBs in the *hprt* gene without inducing cell cycle arrests.

Based on the finding that DSBs generated close to the mutated region enhance reversion frequency stronger than DSBs generated in more remote locations, subsequent experiments were designed to address the question whether there is a hot spot within the mutated region that triggers the reversion event and whether an increase in DSB complexity further enhances this effect.

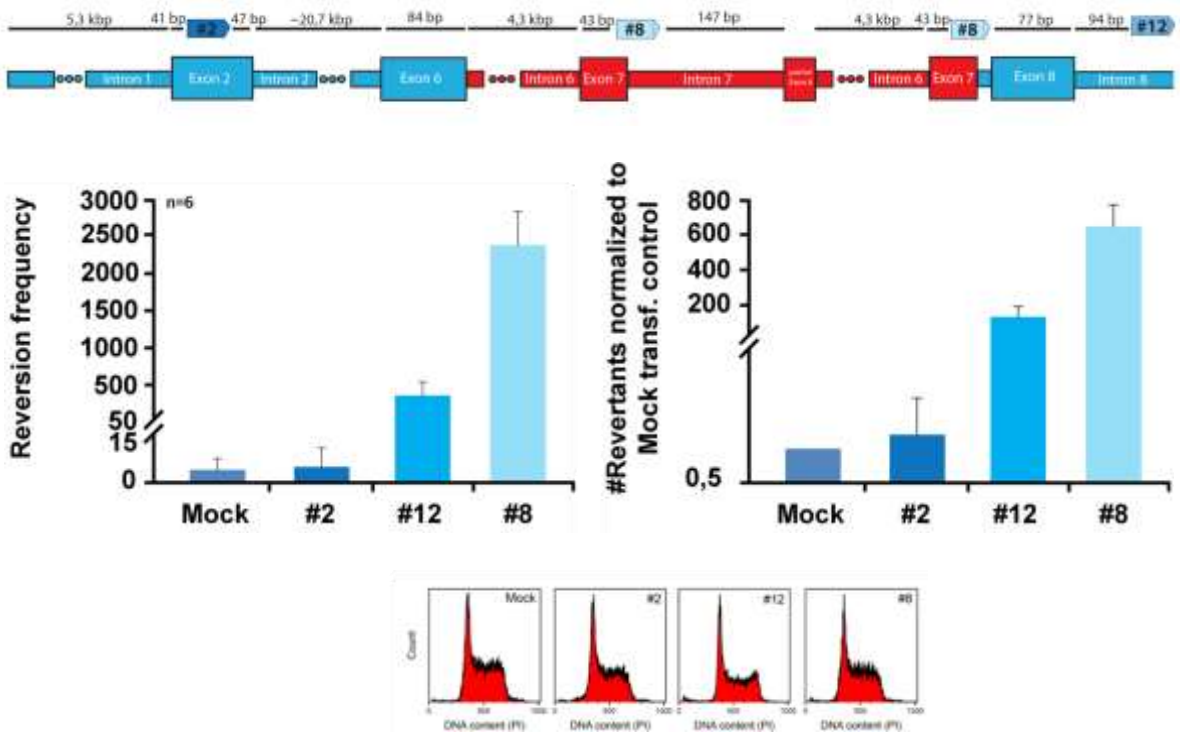

Figure 33: Induction of DSBs within the duplicated region of the *hprt* gene enhances reversion frequency

Guide RNAs (gRNAs) were designed to target specific locations within the *hprt* gene, mainly within the duplicated region as well as outside of mutated region of the SPD8 mutant cell line. The scheme above indicates the mutated *hprt* gene of SPD8 cells. The mutated region with the duplication is

shown in red. gRNA8 recognizes the exon 7/intron 7 junction, gRNA12 the intron 8 that flanks the mutated region 318 bp downstream, and gRNA2 the exon 2 at a region that is located about 20 kb upstream from the duplicated region. Exponentially growing SPD8 cells were cotransfected with Cas9 and gRNA2 (#2), gRNA12 (#12), gRNA8 (#8), or without control gRNA (Mock). To determine transfection efficiency, cells were transfected with a GFP plasmid. The amount of plasmid DNA used for all transfections was 1 µg per million cells. 24 h post transfection the GFP transfected sample was assayed by flow cytometry. The other samples were plated 48 h post transfection in HAT selection media to determine revertant induction and in growth media without selection to determine the plating efficiency. The reversion frequency increases dramatically when DSBs are generated within the mutated region.

3.1.4.1.2 Reversion frequency in SPD8 cells after induction of complex DSBs

We speculated that loss of the exon within the duplicated region of the *hprt* locus will facilitate reversion in SPD8 cells. To test this assumption gRNAs were designed that target the duplicated exon 2 directly (gRNA#13), as well as gRNAs that recognize the sequences that flank exon 2, 5' and 3' (intron 6 by gRNA#11, exon 2/intron 6 junction by gRNA#8 and intron 8 by gRNA#12).

To investigate whether reversion induction has hot spots, SPD8 cells were transfected with Cas9 in conjunction with each of the above gRNAs. Figure 34 shows that DSB generation at the junction of exon 7/intron 7 increases the reversion frequency as compared to DSBs induced in intron 8 or exon 2 (regions outside the mutation). Surprisingly, the induction of a DSB in the intron 6 increases reversion frequency dramatically, by a factor of 1327. This is about three and two times higher than that measured for DSBs induced in exon 7, and the exon 7/intron 7 junction, respectively. This indicates that not the exon itself or the junction of the exon/intron, but the sequence nearby triggers reversion in SPD8 cells.

In the next step we increased the number of DSBs in the mutated region to investigate the effect of complex DSBs on the reversion frequency. We speculated that DSB clusters may further enhance reversion.

To test this, SPD8 cells were transfected with Cas9 in conjunction with one to four different gRNAs that recognize sequences a few hundred base pairs apart. We

regard such DSB clusters as lesions of increased complexity. The distances between DSBs is 120 bp for the gRNA#11 and gRNA#13 pair, 3 bp for the gRNA#13 and gRNA#8 pair, and 338 bp for the gRNA#8 and gRNA#12 pair. Surprisingly, DSB clusters cause a decrease in reversion frequency compared to the single DSBs for all transfection combinations and gene locations. Transfections with three or four gRNAs further decreases reversion frequency compared to the double transfected cells.

These results indicate that the generation of DSBs in close proximity to exon 7 enhances the reversion frequency dramatically. However, DSB clusters reduce reversion frequency. We examined next the role of DSB repair pathways in reversion events generated using the CRISPR/cas9 system.

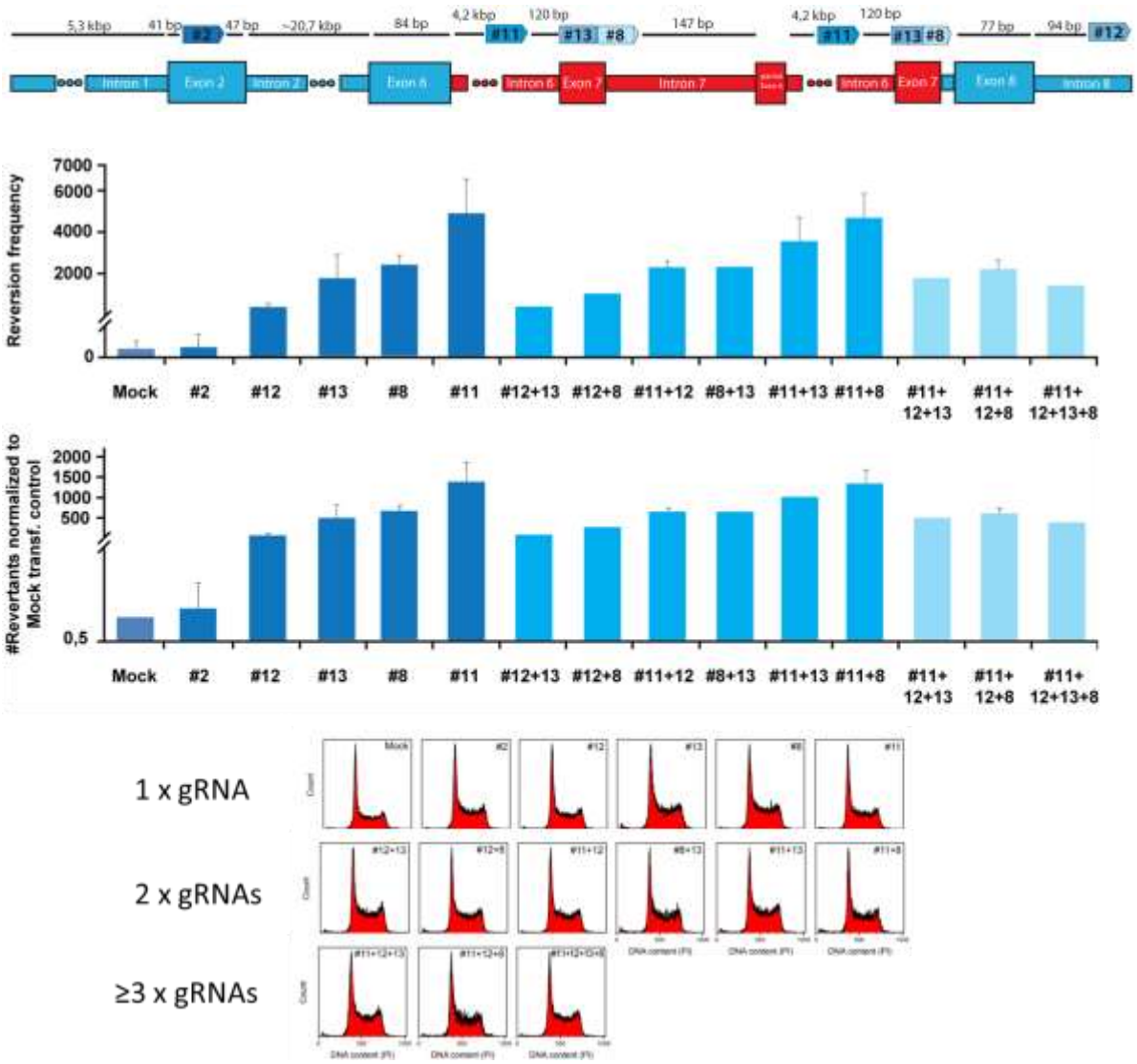

Figure 34: Effect on *hprt* reversion of complex DSBs

SPD8 cells were transfected with one to four different gRNAs in conjunction with Cas9. In addition cells were transfected without gRNA as control, and with GFP as a transfection efficiency control. For each transfection 1 µg plasmid per million cells was used. The transfected cells were plated 48 h later and treated as described in figure 33. The cell cycle distribution was assayed by flow cytometry at the time of transfection (not shown) and 48 h later. Reversion frequency was normalized to the mock transfected control. Induction of DSBs in intron 6 of the mutated region strongly enhanced reversion frequency. Increase in DSB complexity fails to further increase reversion.

3.1.4.1.3 The role of DSB repair pathways in reversion events induced by DSBs of different complexity

The above results demonstrate that simple interruptions in the mutated region facilitate the homologous recombination events causing reversion in SPD8 cells, whereas destabilizing DSB clusters suppress reversion. To determine the role of DSB repair pathways in the events initiated in these conditions, cells were transfected with single (gRNA#8, gRNA#11) and double gRNAs (gRNA#8 + gRNA#11) and plated directly into dishes with media that were supplemented with DMSO, NU7441 (2.5 µM), KU55933 (5 µM), VE821 (2.5 µM) or PJ34 (5 µM). 48 h post transfection the cells were plated to measure reversion.

The flow cytometry analysis in figure 35 shows that induction of single or complex DSBs, with and without inhibitors, leaves unchanged cell cycle distribution 6 h (not shown) and 48 h post transfection. This is in agreement with the results shown above (figure 33 and 34). The absence cell cycle redistribution suggests that one or two DSBs alone are not sufficient for activating a visible checkpoint, even when one of the DSB repair pathways is compromised.

Incubation with NU7441 decreases the normalized reversion frequency after induction of single DSBs from 446 (DMSO gRNA#8) and 1367 (DMSO gRNA#11) to 233.93 and 456.75 respectively, a decrease of a factor of 1.9 and 2.99. Similar reductions were also noted for complex DSBs (2.59 times reduction of the normalized reversion frequency factor from 854 to 329). Similar results are obtained after induction of complex DSBs. This is in contrast to the results obtained

for the IR experiments after NU7441 treatment. It has been reported that high-LET radiation leads to a delayed DNA PKcs phosphorylation and repair compared to low-LET (Anderson 2010), and that inhibition of DNA PKcs may block DNA ends and inhibit thus HRR. Yet, DNA PKcs deficient cells (MO59J) lacking the protein show increase HRR, presumably because ends remain free for other pathways to operate on them. These suggest that the reduction observed in the presence of NU7741 reflect suppression of HRR events in SPD8 cells (Reynolds 2012). We further assume that the results with IR include a component of dose that will require further investigations.

KU55933, an ATM inhibitor, also reduces the reversion frequency by a factor of 2.73 and 3.62 after induction of single DSBs, and by a factor of 1.75 after induction of complex DSBs.

These results are again different from those obtained under similar conditions in cells exposed to IR. These differences may derive from the properties of IR that generate a broad spectrum of DNA damages, while the RNA guided nuclease induce specific DSBs within the *hprt* gene. The results with the CRISPR/Cas9 system suggest that ATM contributes to homologous recombination and therefore its inhibition suppresses reversion events in SPD8 cells.

In contrast to the NU7441 and KU55933, treatment with the ATR inhibitor VE821 increases the reversion frequency factor 2.76 and 1.39 times after induction of single DSBs, and by a factor of 2.15 times after induction of complex DSBs (figure 35). This indicates that ATR under these conditions suppressed homologous recombination. Notably, here again, the opposite effect was observed after exposure to IR. The differences observed may derive from the different type of DSBs generated by IR and nucleases, a role of PARP (D'Silva 1999), as well as by a different role of DNA replication in the outcome.

Incubation with PJ34, a Parp1 inhibitor, reveals no differences in the reversion frequency after single and complex DSB, and only gRNA#11 shows a small reduction by a factor of 1.88. The absence of an effect on the reversion frequency after PJ34 treatment is in agreement with the expectation that alt-EJ process do not support homologous recombination events.

To sum up, the experiments with IR may reflect indirect effects leading to reversion events, while the RNA guided nucleases generate direct effects and trigger homologous recombination. In the latter setting DNA PKcs and ATM enhanced, while ATR suppressed the homologous recombination events underlying the studied reversion.

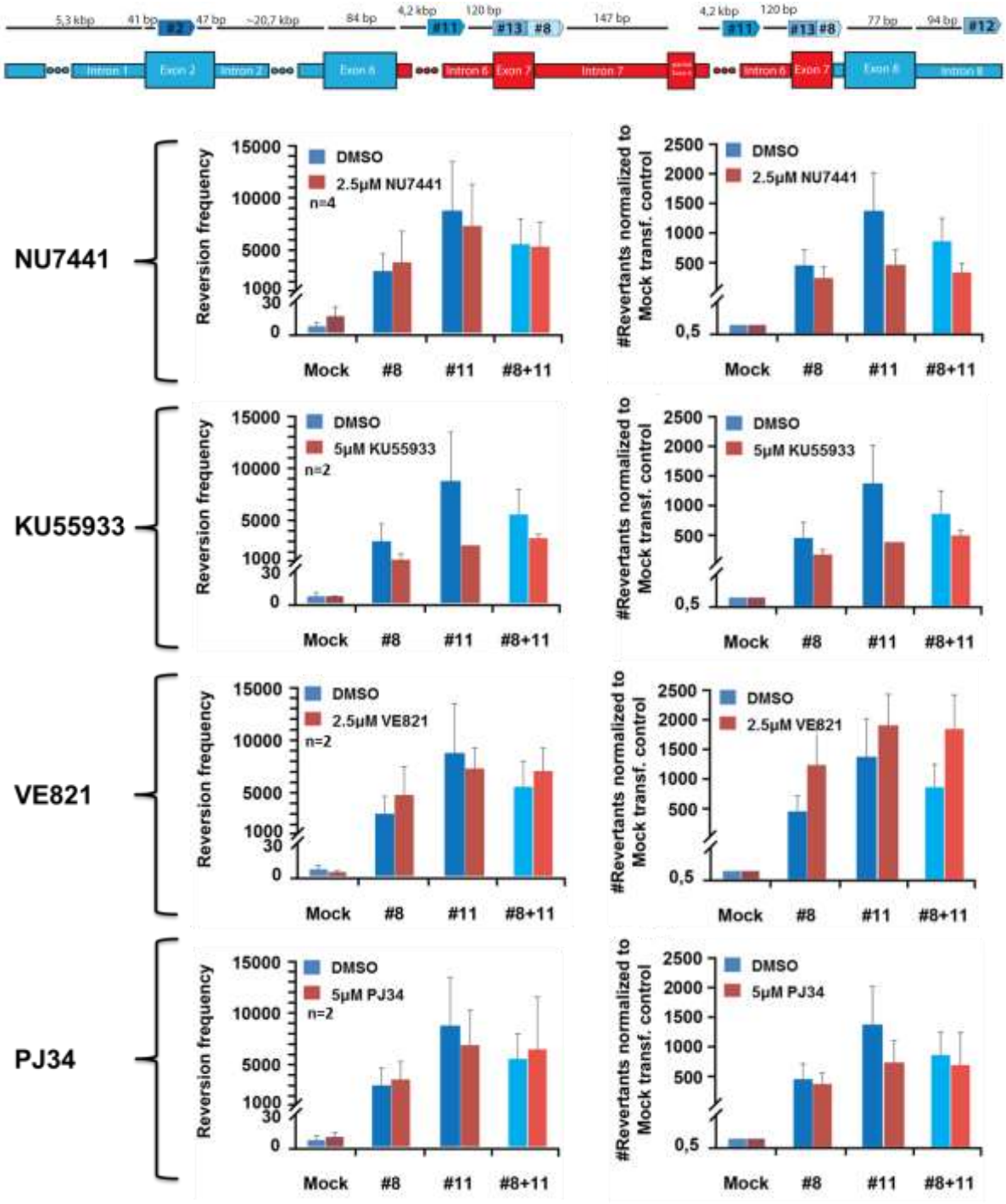

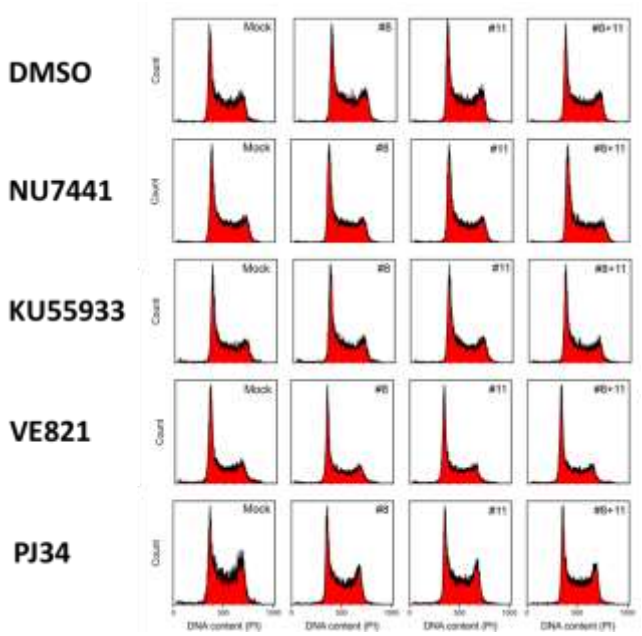

Figure 35: Effects of single DSBs or DSB cluster on the reversion frequency of SPD8 cells

Exponential growing SPD8 cells were transfected with different sets of gRNAs in conjunction with Cas9. In addition cells were transfected without gRNA as a control, and with GFP to measure transfection efficiency. For each transfection 1 µg plasmid per million cells was used. Immediately post transfection cells were plated for 48 h in media supplemented with DMSO, 2.5 µM NU7441, 2.5 µM VE821, 5 µM KU55933 and 5 µM PJ34. Other conditions were as described in figure 33. The cell cycle distribution was assayed by flow cytometry at 48 h after transfection. The reversion events measured were normalized to the mock transfected control (n=3 for NU7441, n=3 for VE821, n=2 for KU55933 and n=4 for PJ34). The data revealed for DNA PKcs and ATM inhibition a suppressive role in the recombination event after induction of single DSBs and DSB clusters.

3.1.4.2 The role of single DSBs and DSB clusters in the induction of reversion events in the SP5 mutant

3.1.4.2.1 Induction of DSBs within the mutated region of SP5 cells enhances the reversion frequency

Similar to the SPD8 mutant, we first examined in the SP5 mutant whether the induction of DSBs within the *hprt* gene, and even within the mutated region affects the reversion frequency. As mentioned above in the SP5 mutant restoration of *hprt* requires a non-homologous recombination event. We inquired how this kind of correction event is initiated, what role DSB complexity plays and how the different DSB repair pathways contribute.

To address the first question we designed gRNAs that recognize sequences within the duplicated region (gRNA#9: intron 1 and gRNA#2: exon 2) and outside of the mutated region (gRNA#8). gRNA#8 recognizes a sequence that is located approximately 25 kb downstream of the mutated region (exon 7/intron 7 junction). The exact recognition locations of the selected gRNAs are shown in figure 36.

To quantitate the reversion efficiency of CRISPR/Cas9 induced DSBs, exponentially growing SP5 cells were transfected with plasmids encoding for gRNA and Cas9 and assayed as described for the SPD8 mutant.

The cell cycle distribution was assayed at the time of transfection and ensured the exponentially growing character of the cells (not shown). Furthermore, cells were analyzed 48 h post-transfection to examine whether the treatment generates noticeable re-distribution of cells in the cell cycle. Such delays could be mediated from the DSBs induced, as well as from off-target DSBs. However, the cell cycle analysis in figure 36 reveals no effect of the treatment and the few DSBs generated on the distribution of cells throughout the cell cycle.

Figure 36 shows that generation of a DSB outside the mutated region of the *hprt* gene (gRNA#8) increases the reversion frequency up to a factor of 1.53 compared to the mock transfected control. However, a more pronounced effect was observed when the DSB was generated within the duplicated region of the *hprt* gene. The

transfection of gRNA#2, which recognizes exon 2 enhanced the reversion frequency by a factor of 70.49. Figure 36 shows that this effect is even more pronounced when intron 1 (gRNA#9) is targeted (increase by a factor of 277.53). Thus, interruptions in the mutated or even more so in the flanking region triggers the non-homologous recombination reversion event. We speculate that for a precise restoration of the *hprt* gene, DSBs in the exon flanking regions facilitate complete removal better than DSBs in the exon itself.

Based on the finding that DSBs in or near the mutated region enhance the reversion frequency in SP5 cells, experiments were carried out to address the question as to whether an increase in DSB complexity further enhances or suppresses this effect.

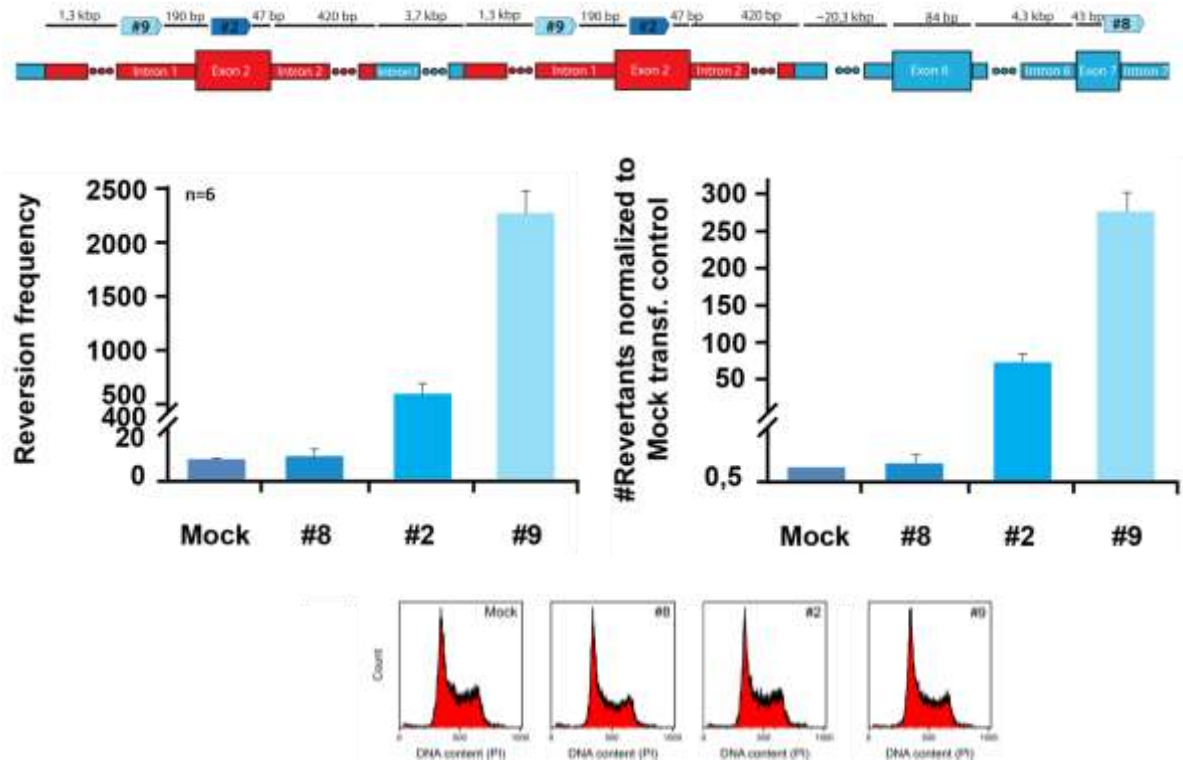

Figure 36: DSBs within the duplicated region of the *hprt* locus enhance the reversion frequency of SP5 cells

Guide RNAs (gRNAs) were designed to target specific locations within the *hprt* gene, mainly within the duplicated region, as well as outside of the mutated region of the SP5 mutant. The scheme above the graph indicates the mutated *hprt* gene of SP5 cells. The mutated region shows the duplication in red, the numbers in brackets (#9, #2 and #8 represent gRNAs that target sequences in intron 1, exon 2 and exon 7/intron 7 junction, respectively). Exponentially growing SP5 cells were cotransfected with Cas9 and gRNA8 (#8), gRNA2 (#2), gRNA9 (#9) or without gRNA as control (Mock). To determine transfection efficiency, cells were transfected with a GFP plasmid. The amount of plasmid DNA used for all transfections was 1 µg per million cells. 24 h post transfection the GFP transfected sample was assayed by flow cytometry. The other samples were plated 48 h post transfection in HAT selection media to determine revertant frequency and in growth media without selection to determine the plating efficiency. In addition cells were fixed in 70% ethanol and after a centrifugation and PI staining their cell cycle distribution was measured by flow cytometry. 7 – 10 d post seed colonies were stained with crystal violet and counted. The reversion frequency was calculated by considering the number of colonies formed in HAT selective media, the transfection efficiency and the plating efficiency. The experiments were carried out n = 6 times. Generation of DSBs within the duplicated region enhanced the frequency of the reversion events dramatically.

3.1.4.2.2 The role of DSB clusters in the reversion frequency of the SP5 mutant

We addressed the question whether DSB clusters at exon 2 enhance or suppress the correction frequency in the *hprt* gene. SP5 cells were cotransfected with gRNAs pairs (gRNA#9, gRNA#2) together with Cas9. The distance between the gRNA#9 and gRNA#2 generated DSBs is about 190 bp. Figure 37 shows that a DSB cluster within the mutated region decreases the reversion frequency compared to single gRNA#2 and gRNA#9 from a factor of 70.49 and 277.53 to 30.49. Such reduction in the presence of complex DSBs was not expected, as experiments with high-LET radiation showed an increase in the frequency of reversion events up to 4.54 times as compared to low LET radiation (see figure 24). We consider this difference to reflect the above discussed indirect role of DSBs in the reversion events of IR, in contrast to the direct role of DSBs generated by the Cas9 system (up to 18.9 rev./10^5 cells for high-LET, up to 2248 rev./10^5 cells for Cas9, see appendix). The reduction observed when DSB clusters were generated indicates that such lesions destabilize chromatin and suppress correction events. Once reversion is activated by a DSB within the mutated region, additional DSBs interfere with the reversion process and impede the recombination event leading to the correction of the *hprt* gene in the SP5 mutant.

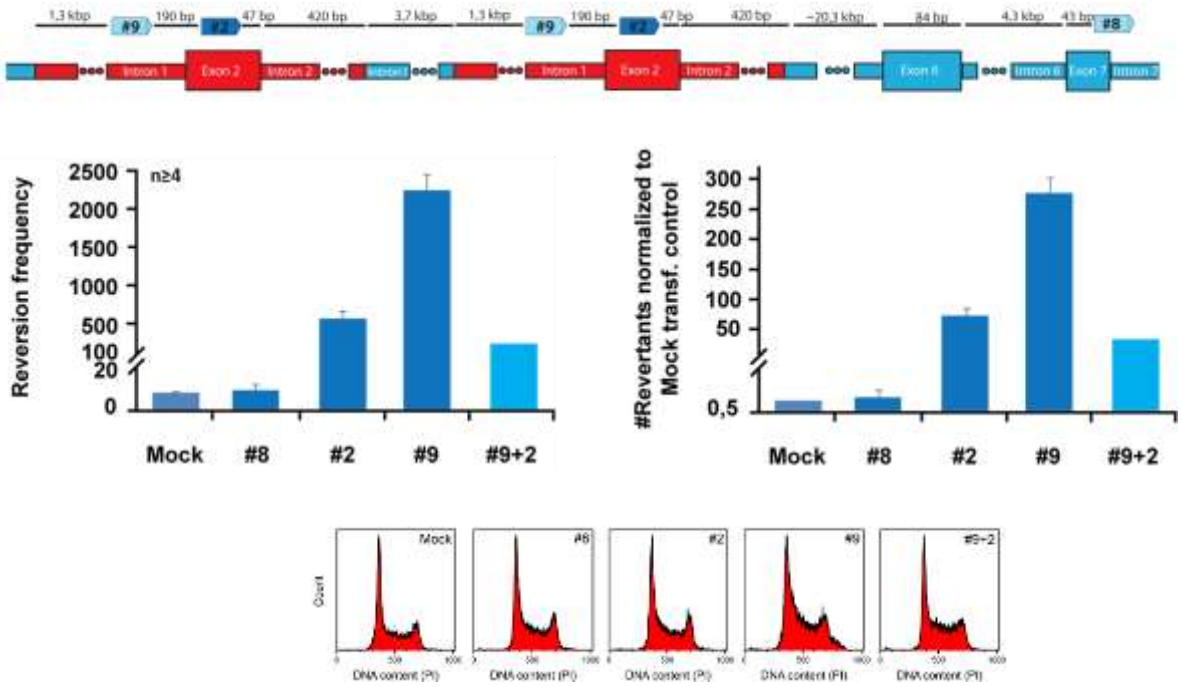

Figure 37: Effect of DSB clusters on the reversion frequency of SP5 cells

SP5 cells were transfected with single and double gRNAs in conjunction with Cas9. In addition cells were transfected without gRNA as control and with GFP to determine transfection efficiency. For each transfection 1 µg plasmid per million cells was used. The transfected cells were plated after 48 h and treated as described in figure 36. The cell cycle distribution was assayed by flow cytometry at the time of transfection (not shown) and 48 h later. Reversion events were normalized to the mock transfected control (n ≥ 4 for single transfections, n = 1 for cotransfections). The analysis of the data reveals a pronounced difference between mock transfected control and the #2, #9 and #9+2 combinations.

3.1.4.2.3 Role of DSB repair pathways in the reversion frequency of the SP5 mutant in the presence of single DSBs and DSB clusters

The generation of single DSBs and DSB clusters within the duplicated region of the *hprt* gene in the SP5 mutant increased the reversion frequency as compared to the mock transfected controls. We wished to determine the role of DSB repair pathways in this effect. SP5 cells were transfected with Cas9 and gRNAs, as described in the previous experiment, with the difference that cells were plated post transfection for 48 h in media supplemented with DMSO, NU7441 (2.5 µM),

KU55933 (5 µM), VE821 (2.5 µM) and PJ34 (5 µM) before determination of reversion frequency and plating efficiency.

The flow cytometry analysis in figure 38 shows that induction of single and complex DSBs, with or without inhibitor, does not affect cell cycle distribution 48 h post transfection. This is in agreement the results presented above (figure 36 and 37).

Figure 38 shows that DNA PKcs inhibitor treatment increases the reversion frequency factor 1.56 (gRNA#2) and 1.58 (gRNA#9) times after induction of single DSBs but not after DSB clusters (#2+#9) as compared to the normalized DMSO control. This indicates that inhibition of DNA PKcs facilitates reversion in the SP5 mutant suggesting that D-NHEJ is not as efficient in the generation of reversions as the pathways remaining active after its inhibition. Inhibition of ATR shows no effect in the reversion frequency after induction of single DSBs (difference of the factor 1.11 for gRNA#2 and 1.15 for gRNA#9), or DSB clusters (difference of the factor of 1.3 for gRNA#2+#9) as compared to the DMSO data (figure 38). This result is different from IR experiments in which VE821 treatment reduced reversion frequency, but as discussed above this most likely reflects secondary effects.

In contrast to ATR, ATM inhibition reduces reversion by 0.64 (gRNA#2) and 0.42 (gRNA#9) after induction of single DSBs and DSB clusters, respectively, as compared to DMSO treated cells. The difference observed after induction of DSB clusters (gRNA#2+#9) is considered within the range of statistical fluctuations.

The function of ATR becomes prominent after resection and causes down-regulation of ATM (Shiotani 2009). Therefore we assume that in the blunt ended DSBs induction ATM plays a more important role in the correction of the non-homologous recombination events. Correction in the *hprt* gene is unlikely after resection.

PJ34 shows no effect on reversion frequency after single DSBs, but an increase at DSB clusters (gRNA#2+#9) compared to the normalized DMSO data. This indicates that DSB clusters utilize alt-EJ for *hprt* correction.

These experiments show that DNA PKcs suppress and ATM enhances non-homologous recombination correction events at the *hprt* locus after induction of single DSBs. At DSB clusters only PARP affects the recombination events.

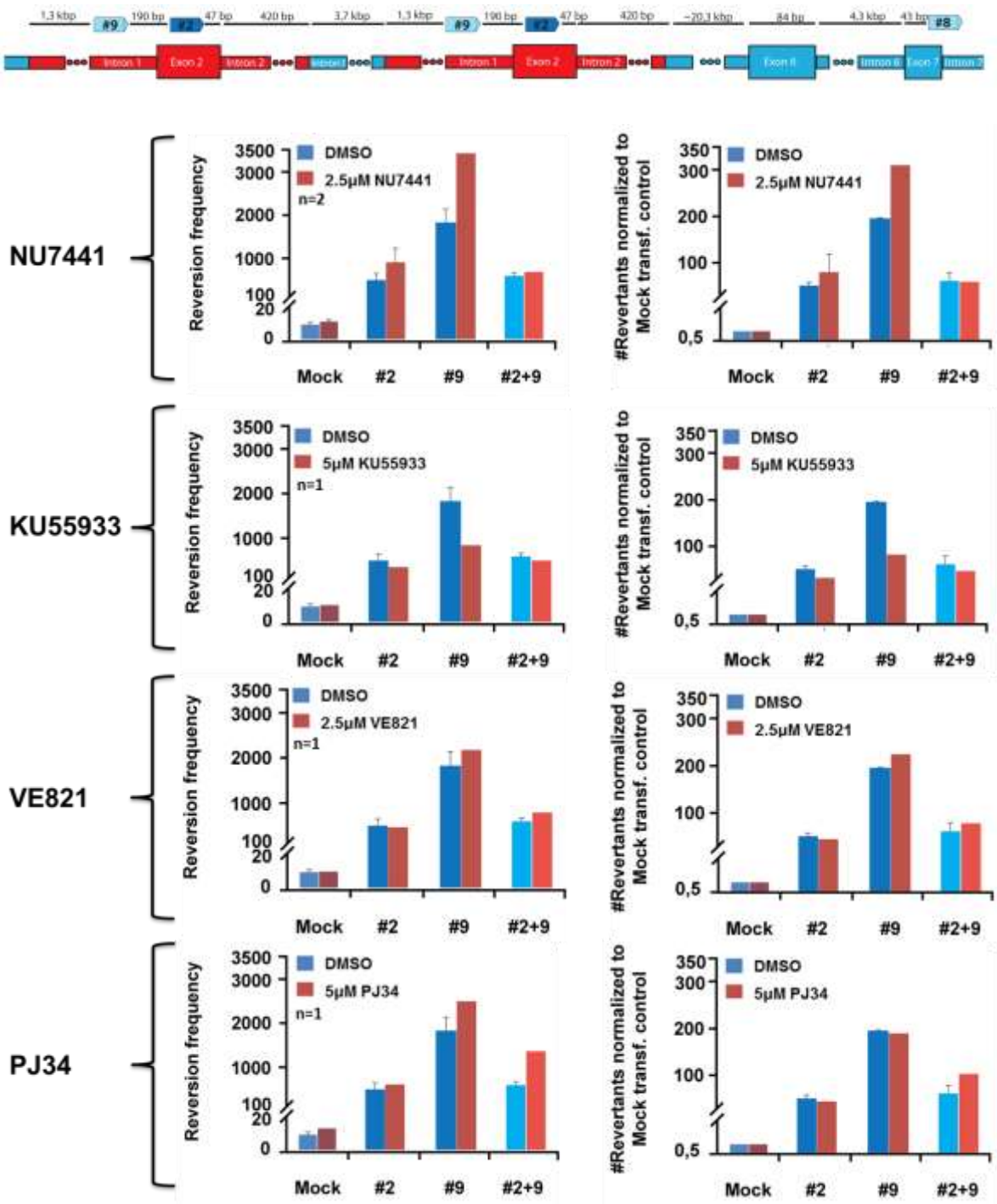
NU7441
KU55933
VE821
PJ34
Reversion frequency
#Revertants normalized to Mock transf. control
DMSO
2.5µM NU7441
n=2
5µM KU55933
n=1
2.5µM VE821
n=1
5µM PJ34
n=1
Mock
#2
#9
#2+9

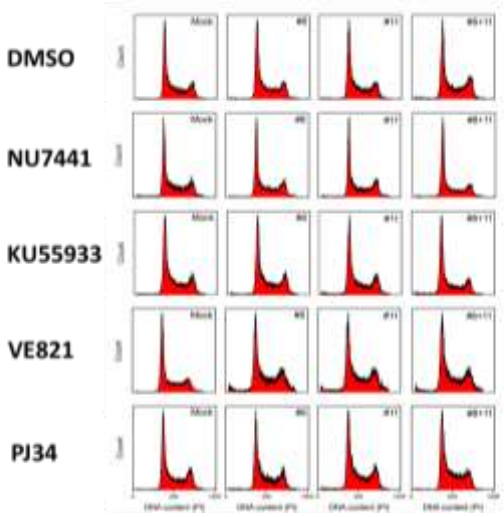

Figure 38: Role of DSB repair pathways on the reversion frequency in the SP5 mutant after induction of single DSBs and DSB clusters

Exponentially growing SP5 cells were transfected with different sets of gRNAs in conjunction with Cas9. In addition cells were transfected without gRNA as control, and with a GFP expressing plasmid as transfection efficiency control. For each transfection 1 µg plasmid per million cells was used. Immediately post transfection cells were plated for 48 h in media supplemented with DMSO, 2.5 µM NU7441, 2.5 µM VE821, 5 µM KU55933 and 5 µM PJ34. Other experimental details were as described in figure 36. Cell cycle distribution was assayed by flow cytometry 48 h after transfection. Reversion events were normalized to the mock transfected control (n = 1 for each inhibitor treatment). The analysis reveals a stimulating role for ATM and suppressive role for DNA PKcs in *hprt* reversion after induction of single DSBs. PJ34 affects the reversion frequency mediated by DSB clusters.

3.2 Mutations at the *hprt* locus by direct induction of DSBs

Mutations evolve spontaneously by endogenous processes like stalled or collapsed replication forks, oxygen radicals as byproducts of the metabolism, or by exogenous insults such as chemotherapeutic agents or IR. Mutations that cause a loss of function of the *hprt* gene can be selected in a forward mutation assay. In the forward mutation selection technique, a purine analogue like 6TG is administrated, which mimics the guanine purine substrate of HPRT. Cells that express a functional

HPRT protein incorporate 6TG into DNA and die, while HPRT deficient cells survive.

We speculated that the generation of DSBs or DSB clusters at the *hprt* gene will enhance mutagenesis. To test this assumption, Chinese hamster V79 cells were used in conjunction with the CRISPR/Cas9 technology.

3.2.1 Mutation induction at the *hprt* locus by single DSBs

The RNA guided nuclease technique described above was used to induce DSBs in V79 wild type cells (figure 39). Cells were transfected with gRNAs together with Cas9. The experiment design was similar to that employed in the SPD8 and SP5 mutants with the difference that cells were routinely cultivated in regular growth media instead of 6TG-containing media and that for selection cells were plated in growth media supplemented with 6TG 84 h after transfection. Mutation induction was calculated by the frequency of 6TG resistant ($6TG^{res}$) cells, the transfection efficiency measured by GFP analysis, and the plating efficiency.

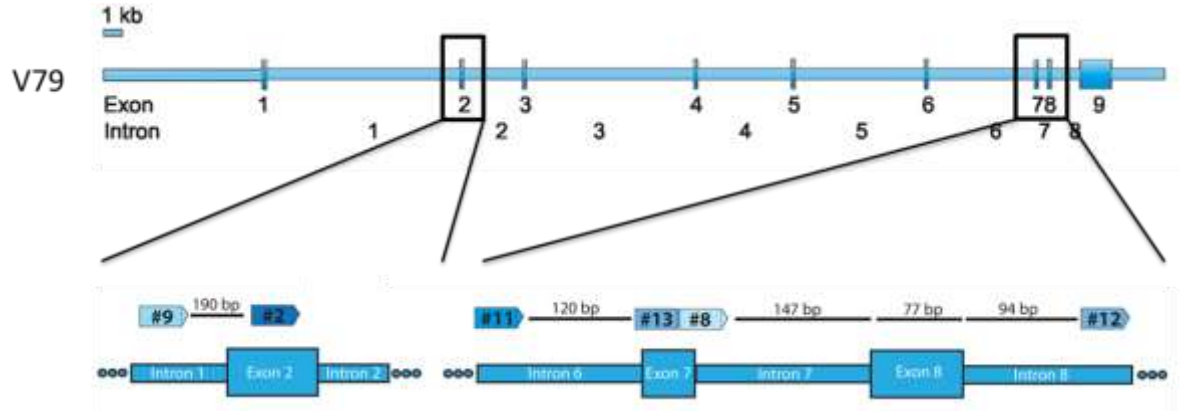

Figure 39: Schematic overview of the gRNAs used to induce DSBs at the *hprt* locus of V79 cells

Figure 40 shows that induction of DSBs in all regions within the *hprt* gene increase the 6TG^{res} frequency. The mutation frequency is different for DSBs generated within an intron or an exon. While a DSB in an intron or exon/intron junction region increases the 6TG^{res} mutation frequency by a factor of 11 - 17, DSBs induced specifically in exon regions (gRNA#2, gRNA#13) shows increases by a factor of 56.92 and 65.91, respectively. Similar to the observations with the SPD8 and SP5 mutants, induction of DSBs by Cas9 in V79 cells has no effect on the cell cycle distribution (figure 40).

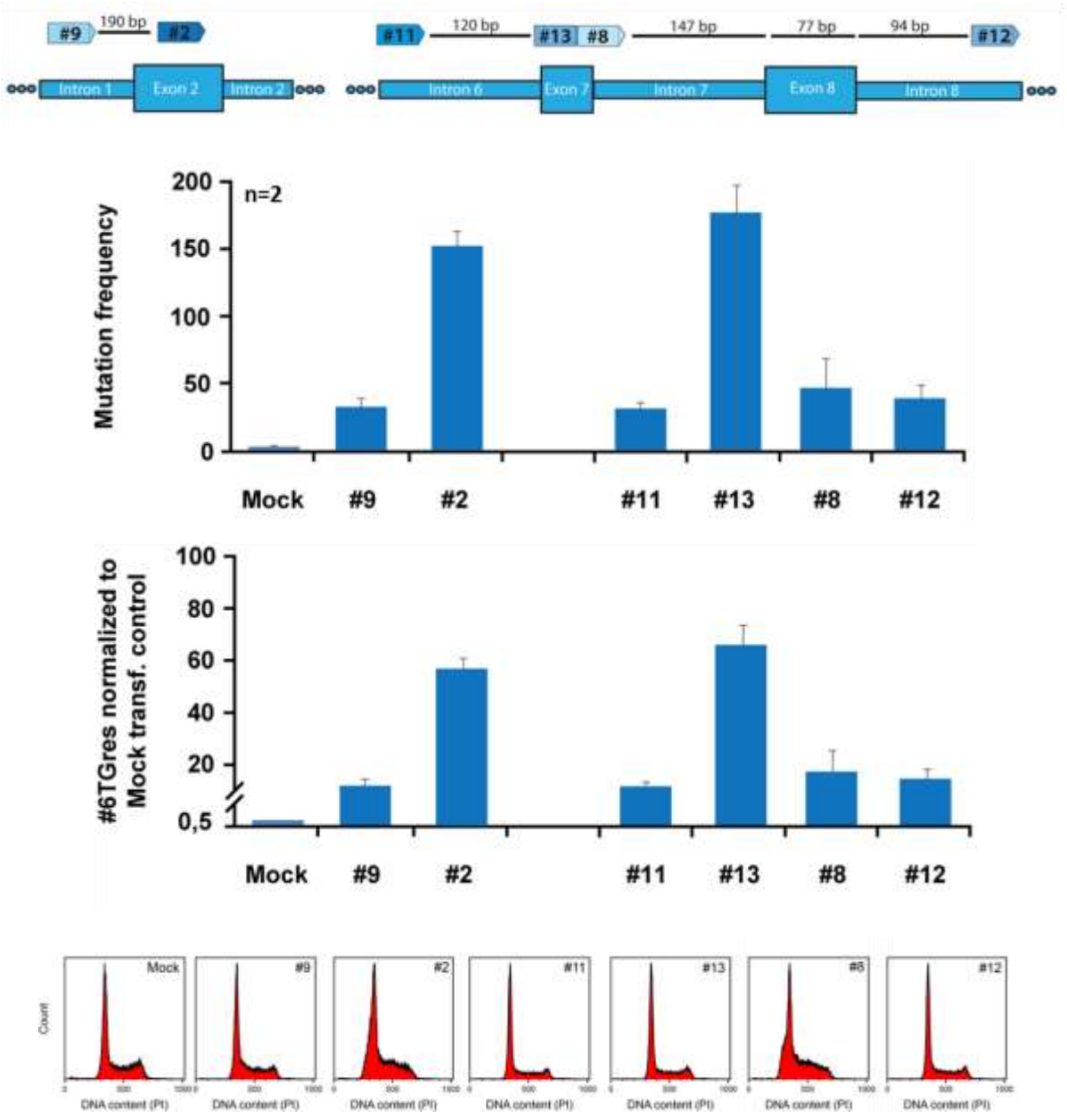

Figure 40: Induction of DSBs by Cas9 increase the mutation frequency in V79 cells

Exponentially growing V79 cells were cotransfected with Cas9 and gRNA9 (#9), gRNA2 (#2), gRNA11 (#11), gRNA13 (#13), gRNA8 (#8), gRNA12 (#12), or without gRNA as control (Mock). In addition cells were transfected with a GFP plasmid and incubated for 24 h to measure transfection efficiency. For each transfection 1 µg plasmid per million cells was used. The cells were plated 84 h post transfection in 6TG selection media to determine the $6TG^{res}$ cells and in growth media without selection to determine the plating efficiency. The cell cycle distribution was assayed by PI staining and flow cytometry. 7 d and 10 d post seeding colonies were stained with crystal violet and counted for plating efficiency and $6TG^{res}$, respectively. The $6TG^{res}$ frequency was calculated by considering the number of colonies formed in 6TG selective media, the transfection efficiency measured by GFP expression and the plating efficiency. The experiments were carried out n=2 times. The generation of a DSB in introns, and more pronouncedly in exons, enhanced mutation frequency in the *hprt* gene.

3.2.3 Induction DSB clusters at the *hprt* locus enhances mutation frequency

The results above show that DSBs increase the probability of mutations at the *hprt* locus. We inquired whether DSB clusters will enhance this effect. The presence of DSB clusters often requires different repair pathways that may be more error prone.

To examine mutagenesis of DSB clusters in V79 cells, we cotransfected gRNAs and Cas9. Figure 41 shows that the induction of DSB clusters flanking the exon 7 region (gRNAs#11+8) increases the mutation frequency by the factor 45.31 compared to the mock transfected control while single DSBs increased mutation frequency by a factor of 17.22 (gRNA#8) and 11.23 (gRNA#11). This effect becomes stronger after induction of DSB clusters flanking exon 8 (factor of 61.79, gRNAs#12+8), and is even more pronounced when exon 7 and exon 8 are removed together by the appropriate DSB clusters (factor of 80.89, gRNAs#11+12). In contrast, induction of DSB clusters that flank a portion of the exon region does not cause further increase compared to the single DSBs. Flow cytometry reveals, similar to the previous experiments, no detectable redistribution of cells in the cell cycle (figure 41).

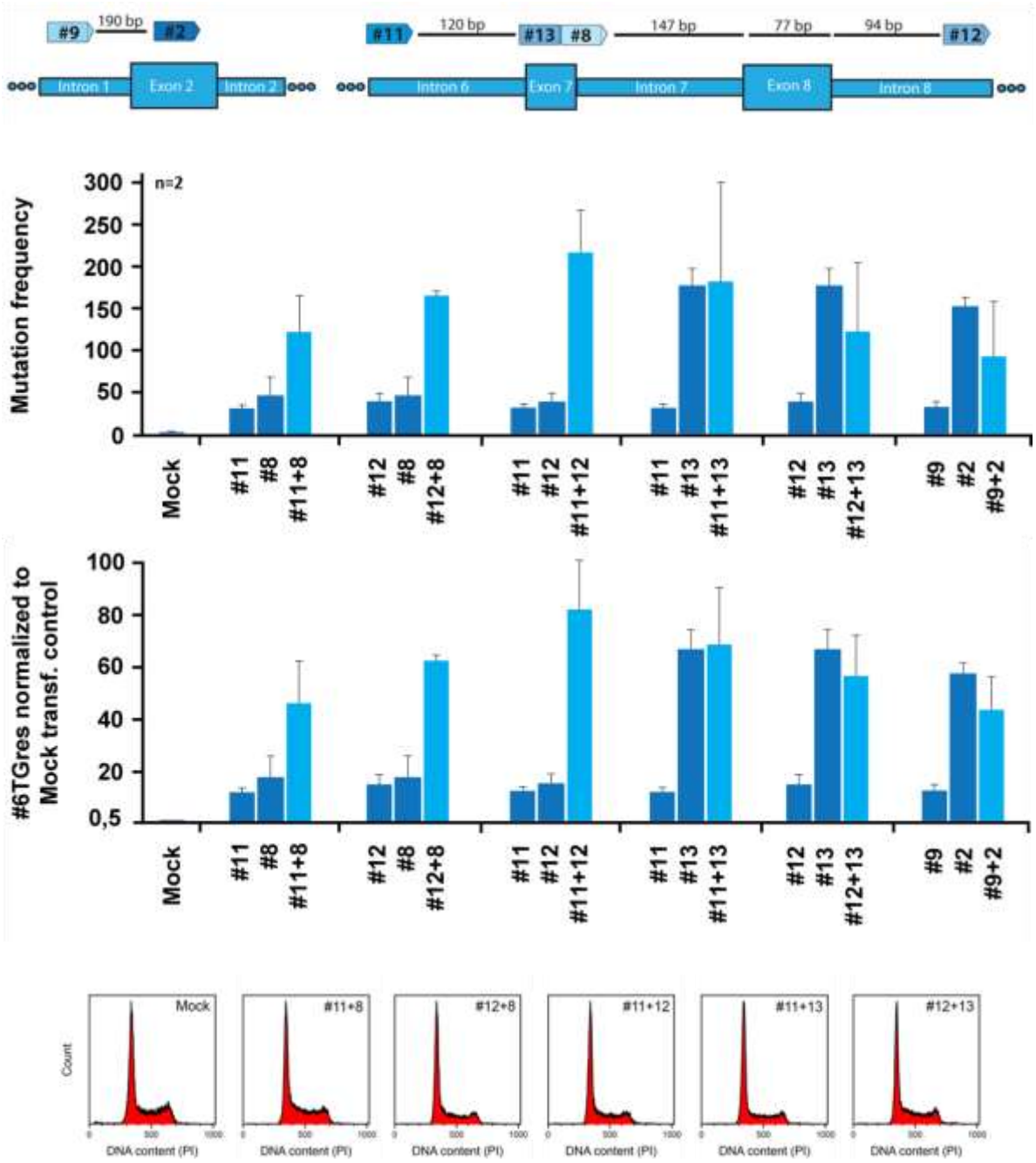

Figure 41: Induction of DSB clusters enhances mutagenesis at the *hprt* locus

V79 cells were transfected with Cas9 together with either one or two gRNAs, or without gRNA as a control (Mock). Analysis of the transfection efficiency and cell cycle distribution was carried out by flow cytometry. For each transfection 1 µg plasmid per million cells was used. Generation and analysis of the 6TG^{res} cells was as described in figure 40. The experiments were carried out n = 2. The cell cycle phases remain unchanged by the associated treatments. Induction of DSB clusters enhances mutation frequency, more pronouncedly when removing whole exons.

3.2.4 Role of DSB repair pathways in *hprt* mutagenesis by single DSBs and DSB clusters

The results above showed that an increase in DSB complexity enhances mutation induction. We speculated that these mutations were the result of error prone DSB repair pathways. To test this and to assess the role of DSB repair pathways in mutagenesis for DSBs of different complexity, V79 cells were transfected with single (gRNA#8, gRNA#11) and double gRNAs (#8+#11) in conjunction with Cas9. Immediately after transfection the cells were plated into media containing DMSO, NU7441 (2.5 µM), KU55933 (5 µM), VE821 (2.5 µM) and PJ34 (5 µM). After 84 h cells were collected and plated according to the $6TG^{res}$ selection protocol. The induction of single DSBs and DSB clusters, with or without inhibitor, has no effect on cell cycle distribution (figure 42).

NU7441 has no effect on mutation frequency after induction of single DSBs, but increases mutation frequency after induction of DSB clusters from a factor of 41 to 470 as compared to the normalized DMSO data. This indicates a protective role for D-NHEJ in the mutagenesis development at complex DSBs that was not expected since D-NHEJ is known to be an error prone repair pathway. However the presence of D-NHEJ factors was shown to suppress a more severely error-prone repair pathway, alt-EJ. Therefore we assume that in the absence of D-NHEJ factors, alt-EJ gains ground. This explains also why mutation induction decreases after induction of single DSBs or DSB clusters in PJ34 treated cells. This shows that in the absence of alt-EJ fewer mutations are forming.

Beside these two error prone repair pathways we examined the error free repair pathway HRR. We expected that in the absence of ATM and ATR activities, which are assumed to affect HRR, the mutation frequency will increase. Surprisingly, figure 42 shows that ATM and ATR inhibition decreases the mutation frequency both after induction of single DSBs and of DSB clusters. However since ATM and ATR have many other functions in the cell and are not involved in HRR exclusively, we assume that HRR most likely does not play a major role in the mutagenesis events recorded here.

Our experiments showed that D-NHEJ reduces the mutation frequency at complex DSBs, which implies that D-NHEJ has a protective role for genome maintenance

and stability. The repair of a DSB via alt-EJ, on the other hand, enhanced mutation induction and contributed to DSB-induced mutagenesis.

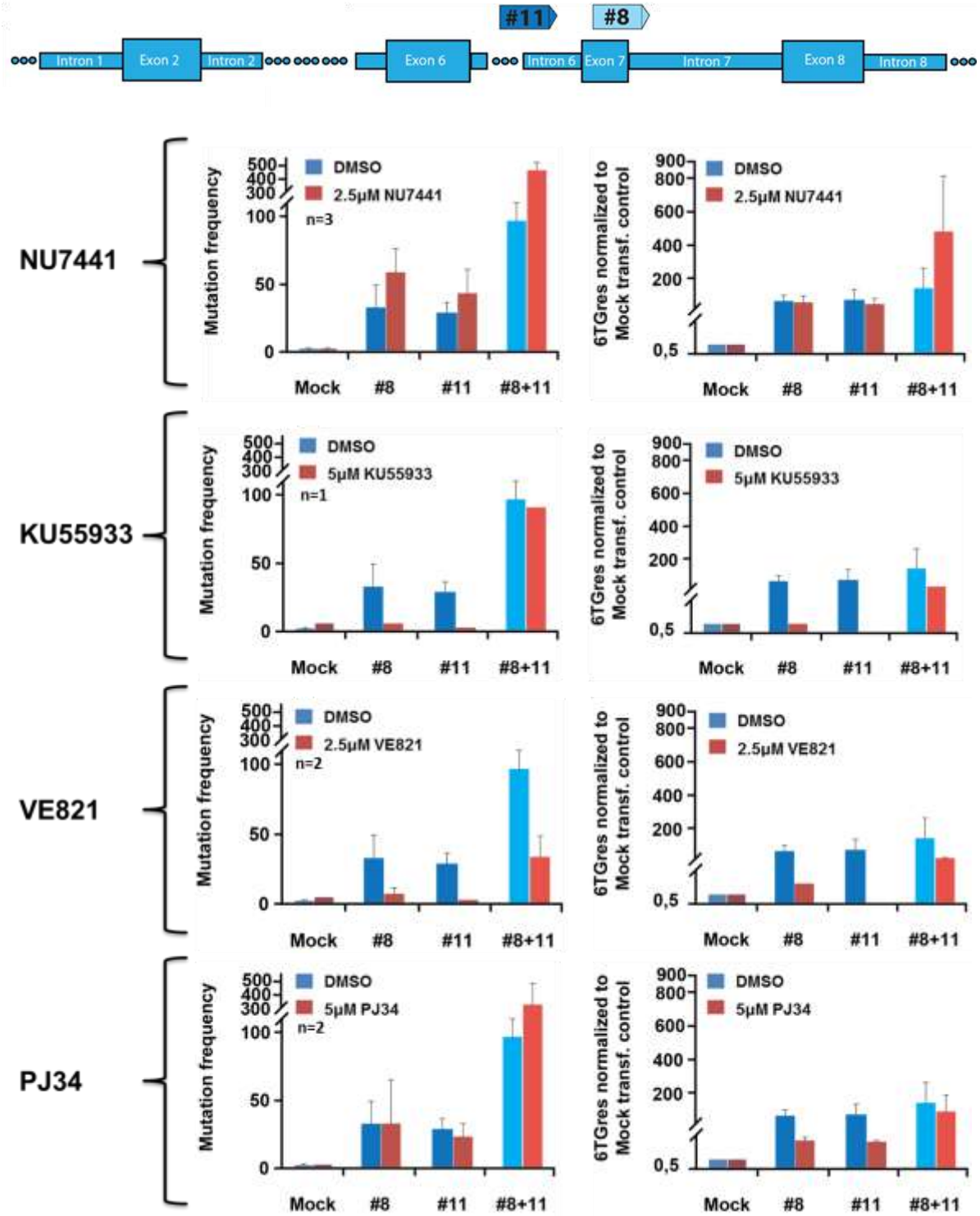

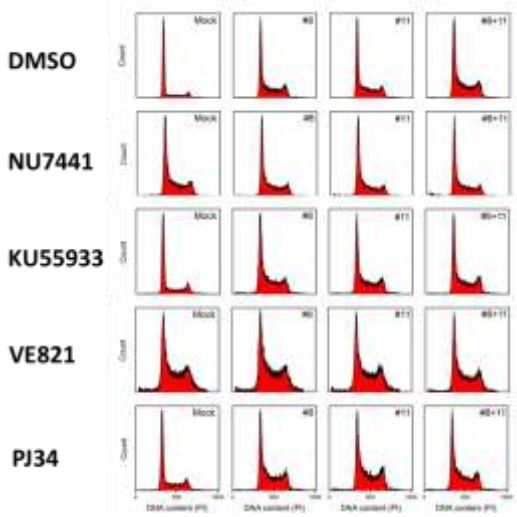

Figure 42: The role of the DSB repair pathways in *hprt* mutation after induction of single DSBs and DSB clusters

V79 cells were transfected with different sets of gRNAs (gRNA#8, gRNA#11, gRNA#8+gRNA#11) together with Cas9. In addition cells were transfection without gRNA as a control, and with GFP as transfection efficiency control. For each transfection 1 µg plasmid per million cells was used. Immediately post transfection cells were grown for 84 h in media supplemented with DMSO, 2.5 µM NU7441, 2.5 µM VE821, 5 µM KU55933 or 5 µM PJ34. Subsequently, cells were plated and mutation frequency determined according to the protocol described in figure 40. The cell cycle distribution was assayed by flow cytometry 84 h after transfection. $6TG^{res}$ mutant frequency was normalized to mock transfected controls (n=3 for NU7441, n=2 for VE821, n=1 for KU55933 and n=2 for PJ34). We observe a stimulating role in mutation induction for ATM, ATR and PARP at single DSBs, while DNA PKcs shows an effect at complex DSBs.

4 Discussion

4.1 Homologous and non-homologous recombination events at *hprt* locus of Chinese hamster mutant cell lines SPD8 and SP5 as a model system to investigate the effects of DSB clustering.

4.1.1 Reverse mutation assay as a tool for the analysis of the biological effects of DSBs

Aim of the present study was to examine the contribution of DSBs of different complexity and of the repair pathways involved in their processing to DNA integrity. We addressed this aim by applying the reverse mutation assay in Chinese hamster *hprt* mutant cell lines (SPD8, SP5), and the forward mutation assay in the Chinese hamster wild type cell line V79. The adapted reverse mutation assay was used to examine the contribution of single DSBs and of DSB clusters to the reversion events, as well as the role of DSB repair pathways in this endpoint. Since reversion events required homologous or non-homologous recombination in SPD8 and SP5 cells, respectively, specific reactions on the DNA could be studies. The forward mutation assay in V79 cells, on the other hand, was used to examine the effect of single DSBs and of DSB clustering on error-prone repair of DSBs.

In the first part of the thesis we used IR of different LET. Low-LET (X-rays) and high-LET (^{241}Am α and ^{56}Fe ions) radiation modalities were chosen to evaluate the effects of the generated DNA damage on the reversion frequency. We demonstrated a 3-fold increase of the biological effect on cell survival for high-LET radiation as compared to low-LET radiation (X-rays) (figure 21). The stronger cell killing potential of high-LET radiation is in line with numerous studies and is explained by the increase in the density of the generated ionizations that cause more complex clustered damage sites than sparsely ionizing low-LET radiation (Hall 2006). CDS and also expected DSB clusters, generate conditions where repair accidents will lead to erroneous repair and thus to cell death. In the case of clustered damage including base damage, it is possible that activation of two or more repair pathways (like base damage repair and DSB repair pathways) within

the limited space of the ionization cluster impedes the function of one or both, and thus it leads eventually to miss-repair events. Since complex DSB clusters are forming after exposure to high LET radiation more likely than after low-LET radiation, a stronger biological effect is expected when using the former radiation modality and this is what the results obtained also demonstrate. In the case of DSB clusters, it is likely that during repair the intervening DNA fragments are lost, exacerbating the radiation effect.

To examine how the restoration of the mutated *hprt* gene takes place in the presence of DSBs of increasing complexity, we introduced the SPD8 and SP5 mutants. In this assay, the spontaneous correction frequency is very low (of the order of magnitude of 10^{-5}) and can be enhanced by diverse DNA damaging agents.

The SPD8 and SP5 mutants showed in our experiments a spontaneous reversion frequency of 0.93±0.13 revertants for 10^5 cells (rev/cells), and of 2.99±0.55 rev/10^5 cells, respectively. These frequencies are close to those reported in the literature (1.5 - 2.7 rev /10^5 cells for SPD8 (Dare 1996, Helleday 1998b) and 3.7±0.9 rev/10^5 cells for SP5 cells, respectively (Dare 1996)). The small differences observed in spontaneous frequency of reversion may derive from differences in the growth conditions.

The validation of the reversion assay was performed using MMC treatment (figure 22). After administration of MMC, the frequency of reversion events increased in both mutants, as it is also described in the literature. The DNA cross linker MMC inhibits DNA replication, which results in blocked or collapsed replication forks and possibly also in the formation of DSBs that initiate reversion (Al-Minawi 2009). However, it is also possible that the increased reversion frequency in the SPD8 and SP5 mutants after MMC treatment is caused by the increased recruitment and activation of repair factors in the proximity to the *hprt* gene. The presence of DNA repair factors may facilitate the DNA recombination processes required for reversion. However, MMC treatment does not directly generate DSBs, therefore an interpretation regarding the possible role of DSBs in reversion is not possible. For such analysis we performed similar experiments using different IR modalities.

4.1.2 The role of DSB repair pathways in reversion events at the *hprt* locus

DSBs are considered the initial step in activation of homologous and non-homologous recombination events causing correction in the SPD8 and SP5 mutants. To address the first aim of the present thesis, we focused on DSB complexity as generated by low and high-LET radiation modalities and examined their impact on reversion. The results of our experiments demonstrated that increase in DSB load and increase in the complexity of DSBs, both increase the frequency of reversion in both mutants (figure 23, figure 24). The increased reversion frequency at higher doses of low-LET and most prominently at high-LET radiation may derive from the fact more DSBs form in the cell.

The effect of DSB complexity on the reversion events can also be explained when we consider the characteristics of the *hprt* gene and emphasizing its early expression properties. Highly expressed genes are known to be clustered in specific regions of chromosomes, termed regions of increased gene expression (RIDGEs) (Falk 2010). In these regions chromatin structure is less condensed. This could enhance the accessibility to DSBs of repair factors, increasing thus the probability of reversion.

The observed effect after exposure to IR is, however, small compared to the background frequency of reversion. This can be explained by the relatively low probability of IR to directly hit the *hprt* gene in the range of doses where reversion analysis is possible. This complication is further enhanced after exposure to high-LET radiation. And yet more reversion events were found after exposure to high LET radiation: We attribute this to the formation of complex DNA damages. The likelihood for a dose of 1 Gy X-rays to generate a DSB at the *hprt* locus is according to the calculations shown in Appendix 7.9 3.1 times in ten thousand. However, the reversion events were found at an even lower frequency after irradiation due to the fact that only very few cells eventually revert. Despite this low probability to hit the *hprt* locus we saw increase in reversion with increasing radiation dose (figure 23; figure 24).

This observed increase in reversion events with increasing radiation dose is in agreement with published studies. In these studies a 2.3-fold increase in the

reversion frequency was found for SPD8 cells after exposure to 3 Gy ɣ-rays (Helleday 1998b), while for SP5 the smaller induction of revertants (1.77 times increase) was found at a similar radiation dose (Zhang 1994). In another study, the same group showed that in SP5 cells exposed to ɣ-rays, reversion frequencies at least two times higher than the background reversion frequency could be measured (Zhang 1992a). The interpretations regarding the mechanisms supporting the recombination events underpinning reversion in the SPD8 and SP5 mutants also vary in literature (Lundin 2002, Fathers 2012, Growth 2012).

Considering the much higher levels of reversion observed using the CRISPR/Cas9 system, we think that our IR results are difficult to interpret conclusively. However, the results obtained suggest that high-LET radiation, i.e. more complex damage, results in increased frequency of reversion. However, we cannot exclude that these effects do not reflect direct damage in the *hprt* gene, but rather to indirect effects.

We also addressed the role of different DSB repair pathways in the induction of reversion events at the *hprt* gene using specific inhibitors and different modalities of IR. For this purpose, specific DNA repair inhibitors were administrated prior to irradiation to inhibit key factors of specific DSB repair pathways. We observed that inhibition of diverse DSB repair pathways only has minor effects on reversion frequency after exposure to both low and high-LET radiations. This further supports the postulate that the observed reversion events are indirect. Since under these conditions the results cannot be interpreted, the results obtained are not discussed further here.

To examine the role of DSB complexity and of DSB repair pathways on reversion at the *hprt* locus in more detail, another approach was taken using RNA guided nucleases to induced DSBs at precisely selected locations in the genome (see 4.1.3.2-4).

4.1.3 Biological consequences of DSBs induced at specific locations in the genome using RNA guided nucleases

4.1.3.1 Reversion events by DSBs generated by Cas9 reveal hot spots at the *hprt* gene in the SPD8 and SP5 mutants

To further investigate the role of DSBs of different complexity and of DSB repair pathways on *hprt* reversion, an RNA guided nuclease technique was adapted. This method allowed us to induce DSBs at specific locations within the *hprt* gene and to simulate DNA damage complexity by inducing DSB clusters.

Our experiments with single DSBs induced at specific locations of the *hprt* gene clearly demonstrated that DSB formation within the locus triggers reversion events with an astonishing frequency (figure 33, figure 36). Moreover, we were able to demonstrate that a DSB within the duplicated exon in these mutants is less likely to cause reversion than a DSB induced in the nearby intron. The pronounced increase in reversion frequency after formation of a DSB at the intron suggests that complete loss of an exon is more beneficial than the generation of a non-functional exon.

Furthermore, we could demonstrate a remarkable increase in reversion frequency after specific DSB induction, as compared to the frequency of reversion events generated after exposure to IR. The reversion events obtained by generation of DSBs within the mutated *hprt* gene are up to 1327- and 277-fold above background in SPD8 and SP5 cells, respectively (figure 34, figure 37). On the other hand, IR induced reversion events are 1.96 – 2.54-fold above background in SPD8 cells (figure 23); and 2.52 - 4.45-fold above background in SP5 cells (figure 24).

This level of differences supports the assumption that IR-induced reversions are not the result of direct hits in the *hprt* gene. While IR generates in addition to modified two ended DSBs, plenty of other modifications like oxidations, base damages or protein-DNA crosslinks, as well as single-stranded breaks, the CRISPR/Cas9 system induces only blunt ended DSBs at the selected genomic locations. One study showed that repair factors are recruited with different affinities to the break site in the presence of blunt or single-base overhangs (D'Silva 1999).

Thus, the type of DSB is important in the coordination of the repair reaction. For example, a clean DSB with compatible ends does not necessarily require additional processing, and may therefore result in different forms of signaling than DSBs with incompatible or modified ends.

In the case of CRISPR/Cas9 system, DSBs are generated through a collaboration of the expressed gRNA and the Cas9 nuclease. A factor that may contribute here to the reversion frequency is the gRNA recognition and the nuclease activity. To prevent off-target sequence recognition, we utilized gRNAs designed to recognize unique sequences that are not present at any another location within the hamster genome. Our cell cycle analysis did not show significant differences after gRNA transfection compared to control transfected cells. Thus, the designed gRNAs are unlikely to generate significant off-target effects. For a more specific validation of the functionality of the designed gRNAs, the surveyor assay or ligation mediated PCR can be used.

Due to the presence of duplications in the *hprt* gene of the SPD8 and SP5 mutants, our gRNA and Cas9 generates two breaks one in normal and one in the duplicated region of the allele. We assume that for gRNAs with this property, loss of the intervening fragment between the two DSBs will occur. This aspect will require further investigations.

Studies revealed that homologous and non-homologous recombination events cause the reversions measured in the SPD8 and SP5 mutants, respectively (Dare 1996, Helleday 1998a, Arnaudeau 2001, Lundin 2002). These groups examined the sequence of revertants generated after various treatments and found in all cases a complete restoration of the wild type gene. Such validation of revertants was not carried out here, but we assume that it reflects complete restoration of the gene as well.

We also addressed the question as to whether increased DSB complexity in the form of DSB clusters influences the reversion rate in the SPD8 and SP5 mutants. For this purpose, we generated gRNAs, which induce Cas9 DSBs in close proximity. We have shown for both mutants that DSB clusters suppress reversion (figure 34, figure 37).

Despite the results obtained with IR, in which increased doses or increased LET enhanced the reversion events (figure 23; figure 24), DSB clusters generated within the mutated *hprt* gene showed the opposite effect (figure 34; figure 37) as compared to single DSBs (figure 33; figure 36). In the case of IR induced damages we speculated that the increased reversion at complex DSBs derives from structural changes in the DNA and an increased accessibility of repair factors near the *hprt* gene. However, the CRISPR/Cas9 technology allowed us to conclusively address this question and to demonstrate that the specific genomic location of single DSBs strongly affects the frequency of correction and that DSB clusters have a negative influence in this correction.

The reduction in the frequency of reversion observed at complex DSBs can be explained by assuming that DSB clusters destabilize chromatin and compromise the DSB repair pathways catalyzing reversion in SPD8 and SP5 cells. It is relevant to point out that reversion events in these mutants require precise genomic modifications that may be generated with reasonable likelihood by HRR and D-NHEJ. They are unlikely to be generated by alt-EJ which may be a likely choice after chromatin destabilization. We conclude that the recombination mechanism in the SPD8 and SP5 mutants is effectively initiated by a DSB within the mutated region and that additional damages in close proximity, interfere with a faithful restoration of the *hprt* gene. This demonstrates that DSB clusters have more severe biological consequences than single DSBs.

4.1.3.2 The role of DSB repair pathways in reversion events of the *hprt* gene

To investigate how DSB repair pathways contribute to the repair of simple or clustered DSBs (aim 6), specific DNA repair inhibitors were administrated at the time of Cas9 mediated DSB induction.

Since the mechanism of reversion differs between the SPD8 and the SP5 mutant, we discuss the results obtained separately.

4.1.3.3 Conditions stimulating homologous recombination events in the SPD8 mutant

It is thought that DSB repair pathway utilization upon DSB induction can be influenced by the properties of the induced DSBs, the cell cycle phase and the abundance of regulatory proteins at the time of DSB induction. DSBs generated by restriction nucleases can be repaired by HRR, D-NHEJ or alt-EJ. In this situation, D-NHEJ and possibly alt-EJ could be able to repair DSBs in an error free manner. However, there is evidence that blunt ended DSBs can be directly ligated by D-NHEJ in an error-free manner, while alt-EJ always results in sequence alterations at the break (Bétermier 2014).

Since all our experiments were performed with cycling cells that were kept in the exponential phase of growth, the generated DSBs could be repaired in theory by all listed DSB repair pathways. It is known that the phase of the cell cycle influences the utilization of DSB repair pathways by restricting HRR to the late S and G_2 phase. In conjunction with this, DNA end resection, an initial step of HRR is actively controlled throughout the cell cycle. Resection is suppressed in G_1 by 53BP1, and is promoted during G_2 by BRCA1. It is also possible that regulator proteins present during specific cell cycle phases facilitate D-NHEJ. Factors like MRN and CtIP that mediate the resection step have lower activity and/or abundance in the G_1 phase of the cell cycle. Other proteins like Ku70/80 when they bind to the DSB may shift DSB repair to D-NHEJ. Along these lines, the strong effect on reversion after inhibition of DNA PKcs can be explained by the increased portion of cells in the G_1 phase of the cell cycle. However, using a different line of argumentation one can also hypothesize that the reduction in HRR-dependent reversion in this mutant after treatment with an inhibitor of DNA PKcs indicates that DNA PKcs is also utilized and is regulating HRR.

HRR is involved in the repair of DSBs in the process of homologous recombination. HRR is known to operate predominantly in S and G_2 phase of the cell cycle. This requirement derives from the fact that in these phases of the cell cycle a sister chromatid is available to provide template function and resection proteins are present at higher levels such as CtIP (Ottaviani 2014). To study the effect of cell cycle phase in the reversion events generated with the Cas9 system will require

synchronized cells and an inducible Cas9 system. Such systems are considered at present in the laboratory.

Here we have focused on asynchronous cell population and demonstrate that factors of HRR play distinct roles in the homologous recombination correction events. While ATM was shown to facilitate the reversion events, ATR did not. ATM and ATR are known to regulate the G_1 and S/G_2 phase checkpoints via CHK2 and CHK1, respectively. One study suggested that ATM plays a dual role throughout the cell cycle: it regulates HRR in G_2 and D-NHEJ in G_1 and G_0 (Beucher 2009). Thus, the increased reversion observed in the presence of ATM may reflect ATM stimulation of HRR, and possibly also of D-NHEJ. Stimulation of D-NHEJ could suppress alt-EJ pathway. We speculate that ATM favors the processes required for reversion predominantly during S and G_2 phase of the cell cycle, while in G_1 DNA PKcs (D-NHEJ) takes over.

We could show that PARP inhibition reduces reversion. The opposite effect was expected since PARP inhibition is associated with decrease in the alt-EJ, which always results in sequence alterations at the break site. However, there is a study suggesting a role for PARP1 in the stimulation of ATM activity, which triggers homologous recombination (Bryant 2006). It has also been reported that PARP interacts with DNA PKcs. Therefore we speculate that PARP inhibition could also lead to inhibition of DNA PKcs. Thus, an effect of PARP on DNA PKcs, the major component of D-NHEJ that was shown to contribute to the correction events (figure 35), could explain the reduction observed (Bryant 2006).

4.1.3.4 Non-homologous recombination events are stimulated by ATM and suppressed by DNA PKcs after induction of single DSBs in SP5 cells

We consider that only HRR and D-NHEJ, or some form of SSA, allow reversion, while the alt-EJ is less efficient in this due to its mutagenic character. However, we cannot exclude the possibility that alt-EJ allows reversion under certain conditions. In the reversion assay using the SP5 mutant, non-homologous recombination is thought to operate and we could demonstrate that alt-EJ does not contribute when single DSBs mediate reversion. However, alt-EJ may be involved when DSB clusters induce reversion. Thus, increasing DSB complexity may allow the function of error-prone DSB repair pathways in the reversion events.

Notably, in this endpoint, we could demonstrate a role for DNA PKcs and ATM after induction of single DSBs. The observation that DNA PKcs appears involved in reversion events induced by single DSBs, but not by DSB clusters can be explained by compromised function of the kinase in the latter setting. It has been reported that low-LET radiation generates a more suitable substrate for DNA PKcs than high-LET radiation (Anderson 2010).

We could demonstrate a stimulating role for ATM in the reversion process. This can be explained by the generated ends at the DSBs (Shiotani 2009) (see 3.1.4.2.3). One study suggested that ATM activity counteracts alt-EJ and decreases its efficiency in G_1 phase of the cell cycle (Muraki 2013). A diminished activity of alt-EJ will facilitate the repair by HRR and D-NHEJ after the induction of a single DSB.

As discussed above, chromatin structure may also play an important role in determining the DSB repair pathway choice. Therefore we speculate that the function of ATM to phosphorylate a heterochromatin building factor, KAP-1, and to relax chromatin locally (Geuting 2013) also facilitates reversion in SP5 cells. The release of ATM from single DSBs during the resection process, could suppress D-NHEJ and contribute thus to the non-homologous recombination event underpinning resection in the SP5 mutant.

The error prone repair pathway alt-EJ is facilitated by the limited resection. However, as mentioned earlier alt-EJ does not show detectable contribution to reversion after single DSBs induction.

We could conclude that an increase in complexity increased the involvement of the error-prone alt-EJ repair pathways, which results in lower number of reversion events. To examine directly the role of alt-EJ in mutation induction for single DSBs and DSB clusters we utilized the direct mutation assay (aim 7) (see 4.2).

4.2 Increased mutagenesis at DSB clusters

Mutations are aberrations or interruptions of sequence information at the DNA and promote cancer development. DSBs are severe lesions and are repaired mainly by HRR, D-NHEJ or when the above two processes are compromised by alt-EJ. However, not all DSB repair pathways restore the original sequence information at the breaks and therefore may contribute to the increase in mutation frequency. One factor that may increase mutation risk is the induction of complex DSBs. To study this question in more detail we generated DSB clusters at different levels of complexity at the *hprt* gene in wild type V79 Chinese hamster cells. The occurrence of spontaneous mutations at the *hprt* gene was found very low at about $3.7x10^{-7}$ mutations per generation. This allows us to clearly distinguish between induced mutations and background mutations (Telleman 1996).

To address aim 7 whether with increase in DSB complexity, here modeled by DSB clusters, increases the risk of mutagenesis, we applied the RNA guided nuclease system using the gRNAs designed for the SPD8 and SP5 mutants.

Our experiments showed that the generation of DSB within the *hprt* gene increases mutation induction after targeting the intron or intron/exon junctions. However, the mutation rate was more pronounced when the exon region was targeted (figure 40). This reflects the importance of each exon in gene function. However, the elevated mutation frequency upon DSB induction in the intron regions also indicates the vulnerability of these gene regions.

The increased mutation induction after Cas9 mediated DSB generation at the *hprt* gene could be explained by the fact that the induced DSBs are repaired by error-prone DSB repair pathways such as D-NHEJ or alt-EJ, causing thus loss or alterations in DNA sequence by insertions or small deletions for D-NHEJ, or large deletions and chromosomal translocations for alt-EJ. Deletions could include not only intron but also exon regions, or could derive from translocation events. The latter seems though unlikely, as translocations are frequently lethal. The lower mutagenic potential of intron induced DSBs showed the repair errors are better tolerated in these genomic regions. Our results of the exon and intron targeted DSBs are in line with another study which reported that deletions involving exon and intron DNA, as well as intron DNA alone were sufficient to inactivate the *hprt* gene and to result in a selectable HPRT phenotype (Bao 1995).

A biologically more severe type of DNA damage are DSB clusters. We demonstrated that DSB clusters that excised one or two flanking exons dramatically increased mutation induction, while DSB clusters of intron or intron/exon junctions had effects similar to single DSBs (figure 41). DSB clusters are generated in nature for example after high-LET exposure including particles present in space radiation. Studies have shown that high-LET radiation often results in an extensive release of many small DNA fragments (30% of all fragments at 1 Gy) as compared to low-LET radiation (3% of all fragments at 1 Gy), most likely as a consequence of the increased formation of DSB clusters (Li 2012). In another study DSB clusters generated with an I-SceI based system were shown to have a higher cell killing potential (Schipler 2013). The importance of DSB clusters in genome stability could be also documented here using the CRISPR/Cas9 system. Furthermore, we could demonstrate that the formation of DSB cluster in specific locations within the DNA contributes to mutagenesis. The increase in the mutation frequency at complex DSBs can be explained by a functional abrogation of D-NHEJ and HRR and over-activation of alt-EJ.

To sum up the results for aim 7, we could show that the location and the complexity of the induced DSBs are of importance and contribute strongly to mutagenesis.

We assumed that with increasing DSB complexity the risk of miss-rejoining events increases. Therefore we next addressed the question of aim 8, how the repair

pathways contribute under these conditions. We could show that the role of DSB repair pathways differs between single DSBs and DSB clusters (figure 42). The inhibition of DNA PKcs revealed an increase in the mutation frequency at DSB clusters. Thus the faster operating D-NHEJ has a protective role. This effect can be explained by the ability of D-NHEJ to rejoin DSB ends, even when this happens with small sequence alterations (Bétermier 2014). Another study reported that upon D-NHEJ inhibition mutation induction increases after exposure to high-LET radiation (Li 2012).

In the CRISPR/Cas9 system, the generated blunt ended DSBs are thought to be repaired accurately by D-NHEJ, with miss-repair events contributing only about 5% of the rejoining events (Wyatt 2015). The protective role of D-NHEJ at DSB clusters can also be explained by its role in suppressing alt-EJ. Inhibition of D-NHEJ may facilitate alt-EJ and could lead to the increase in mutation frequency observed.

Inhibition of alt-EJ on the other hand (figure 42) did generate any effect on mutation induction. This indicates that under the conditions tested HRR and D-NHEJ were still functional, and since alt-EJ predominantly operates as backup it failed to contribute. However, the absence of an effect even at DSB clusters points to additional contributions that require further investigations.

To investigate the role of alt-EJ in more detail, experiments could be performed in which both repair pathways, HRR and D-NHEJ are inhibited. It will be interesting to establish how ATM and ATR contribute to mutagenesis. Information on pathway function and outcome could also be obtained by sequence analysis of the mutated *hprt* gene.

To sum up the findings of aim 7 and aim 8, demonstrate that the mutagenic risk increases with increasing complexity of the DSB. Furthermore we revealed that D-NHEJ prevents mutagenesis at complex DSBs, while alt-EJ contributes to DSB related mutagenesis events predominantly at single DSBs.

5 Summary

Double strand breaks (DSBs) are the most severe form of DNA lesions that are repaired in higher eukaryotes by DNA PK-dependent non-homologous end-joining (D-NHEJ), homologous recombination repair (HRR) or alternative non-homologous end-joining (alt-EJ). From all DSB repair pathways, only HRR has a build-in mechanism to completely restore the DNA sequence around the breaks, while D-NHEJ is frequently associated with errors. Alt-EJ is commonly associated with chromosomal translocations, large deletions and in general genomic instability. However, it is still not known how increasing DSB complexity affects DSB repair pathway choice. To address this question, two different approaches were introduced in the present thesis.

In the first approach we studied reversion in the Chinese hamster *hprt* mutants, SPD8 and SP5. Using this biological model system, we could study the role of DSB complexity in reversion induction and the contribution of DSB repair pathways to the correction events induced. It is particularly useful that reversion in the SPD8 and SP5 mutant require homologous and non-homologous recombination, respectively. Reversion results generated after exposure of SPD8 and SP5 cells to low and high-linear energy transfer (LET) ionizing radiation showed only limited induction of reversions that was difficult to interpret as deriving from DSBs of different complexity.

Therefore, we specifically induced DSBs within the *hprt* gene by applying the RNA guided nuclease technique (CRISPR/Cas9). Our results revealed that a single DSB generated directly in the exon flanking intron region of the mutated region in SPD8 and SP5 cell lines efficiently triggers reversion, while DSBs in the surrounding region triggers reversion markedly less efficiently.

Furthermore we could document that DSB clusters impair the correction mechanisms in SPD8 and SP5 cell lines. DSB clusters are apparently more difficult to handle and compromise repair events supporting reversion. The DSB repair pathway analysis carried out using specific inhibitors revealed distinct repair pathway contributions in the SPD8 and SP5 mutants. D-NHEJ and partially HRR facilitated the homologous recombination events supporting reversion in SPD8

cells, whereas D-NHEJ interfered with the process of non-homologous recombination in SP5 cells. Thus, we could demonstrate that D-NHEJ is not always error prone.

In the second approach we have adapted the forward mutation assay in the Chinese hamster V79 cells and examined the contribution of single DSBs as well as of DSB clusters, and or DSB repair pathways to mutagenesis. We found that the induction of a DSB within intron or intron/exon junctions, and even more pronouncedly in exon regions, enhance mutagenesis, confirming that DSBs is a severe DNA lesion. Increase in DSB complexity in the form of DSB clusters, further increase mutation induction particularly when the DSB cluster removes an entire exon or several exons. They generate less severe effects when generated in introns or intron/exon junctions. The DSB repair pathway investigation revealed a protective role for D-NHEJ at complex DSBs. In contrast alt-EJ contributed predominantly to DSB related mutagenesis at single DSBs.

The exact mechanisms as to how repair pathways coordinate their activities and contribute to genome stability could not be explained conclusively by our experiments. The further elucidation of this highly important aspect of genomic stability will be the focus of future studies in the Institute of Medical Radiation Biology.

Zusammenfassung

Doppelstrangbrüche (DSBs) sind die schwerste Form von DNA-Schäden, die in höheren Eukaryonten durch DNA-PK-abhängigen nicht-homologen End-Verknüpfung (D-NHEJ), homologer Rekombinationsreparatur (HRR) oder alternativer nicht-homologen End-Verknüpfung (alt-EJ) repariert werden. Von allen DSB-Reparaturwegen hat nur HRR einen eingebauten Mechanismus, um die DNA-Sequenz an der Bruchstelle vollständig wiederherzustellen, während D-NHEJ häufig mit Reparaturfehlern einhergeht. Alt-EJ ist oft mit chromosomalen Translokationen, großen Deletionen und im Allgemeinen mit genomischer Instabilität assoziiert. Bis heute ist jedoch nicht bekannt, wie die zunehmende Komplexität von DSBs sich auf die Wahl der DSB-Reparaturwege auswirkt. Um dieser Frage nachzugehen wurden zwei unterschiedliche Ansätze in der vorliegenden Arbeit verfolgt.

Im ersten Ansatz untersuchten wir die Reversions-Ereignisse in chinesischen-Hamster *hprt* Mutanten Zelllinien, SPD8 und SP5. Mit diesem biologischen Modellsystem konnten wir die Rolle der DSB Komplexität in der Reversions-Induktion und den Beitrag der DSB-Reparaturwege in den induzierten Reversions-Ereignissen untersuchen. Im Übrigen zeichnen die SPD8 und SP5 Mutanten dahingehend aus, dass sie ihre Mutation über homologe bzw. nicht-homologe Rekombinations-Ereignisse korrigieren. Die erzielten Ergebnisse der Reversionsuntersuchung nach Exposition von SPD8- und SP5-Zellen mit niedriger- und hoher-linearer Energietransfer (LET) Strahlung zeigten nur geringe Reversions-Induktionen, die eine Interpretation der DSBs unterschiedlicher Komplexität erschwerten.

Durch Anwendung der CRISPR/Cas9 Technik konnten wir DSBs speziell im *hprt*-Gen induzieren. Unsere Ergebnisse zeigten, dass ein einzeln generierter DSB in der Exon-Intron flankierenden Region innerhalb der Mutation in SPD8- und SP5-Zelllinien einen direkten Reversions-Effekt auslöst, wohingegen DSBs in anderen Regionen zu einer deutlich geringeren Reversion führen.

Darüber hinaus konnten wir zeigen, dass DSB-Cluster die Korrekturmechanismen in SPD8 und SP5 Zelllinien beeinträchtigen. DSB-Cluster sind offenbar schwieriger

zu verarbeiten und verhindern Reparatur-Ereignisse wie die der Reversion. Die durchgeführte DSB-Reparatur Analyse unter Verwendung spezifischer Inhibitoren zeigte deutliche Beiträge der verwendeten DSB-Reparaturwege in SPD8 und SP5 Mutanten. D-NHEJ und teilweise HRR erleichtern die Reversion der homologen Rekombination in SPD8 Zellen, während D-NHEJ den Prozess der nicht-homologen Rekombination in SP5 Zellen stört. Somit konnten wir zeigen, dass D-NHEJ nicht immer fehleranfällig operiert.

Im zweiten Ansatz haben wir den Vorwärts-Mutations Assay in chinesischen Hamster V79-Zellen angewendet und den Beitrag der einzelnen DSBs sowie der DSB-Cluster und/oder der DSB Reparaturwege zur Mutagenese hin untersucht. Dabei war festzustellen, dass die Induktion eines DSBs innerhalb des Introns oder des Intron/Exon-Übergangs und noch stärker in Exon Regionen zu einer erhöhten Mutagenese führt. Somit konnten wir bestätigen, dass DSBs schwere DNA-Schäden verursachen. Die Erhöhung der DSB Komplexität in Form von DSB-Cluster führte zu einer weiteren Erhöhung der Mutations-Induktion, insbesondere in Fällen, in denen ein DSB-Cluster ein ganzes Exon oder mehrere Exons entfernt. Die DSB-Cluster zeigten weniger schwere Auswirkungen, wenn sie in Introns oder an Intron/Exon-Übergängen generiert werden. Die Untersuchung des DSB-Reparaturwegs ergab eine protektive Rolle für D-NHEJ bei komplexen DSBs. Im Gegensatz dazu hat alt-EJ überwiegend bei einzel-DSBs zur Mutagenese beigetragen.

Die genauen Mechanismen, durch die Reparaturwege ihre Aktivität koordinieren und das Genom stabilisiert wird, konnten nicht abschließend durch unsere Experimente geklärt werden. Weitere Untersuchungen, die diesen wichtigen Aspekt berücksichtigen, werden schwerpunktmäßig in zukünftigen Studien am Institut für Medizinische Strahlenbiologie durchgeführt.

6 Literature

Al-Minawi, A. Z., Lee, Yin-Fai, Hakansson, D., Johansson, F., Lundin, C., Saleh-Gohari, N., Schultz, N., Jenssen, D., Bryant, HE., Meuth, M., Hinz, JM., Helleday, T. (2009). "The ERCC1/XPF endonuclease is required for completion of homologous recombination at DNA replication forks stalled by inter-strand cross-links." Nucleic Acids Research **37**(19): 6400-6413.

Anderson, J. A., Harper, J. V., Cucinotta, F. A., O'Neill, P. (2010). "Participation of DNA-PKcs in DSB Repair after Exposure to High- and Low-LET Radiation." Radiation Research **174**(2): 195-205.

Arnaudeau, C., Helleday, T., Jenssen, D. (1999). "The RAD51 protein supports homologous recombination by an exchange mechanism in mammalian cells." Journal of Molecular Biology **Jun 25;289(5):1231-8**.

Arnaudeau, C., Lundin, C., Helleday, T. (2001). "DNA double-strand breaks associated with replication forks are predominantly repaired by homologous recombination involving an exchange mechanism in mammalian cells." Journal of Molecular Biology **Apr 13;307(5):1235-45**.

Arnaudeau, C., Rozier, L., Cazaux, C., Defais, M., Jenssen, D., Helleday, T. (2001). "RAD51 supports spontaneous non-homologous recombination in mammalian cells, but not the corresponding process induced by topoisomerase inhibitors." Nucleic Acids Research **Feb 1;29(3):662-7**.

Audebert, M., Salles, B., Calsou, P. (2004). "Involvement of Poly(ADP-ribose) Polymerase-1 and XRCC1/DNA Ligase III in an Alternative Route for DNA Double-strand Breaks Rejoining." Journal of Biological Chemistry **279**: 55117-55126.

Bakkenist, C. J., Kastan, M. B. (2003). "DNA damage activates ATM through intermolecular autophosporylation and dimer dissociation." Nature(Jan 30;421 (6922):499-506).

Bakr, A., Oing, C., Köcher, S., Borgmann, K., Dornreiter, I., Petersen, C., Dikomey, E., Mansour, W.Y. (2015). "Involvement of ATM in homologous recombination after end resection and RAD51 nucleofilament formation." Nucleic Acids Research **43**(6): 3154-3166.

Bao, C. Y., Ma, A. H., Evans, H. H., Horng, M. F., Mencl, J., Hui, T. E., Sedwick, W. D. (1995). "Molecular analysis of hypoxanthine phosphoribosyltransferase gene deletions induced by alpha- and X-radiation in human lymphoblastoid cells." Mutation Research **Jan;326(1):1-15**.

Barrangou, R. (2012). "RNA-mediated programmable DNA cleavage." Nature Biotechnology **Sep;30(9):836-8**.

Berg, J. M., Tymoczko, J. L., Stryer, L. (2002). Biochemistry. 5th edition, New York: W H Freeman.

Bétermier, M., Bertrand, P., Lopez, B. S. (2014). "Is Non-Homologous End-Joining Really an Inherently Error-Prone Process?" PLoS Genetics **10**(1): e1004086.

Beucher, A., Birraux, J., Tchouandong, L., Barton, O., Shibata, A., Conrad, S., Goodarzi, A. A., Krempler, A., Jeggo, P. A., Löbrich, M. (2009). "ATM and Artemis promote homologous recombination of radiation-induced DNA double-strand breaks in G2." EMBO Journal **28**(21): 3413-3427.

Boboila, C., Oksenych, V., Gostissa, M., Wang, J. H., Zha, S., Zhang, Y., Chai, H., Lee, CS., Jankovic, M., Saez, LM. A., Nussenzweig, Michel C., McKinnon, P. J., Alt, F. W., Schwer, B. (2012). "Robust chromosomal DNA repair via alternative end-joining in the absence of X-ray repair cross-complementing protein 1 (XRCC1)." Proceedings of the National Academy of Sciences of the United States of America **109**(7): 2473-2478.

Bradly, M. O., Bhuyan, B., Francis, M. C., Langenbach, R., Peterson, A., Huberman, E. (1981). "Mutagenesis by chemical agents in V79 chinese hamster cells: a review and analysis of the literature. A report of the Gene-Tox Program." Mutation Research **Sep;87(2):81-142**.

Brem, R., Karran, P. (2012). "Oxidation-mediated DNA cross-linking contributes to the toxicity of 6-thioguanine in human cells." Cancer Research **Sep 15;72(18):4787-95**.

Brinkrolf, K., Rupp, O., Laux, H., Kollin, F., Ernst, W., Linke, B., Kofler, R., Romand, S., Hesse, F., Budach, WE., Galosy, S., Mueller, D., Noll, T., Wienberg, J., Jostock, T., Leonard, M., Grillari, J., Tauch, A., Goesmann, A., Helk, B., Mott, JE., Puhler, A., Borth, N. (2013). "Chinese hamster genome sequenced from sorted chromosomes." Nature Biotechnology **Aug;31(8):694-5**.

Brown, M. L. F., D. Bürkle, A. Chang, Y. (2002). "Role of poly(ADP-ribosyl)ation in DNA-PK_{cs}-independent V (D)J recombination." Proceedings of the National Academy of Sciences of the United States of America **99**: 4532-4537.

Bryant, H. E. H., T. (2006). "Inhibition of poly (ADP-ribose) polymerase activates ATM which is required for subsequent homologous recombination repair." Nucleic Acids Research **34**(6): 1685-1691.

Bugg, C. E., Thewalt, U. (1970). "The crystal and molecular structure of 6-thioguanine." Journal of the American Chemical Society **Dec 16;92(25):7441-5**.

Cariello, N. F., Skopek, T. R. (1993). "In vivo mutation at the human HPRT locus." Trends in Genetics **Sep;9(9):322-6**.

Caskey, C. T., Kruh, G. D. (1979). "The HPRT locus." Cell **Jan;16(1):1-9**.

Chinault, A. C., Caskey, C. T. (1984). "The hypoxanthine phosphoribosyltransferase gene: a model for the study of mutation in mammalian cells." Prog Nucleic Acid Res Mol Biol **31:295-313**.

Cimprich, K. A. C., D. (2008). "ATR: an essential regulator of genome integrity." Nature Reviews. Molecular Cell Biology **9**(8): 616-627.

D'Silva, I., Pelletier, J.D., Lagueux, J., D'Amours, D., Chaudhry, M.A., Weinfeld, M., Lees-Miller, S. P.,Poirier, G.G. (1999). "Relative affinities of poly(ADP-ribose) polymerase and DNA-dependent protein kinase for DNA strand interruptions." Biochimica et Biophysica Acta **1430**: 119-126.

Dantzer, F., de la Rubia, G., Menissier-de Murcia, J., Hostomsky, Z., de Murcia, G., Schreiber, V. (2000). "Base Excision Repair Is Impaired in Mammalian Cells Lacking Poly(ADP-ribose) Polymerase-1." Biochemistry **39**: 7559-7569.

Dare, E., Zhang, L. H., Jenssen, D. (1996). "Characterization of mutants involving partial exon duplications in the hprt gene of Chinese hamster V79 cells." Somat cell mol genet **May;22(3):201-10**.

Davis, A. J., Chen, B. P. C., Chen, D. J. (2014). "DNA-PK: A dynamic enzyme in a versatile DSB repair pathway." DNA Repair **17**: 21-29.

Davis, A. J., Chen, D. J. (2013). "DNA double strand break repair via non-homologous end-joining." Translational Cancer Research **2**(3): 130-143.

DeFazio, L. G., Stansel, R.M., Griffith, J. D., Chu, G. (2002). "Synapsis of DNA ends by DNA-dependent protein kinase." EMBO Journal **21**: 3192-3200.

Deltcheva, E., Chylinski, K., Sharma, C. M., Gonzales, K., Chao, Y., Pirzada, Z. A., Eckert, M. R., Vogel, J., Charpentier, E. (2011). "CRISPR RNA maturation by trans-encoded small RNA and host factor RNase III." Nature **Mar 31;471(7340):602-7**.

DiBiase, S. J., Zeng, Z-C., Chen, R., Hyslop, T., Curran, W.J., Jr., Iliakis, G. (2000). "DNA-dependent protein kinase stimulates an independently active, nonhomologous, end-joining apparatus." Cancer Research **60**: 1245-1253.

Dueva, R., Iliakis, G. (2013). "Alternative pathways of non-homologous end joining (NHEJ) in genomic instability and cancer." Translational Cancer Research **2**(3): 163-177.

Falk, M., Lukasova, E., Kozubek, S. (2010). "Higher-order chromatin structure in DSB induction, repair and misrepair." Mutation Research/Reviews in Mutation Research **704**(1–3): 88-100.

Farrel, S. A., Worton, R. G. (1977). "Chromosome loss is responsible for segregation at the HPRT locus in Chinese hamster cell hybrids." Somatic Cell Genetics **Sep;3(5):539-51**.

Fathers, C., Drayton, R. M., Solovieva, S., Bryant, H. E. (2012). "Inhibition of poly(ADP-ribose) glycohydrolase (PARG) specifically kills BRCA2-deficient tumor cells." Cell Cycle **11**(5): 990-997.

Flynn, R. L., Zou, L. (2011). "ATR: a master conductor of cellular responses to DNA replication stress." Trends in Biochemical Sciences **36**(3): 133-140.

Friedberg, E. C., Walker, G.C., Siede, W., Wood, R. D., Schultz, R.A., Ellenberger, T. (2006). DNA Repair and Mutagenesis. Washington, D.C., ASM Press.

Fuscoe, J. C., Zimmerman, LJ., Fekete, A., Setzer, R. W., Rossiter, B. J. (1992). "Analysis of X-ray-induced HPRT mutations in CHO cells: insertions and deletions." Mutation Research **Oct;269(2):171-83**.

Gasiunas, G., Barrangou, R., Horvath, P., Siksnys, V. (2012). "Cas9-crRNA ribonucleoprotein complex mediates specific DNA cleavage for adaptive immunity in bacteria." Proceedings of the National Academy of Sciences of the United States of America **Sep 25;109(39):E2579-86**.

Geuting, V., Reul, C., Löbrich, M. (2013). "ATM Release at Resected Double-Strand Breaks Provides Heterochromatin Reconstitution to Facilitate Homologous Recombination." PLoS Genetics **9**(8): e1003667.

Growth, P., Orta, M., Elvers, I., Majumder, M., Lagerqvist, A., Helleday, T. (2012). "Homologous recombination repairs secondary replication induced DNA double-strand breaks after ionizing radiation." Nucleic Acids Research **Vol 40, no 14**.

Gu, J., Lu, H., Tippin, B., Shimazaki, N., Goodman, M. F., Lieber, M. R. (2007). "XRCC4:DNA ligase IV can ligate incompatible DNA ends and can ligate across gaps." EMBO Journal **Feb 21;26(4):1010-23**.

Guirouilh-Barbat, J., Huck, S., Bertrand, P., Pirzio, L., Desmaze, C., Sabatier, L., Lopez, B. S. (2004). "Impact of the KU80 pathway on NHEJ-induced genome rearrangements in mammalian cells." Molecular Cell **Jun 4;14(5):611-23**.

Gunderson, L. L., Tepper, J. E., Bogart, J. A. (2015). Clinical Radiation Oncology, Elsevier.

Haince, J. F., McDonald, D., Rodrigue, A., Dery, U., Masson, J. Y., Hendzel, M. J., Poirier, G. G. (2008). "PARP1-dependent kinetics of recruitment of MRE11 and NBS1 proteins to multiple DNA damage sites." Journal of Biological Chemistry: 283(282):1197-1208.

Hall, E. J., Giaccia, A. J. (2006). Radiobiology for the Radiologist. Philadelphia, Baltimore, New York, London, Buenos Aires, Hong Kong, Sydney, Tokyo, Lippincott Williams & Wilkins.

Harper, J. W., Elledge, S. J. (2007). "The DNA Damage Response: Ten Years After." Molecular Cell **28**(5): 739-745.

Helleday, T., Arnaudeau, C., Jenssen, D. (1998a). "A partial hprt gene duplication generated by non-homologous recombination in V79 chinese hamster cells is eliminated by homologous recombination." Journal of Molecular Biology **Jun19;279(4):687-94**.

Helleday, T., Arnaudeau, C., Jenssen, D. (1998b). "Effects of carcinogenic agents upon different mechanisms for intragenic recombination in mammalian cells." Carcinogenesis **Jun;19(6):973-8**.

Heyer, W., Li, X., Rolfsmeier, M., Zhang, XP. (2006). "Rad54: the Swiss Army knife of homologous recombination?" Nucleic Acids Research **34**(15): 4115-4125.

Heyer, W. E., K. T., Liu, Jie. (2010). "Regulation of Homologous Recombination in Eukaryotes." Annual Review of Genetics **44**: 113-139.

Howard, W. J., Kerson, L. A., Appel, S. H. (1970). "Synthesis de novo of purines in slices of rat brain and liver." J of neurochem **Jan;17(1):121-3**.

Hsie, A. W., Xu, Z., Yu, Y., An, J., Meltz, M. L., Schwartz, J. L., Hrelia, P. (1993). "Quantitative and molecular analysis of genetic risk: a study with ionizing radiation." Environ health perspect **Oct;101 Suppl 3:213-8**.

Iliakis G., Murmann, T., Soni, A (2015). "Alternative end-joining repair pathways are the ultimate backup for abrogated classical non-homologous end-joining and homologous recombination repair: Implications for the formation of chromosome

translocations." Mutation Research/Genetic Toxicology and Environmental Mutagenesis **in press**.

Jackson, S. P. (2002). "Sensing and repairing DNA double-strand breaks." Carcinogenesis **23**: 687-696.

Jackson, S. P., Bartek, J. (2009). "The DNA-damage response in human biology and disease." Nature **461**(7267): 1071-1078.

Jinek, M., Chylinski, K., Fonfara, I., Hauer, M., Doudna, J. A., Charpentier, E. (2012). "A programmable dual-RNA-guided DNA endonuclease in adaptive bacterial immunity." Science **Aug 17;337(6096):816-21**.

Jinnah, H. A., de Gregorio, L., Harris, J. C., Nyhan, W. L., O'Neill, J. P. (2000). "The spectrum of inherited mutations causing HPRT deficiency: 75 new cases and a review of 196 previously reported cases." Mutation Research **Oct; 463(3):309-26**.

Kass, E. M., Helgadottir, H. R., Chen, CC., Barbera, M., Wang, R., Westermark, U. K., Ludwig, T., Moynahan, M. E., Jasin, M. (2013). "Double-strand break repair by homologous recombination in primary mouse somatic cells requires BRCA1 but not the ATM kinase." Proceedings of the National Academy of Sciences of the United States of America **110**(14): 5564-5569.

Kedar, P. S., Stefanick, D. F., Horton, J. K., Wilson, S. H. (2012). "Increased PARP-1 association with DNA in alkylation damaged, PARP-inhibited mouse fibroblasts." Molecular Cancer Research **Mar;10(3):360-8**.

Keebaugh, A. C., Sullivan, R. T., NISC Comparative Sequencing Program, Thomas, J. W. (2007). "Gene duplication and inactivation in the HPRT gene family." Genomics **Jan;89(1):134-42**.

Kelley, M. R. (2012). DNA repair in cancer therapy: molecular targets and clinical applications, Elsevier.

Khan, F. M. (2009). The physics of radiation therapy. Philadelphia, Lippincott Williams & Wilkins.

Kim, M. Y., Zhang, T., Kraus, W. L. (2005). "Poly(ADP-ribosyl)ation by PARP-1: `PAR-laying' NAD+ into a nuclear signal." Genes & Development **19**(17): 1951-1967.

Kim, S. H., Moores, J. C., David, D., Respess, J. G., Jolly, D. J., Friedmann, T. (1986). "The organization of the human HPRT gene." Nucleic Acids Research **Apr 11;14(7):3103-18**.

Köcher, S., Rieckmann, T., Rohaly, G., Mansour, W. Y., Dikomey, E., Dornreiter, I., Dahm-Daphi, J. (2012). "Radiation-induced double-strand breaks require ATM but not Artemis for homologous recombination during S-phase." Nucleic Acids Research **40**(17): 8336-8347.

Kraft, G. (2005). Tumortherapie mit schweren Ionen, Physikalische und biologische Grundlagen, Technische Realisierung an der GSI, Klinische Ergebnisse, Verein zur Foerderung der Tumortherapie mit schweren Ionen e.V.

Krajewska, M., Fehrmann, R. S. N., de Vries, E. G. E., van Vugt, Marcel A. T. M. (2015). "Regulators of homologous recombination repair as novel targets for cancer treatment." Frontiers in Genetics **6**: 96.

Lee, J., Paull, T. T. (2005). "ATM Activation by DNA Double-Strand Breaks Through the Mre11-Rad50-Nbs1 Complex." Science **308**(5721): 551-554.

Li, Y., Qian, H., Wang, Y., Cucinotta, F. A. (2012). "A Stochastic Model of DNA Fragments Rejoining." PLoS ONE **7**(9): e44293.

Lindahl, T. (1993). "Instability and decay of the primary structure of DNA." Nature **362**: 709-715.

Linder (2005). Expression and regulation of human xanthine oxireductase.

Lossaint, G., Besnard, E., Fisher, D., Piette, J., Dulic, V. (2011). "Chk1 is dispensable for G2 arrest in response to sustained DNA damage when the ATM/p53/p21 pathway is functional." Oncogene **108**(21): 8663-8667.

Lundin, C., Erixon, K., Arnaudeau, C., Schultz, N., Jenssen, D., Meuth, M., Helleday, T. (2002). "Different Roles for Nonhomologous End Joining and Homologous Recombination following Replication Arrest in Mammalian Cells." Molecular and Cellular Biology **22**: 5869-5878.

Madabhushi, R., Gao, F., Pfenning A. R., Pan, L., Yamakawa, S., Seo, J., Rueda, R., Phan TX., Yamakawa, H., Pao, PC., Stott, RT., Gjonesk, E., Nott, A., Cho, S., Kellis, M., Tsai, LH. (2015). "Activity-induced DNA breaks govern the expression of neuronal early-response genes." Cell **Jun 18;161(7):1592-605**.

Madison, D. L., Stauffer, D., Lundblad, J. R. (2011). "The PARP inhibitor PJ34 causes a PARP1-independent, p21 dependent mitotic arrest." DNA Repair **10**(10): 1003-1013.

Mansour, W. Y., Rhein, T., Dahm-Daphi, J. (2010). "The alternative end-joining pathway for repair of DNA double-strand breaks requires PARP1 but is not dependent upon microhomologies." Nucleic Acids Research **38**(18): 6065-6077.

Mari, P., Florea, B. I., Persengiev, S. P., Verkaik, N. S., Bruggenwirth, H. T., Modesti, M., Giglia-Mari, G., Bezstarosti, K., Demmers, J. A. A., Luider, T. M., Houtsmuller, A. B., van Gent, D. C. (2006). "Dynamic assembly of end-joining complexes requires interaction between Ku70/80 and XRCC4." Proceedings of the National Academy of Sciences of the United States of America **103**(49): 18597-18602.

Marraffini, L. A., Sontheimer, E. J. (2010). "CRISPR interference: RNA-directed adaptive immunity in bacteria and archaea." Nature Reviews. Genetics **Mar;11(3):181-90**.

Matsuoka, A., Lundin, C., Johansson, F., Sahlin, M., Fukuhara, K., Sjoberg, BM., Jenssen, D., Onfelt, A. (2004). "Correlation of sister chromatid exchange formation through homologous recombination with ribonucleotide reductase inhibition." Mutation Research **Mar 22;547(1-2):101-7**.

McVey, M., Lee, S. E. (2008). "MMEJ repair of double-strand breaks (director's cut): deleted sequences and alternative endings." Trends in Genetics **24**(11): 529-538.

Melton, D. W., Konecki, D. S., Brennand, J., Caskey, C. T. (1984). "Structure, expression, and mutation of the hypoxanthine phosphoribosyltransferase gene." Proceedings of the National Academy of Sciences of the United States of America **Apr;81(7)::2147-51**.

Mladenov, E., Iliakis, G. (2011). "Induction and Repair of DNA Double Strand Breaks: The Increasing Spectrum of Non-homologous End Joining Pathways." Mutation Research **711**: 61-72.

Muraki, K., Han, L., Miller, D., Murnane, J. P. (2013). "The Role of ATM in the Deficiency in Nonhomologous End-Joining near Telomeres in a Human Cancer Cell Line." PLoS Genetics **9**(3): e1003386.

Nikjoo, H., O'Neill, P.O., Terrissol, M., Goodhead, D.T. (1999). "Quantitative modelling of DNA damage using Monte Carlo track structure method." Radiation and Environmental Biophysics **38**: 31-38.

Noll, D. M., Mason, T. M., Miller, P. S. (2006). "Formation and repair of interstrand cross-links in DNA." Chem Rev **Feb;106(2):277-301**.

Ottaviani, D., LeCain, M., Sheer, D. (2014). "The role of microhomology in genomic structural variation." Trends in Genetics **30**(3): 85-94.

Paul, K., Wang, M., Mladenov, E., Bencsik-Theilen, A. A., Bednar, T., Wu, W., Arakawa, H., Iliakis, G. (2013). "DNA ligases I and III cooperate in alternative non-homologous end-joining in vertebrates." PLoS ONE **8**(3): e59505.

Polo, S. E., Jackson, S. P. (2011). "Dynamics of DNA damage response proteins at DNA breaks: a focus on protein modifications." Genes & Development **25**(5): 409-433.

Prevo, R., Fokas, E., Reaper, P. M., Charlton, P. A., Pollard, J. R., McKenna, W. G., Muschel, R. J., Brunner, T. (2012). "The novel ATR inhibitor VE-821 increases sensitivity of pancreatic cancer cells to radiation and chemotherapy." Cancer Biology & Therapy **13**(11): 1-10.

Ren, X., Li, F., Jeffs, G., Zhang, X., Xu, YZ., Karran. P (2010). "Guanine sulphinate is a major stable product of photochemical oxidation of DNA 6-thioguanine by UVA irradiation." Nucleic Acids Research **Apr;38(6):1832-40**.

Reynolds, P., Anderson, J. A., Harper, J. V., Hill, M. A., Botchway, S. W., Parker, A. W., O'Neill, P. (2012). "The dynamics of Ku70/80 and DNA-PKcs at DSBs induced by ionizing radiation is dependent on the complexity of damage." Nucleic Acids Research **40**(21): 10821-10831.

Rogakou, E. P., Boon, C., Redon, C., Bonner, W. M. (1999). "Megabase chromatin domains involved in DNA double-strand breaks *in vivo*." Journal of Cell Biology **146**: 905-915.

Rosidi, B., Wang, M., Wu, W., Sharma, A., Wang, H., Iliakis, G. (2008). "Histone H1 functions as a stimulatory factor in backup pathways of NHEJ." Nucleic Acids Research **36**(5): 1610-1623.

Rossiter, B. J., Fuscoe, J. C., Muzny, D. M.,Fox, M., Caskey, C. T. (1991). "The Chinese hamster HPRT gene: restriction map, sequence analysis, and multiplex PCR deletion screen." Genomics **Feb;9(2):247-56**.

Saha, J., Wang, M., Cucinotta, F. A. (2013). "Investigation of switch from ATM to ATR signaling at the sites of DNA damage induced by low and high LET radiation." DNA Repair **12**(12): 1143-1151.

Sahasranaman, S., Howard, D., Roy, S. (2008). "Clinical pharmacology and pharmacogenetics of thiopurines." Eur J Clin Pharmacol **Aug;64(8):753-67**.

Schipler, A. (2013). Homing endonuclease-based model systems for the study of DNA double strand break induced cell signalling and repair, Dissertation, University of Duisburg-Essen.

Schipler, A., Iliakis, G. (2013). "DNA double-strand-break complexity levels and their possible contributions to the probability for error-prone processing and repair pathway choice." Nucleic Acids Research **41**(16): 7589-7605.

Sculley, D. G., Dawson, P. A., Emmerson, B. T., Gordon, R. B. (1992). "A review of the molecular basis of hypoxanthine-guanine phosphoribosyltransferase (HPRT) deficiency." Hum Genet **Nov;90(3):195-207**.

Sherer, M. V., PJ. Ritenour, ER (2011). Radiation protection in medical radiography, Elsevier.

Shiotani, B., Zou, L. (2009). "Single-Stranded DNA Orchestrates an ATM-to-ATR Switch at DNA Breaks." Molecular Cell **33**(5): 547-558.

Singh, S. K., Bencsik-Theilen, A., Mladenov, E., Jakob, B., Taucher-Scholz, G., Iliakis, G. (2013). "Reduced contribution of thermally labile sugar lesions to DNA double strand break formation after exposure to heavy ions." Radiation Oncology **8**: 77.

Sleeth, K. M., Sorensen, C. S., Issaeva, N., Dziegielewski, J., Bartek, J., Helleday, T. (2007). "RPA Mediates Recombination Repair During Replication Stress and Is Displaced from DNA by Checkpoint Signalling in Human Cells." Journal of Molecular Biology **373**: 38-47.

Soni, A., Siemann, M., Grabos, M., Murmann, T., Pantelias, G. E., Iliakis, G. (2014). "Requirement for Parp-1 and DNA ligases 1 or 3 but not of Xrcc1 in chromosomal translocation formation by backup end joining." Nucleic Acids Research **42**(10): 6380-6392.

Stout, J. T., Caskey, C. T. (1985). "HPRT: gene structure, expression, and mutation." Annual Review of Genetics **19:127-48**.

Szybalski, W., Szybalski, E. H. (1962). "Drug sensitivity as a genetic marker for human cell lines." Med Bull (Ann Arbor) **Sep-Oct;28:277-93**.

Telleman, P., Overkamp, W. J., Zdzienicka, M. Z. (1996). "Spectrum of spontaneouslz occurring mutations in the HPRT gene of the Chinese hamster V79 cell mutant V-H4, which is homologous to Fanconi anemia group A." Mutagenesis **Mar;11(2):155-9**.

Thacker, J. (1986). "The nature of mutants induced by ionising radiation in cultured hamster cells. III. Molecular characterization of HPRT-deficient mutants induced by gamma-rays or alpha-particles showing that the majority have deletions of all or part of the hprt gene." Mutation Research **May;160(3):267-75**.

Thacker, J., Fleck, E. W., Morris, T., Rossiter, B. J., Morgan, T. L. (1990). "Localization of deletion breakpoints in radiation-induced mutants of the hprt gene in hamster cells." Mut Res **Oct;232(2):163-70**.

Tomimatsu, N., Mukherjee, B., Deland, K., Kurimasa, A., Bolderson, E., Khanna, K. K., Burma, S. (2012). "Exo1 plays a major role in DNA end resection in humans and influences double-strand break repair and damage signaling decisions." DNA Repair **11**(4): 441-448.

van den Bosch, M., Bree, R. T., Lowndes, N. F. (2003). "The MRN complex: coordinating and mediating the response to broken chromosomes." EMBO Reports **4**(9): 844-849.

Walker, J. R., Corpina, R.A., Goldberg, J. (2001). "Structure of the Ku heterodimer bound to DNA and its implications for double-strand break repair." Nature **412**: 607-614.

Wang, H., Rosidi, B., Perrault, R., Wang, M., Zhang, L., Windhofer, F., Iliakis, G. (2005b). "DNA Ligase III as a Candidate Component of Backup Pathways of Nonhomologous End Joining." Cancer Research **65**(10): 4020-4030.

Wang, H., Wang, H., Powell, S.N., Iliakis, G., Wang, Y. (2004). "ATR Affecting Cell Radiosensitivity Is Dependent on Homologous Recombination Repair but Independent of Nonhomologous End Joining." Cancer Research **64**: 7139-7143.

Wang, H., Wang, M., Wang, H., Böcker, W., Iliakis, G. (2005). "Complex H2AX phosphorylation patterns by multiple kinases including ATM and DNA-PK in human cells exposed to ionizing radiation and treated with kinase inhibitors." Journal of Cellular Physiology **202**: 492-502.

Wang, H., Zeng, Z-C., Bui, T-A., Sonoda, E., Takata, M., Takeda, S., Iliakis, G. (2001b). "Efficient rejoining of radiation-induced DNA double-strand breaks in vertebrate cells deficient in genes of the RAD52 epistasis group." Oncogene **20**: 2212-2224.

Wang, H., Zeng, ZC., Perrault, A.R., Cheng, X., Qin, W., Iliakis, G. (2001a). "Genetic evidence for the involvement of DNA ligase IV in the DNA-PK-dependent pathway of non-homologous end joining in mammalian cells." Nucleic Acids Research **29**: 1653-1660.

Wang, M., Wu, W., Wu, W., Rosidi, B., Zhang, L., Wang, H., Iliakis, G. (2006). "PARP-1 and Ku compete for repair of DNA double strand breaks by distinct NHEJ pathways." Nucleic Acids Research **34**(21): 6170-6182.

Ward, J. F. (1985). "Biochemistry of DNA lesions." Radiation Research **104**: S103-S111.

Ward, J. F., Evans, J.W., Limoli, C.L., Calabro-Jones, P.M. (1987). "Radiation and hydrogen peroxide induced free radical damage to DNA." British Journal of Cancer **55**: 105-112.

Waters, T. R., Swann, P. F. (1997). "Cytotoxic mechanism of 6-thioguanine: hMutSalpha, the human mismatch binding heterodimer, binds to DNA containing S6-methylthioguanine." Biochemistry **Mar 4;36(9):2501-6**.

Williams, R. S., Moncalian, G., Williams, J. S., Yamada, Y., Limbo, O., Shin, D. S., Groocock, L. M., Cahill, D., Hitomi, C., Guenther, G., Moiani, D., Carney, J. P., Russell, P., Tainer, J. A. (2008). "Mre11 Dimers Coordinate DNA End Bridging and Nuclease Processing in Double-Strand-Break Repair." Cell **135**(1): 97-109.

Wu, W., Wang, M., Wu, W., Singh, S. K., Mussfeldt, T., Iliakis, G. (2008). "Repair of radiation induced DNA double strand breaks by backup NHEJ is enhanced in G2." DNA Repair **7**(2): 329-338.

Wyatt, D., Ramsden, D., (2015). CRISPR 101: Non-Homologous End Joining. blog.addgene.org/crispr-101-non-homologous-end-joining, Addgene.

Xu, T., Li, Y., Van Nostrand, J. D., He, Z., Zhou, J. (2014). "Cas9-based tools for targeted genome editing and transcriptional control." Appl Environ Microbiol **Mar;80(5):1544-52**.

Yan, T., Berry, S. E., Desai, A. B., Kinsella, T. J. (2003). "DNA mismatch repair (MMR) mediates 6-thioguanine genotoxicity by introducing single-strand breaks to signal a G2-M arrest in MMR-proficient RKO cells." Clinical Cancer Research **Jun;9(6):2327-34**.

Yoo, S., Dynan, W.S. (1999). "Geometry of a complex formed by double strand break repair proteins at a single DNA end: recruitment of DNA-PKcs induces inward translocation of Ku protein." Nucleic Acids Research **27**: 4679-4686.

Zhang, L. H., Jenssen, D. (1992a). "Reversion of the hprt mutant clone SP5 by intrachromosomal recombination." Carcinogenesis **Apr;13(4)609-15**.

Zhang, L. H., Jenssen, D. (1994). "Studies on intrachromosomal recombination in SP5/V79 Chinese hamster cells upon exposure to different agents related to carcinogenesis." Carcinogenesis **Oct;15(10):2303-10**.

Zhang, Y., Jasin, M. (2011). "An essential role for CtIP in chromosomal translocation formation through an alternative end-joining pathway." Nature Structural & Molecular Biology **18**(1): 80-84.

7 Appendix

7.1 List of abbreviations

°C	Degree Celsius
%	percent
α	Alpha
ɣ	Gamma
δ	Delta
6-(me)TG	(methylated) 6-thioguanine
$6TG^{res}$	6-Thioguanine resistant
6-TGMP	6-Thioguanyl monophosphate
9-1-1 complex	Rad9-Rad1-Hus1 complex
ADP	Adenosine diphosphate
Alt-EJ	Alternative non-homologous end-joining
Am	Americium
APRT	Adenine phosphoribosyl transferase
ATM	Ataxia-telangiectasia mutated
ATR	ATM and Rad3-related
ATRIP	ATR-interacting protein
BIR	Break-induced replication
BLM	Bloom helicase
bp	Base pairs
BRCA1	Breast cancer susceptibitility protein 1
BRCA2	Breast cancer susceptibility protein 2
CDS	Cluster damage sites
CHK1 / CHK2	Checkpoint kinase 1 / Checkpoint kinase 2
CRISPR/Cas endonuclease	Clustered regularly interspaced short palindromic repeat Cas-based RNA guided DNA
crRNA	CRISPR RNA
CSR	Class switch recombination
CtIP	C-terminal binding protein interacting protein
d	Days

dHJ	Double Holliday junction
DDR	DNA damage response
DHFR	7,8-dihydrofolate reductase
D-loop	Displacement loop
DMSO	Dimethyl sulfoxide
DNA	Deoxyribonucleic acid
DNA PK-cs	DNA-dependent protein kinase, catalytic subunit
D-NHEJ	DNA-PK dependent non-homologous end-joining
DSB	Double strand break
e.g.	exempli gratia
eV / MeV / GeV	Electronvolt / Megaelectronvolt / Gigaelectronvolt
et al.	et alii
FACS	Flourescence activated cell sorting
FBS	Fetal bovine serum
Fe	Iron
g	Gravity
G_1-Phase / G_2-Phase	Cell cycle phase gap 1/ Cell cycle phase gap 2
GeV	Gigaelectronvolt
GFP	Green flourescent protein
gRNA	Guide RNA
GSI	Facility of the Helmholtz Center for Heavy Ion Research
Gy	Gray
h	Hour
H1	Histone 1
HAT	Hypoxanthine aminopterin thymidine
HPRT	Hypoxanthine guanine phosphoribosyl transferase
HRR	homologous recombination repair
ɣ-H2AX	Phosphorylated form of histone H2AX at Ser-139
i.e.	Id est
IMP/GMP/AMP	Inosine-/Guanine-/Adenosine- monophosphate
IR	Ionizing radiation
J	Joule
kb	Kilo base

kDa	Kilo Dalton
kg	Kilogram
LET	Linear energy transfer
M	Molar (mol/l)
mA	Milliampere
ml	Milliliter
mm	Millimeter
MDC1	DNA damage checkpoint protein 1
MMC	Mitomycin C
MMEJ	Microhomology mediated end-joining
MMR	DNA mismatch repair
MRN	Mre11-Rad50-Nbs1 complex
NBS1	Nijmegen breakage syndrome 1
PAM	Protospacer adjacent motif
PARP-1	Poly(ADP-ribose)polymerase1
PCR	Polymerase chain reaction
PE	Plating efficiency
PI	Propidium iodide
PIKK	Phosphatidylinositol-3 kinase-like kinase family
PLL	Poly-L-lysine
PRPP	5-phosphoribosyl-1-pyrophosphate
rev.freq.	Reversion frequency (10^{-5} cells)
RBE	Relative biological effectiveness
RIDGE	Regions of increased gene expression
RNF8/168	Ring finger protein 8/168
RPA	Replication protein A
rpm	Rounds per minute
S-Phase	Cell cycle synthesis phase
SDSA	Synthesis dependend strand annealing
SF	Surviving fraction
SIS	Heavy ion synchroton facility of the GSI
ssDNA	Single-stranded DNA
SSB	Single strand break
SSO	Single-strand overhangs

TALEN	Transcription activator-like effector nucleases
(d)TMP	(deoxy)Thymidine monophosphate
tracrRNA	Trans-acting crRNA
UV(A)	Ultraviolet light (A)
V(D)J	Variable (diversity) joining
WRN	Werner
XRCC	X-ray repair cross complementation protein group
ZFN	Zinc finger nucleases

7.2 Clonogenic survival data obtained with SPD8 cell line

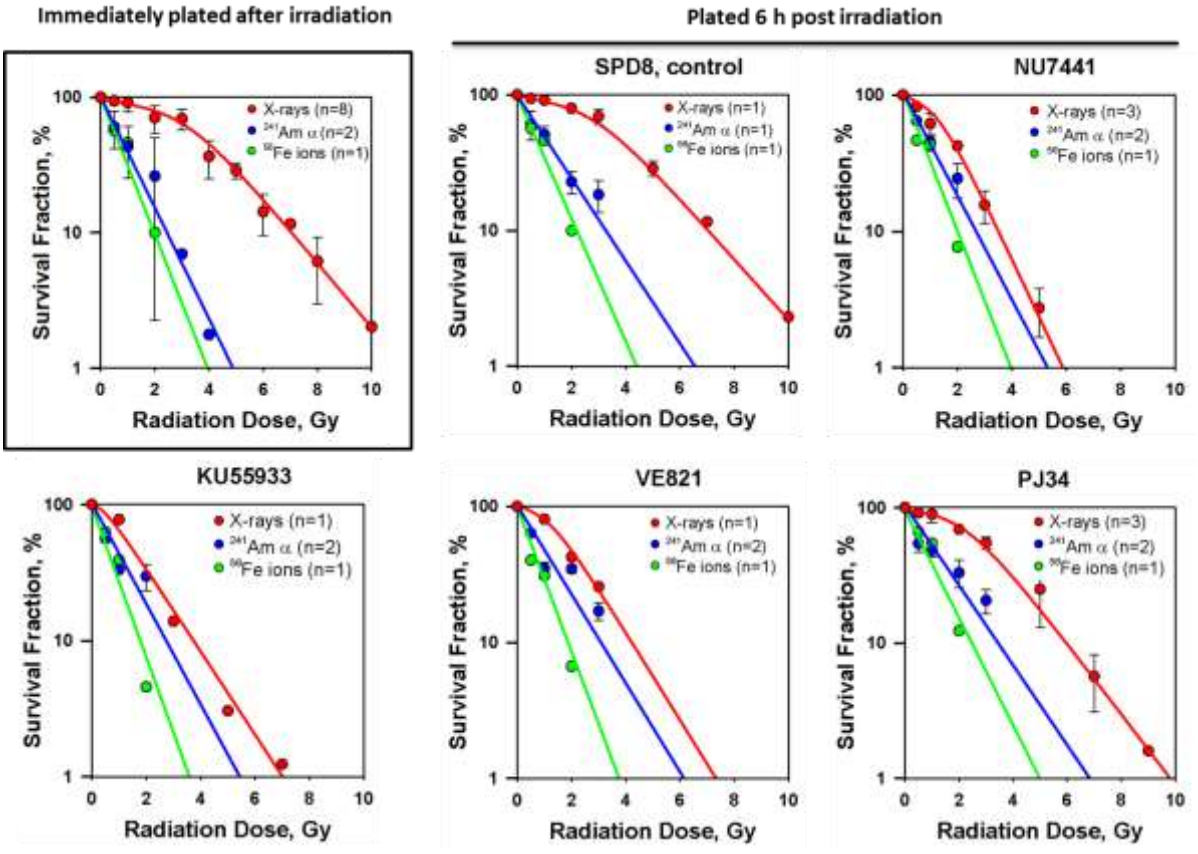

Overview about the clonogenic survival curves. Despite the indications in these figures the ^{56}Fe ion exposed cells were plated 12 h post irradiation.

7.3 Reversion frequency data obtained with SPD8 cells

Mitomycin C	Rev. frequency (Rev./10^5 cells)
0 nM	0.93
100 nM	2.67
250 nM	1.13
500 nM	0.94

#gRNA	Rev. frequency (Rev./10^5 cells)
Mock	3.57±1.8
#2	4.27±5.8
#12	340±184
#13	1736±1142
#8	2367±455
#11	4882±1654

#gRNA	Rev. frequency (Rev./10^5 cells)
#12+13	422
#12+8	1017
#11+12	2287±297
#8+13	2305
#11+13	3543±1157
#11+8	4668±1155

#gRNA	Rev. frequency (Rev./10^5 cells)
#11+12+13	1760
#11+12+8	2198±428
#11+12+13+8	1412

	X-rays				
Dose (Gy)	DMSO	NU7741	KU55933	VE821	PJ34
0	0.93±0.13	1.35±0.26	1.24	1.06	1.85±0.06
1	1.19±0.13	1.99±0.01	1.45	1.19	1.81±0.46
3	1.23±0.19	1.89±0.06	1.02	1.63	2.63±0.2
5	2.05±0.45	8.5±3.37			2.33±1.25

	^{241}Am α particles				
Dose (Gy)	DMSO	NU7741	KU55933	VE821	PJ34
0	1.11	0.94±0.01	0.91±0.01	0.86±0.25	1.38±0.04
0.5	1.63±0.29	1.22±0.05	1.63±0.56	0.61±0.2	2.44±0.48
1	1.91±0.75	1.96±0.39	1.36±0.44	1.1±0.08	1.97±0.91
2	2.18±0.73	1.87±0.13	1.17±0.57	1.34±0.16	2.16±0.64
3	1.54	2.3±0.51	1.93±0.38	0.48±0.09	2.71±0.57

	^{56}Fe-ions				
Dose (Gy)	DMSO	NU7741	KU55933	VE821	PJ34
0	0.93	1.35	2.78	1.06	1.85
0.5	2.25	4.64	5.62	0.77	4.22
1	2.37	5.42		2.19	6.87
2	1.82	28.21	32.56	0	9.75

	Treatment				
#gRNA	DMSO	NU7741	KU55933	VE821	PJ34
Mock	6.27±3.59	15.56±8.75	6.31±0.29	3.74±1.14	9.18±3.98
#8	2798±1648	3640±2947	1029±570	4600±2691	3365±1723
#11	8577±4670	7107±3980	2385	7097±1965	6687±3423
#8+11	5357±2429	5130±2357	3086±386	6873±2157	6291±5057

7.4 Clonogenic survival data obtained with SP5 cells

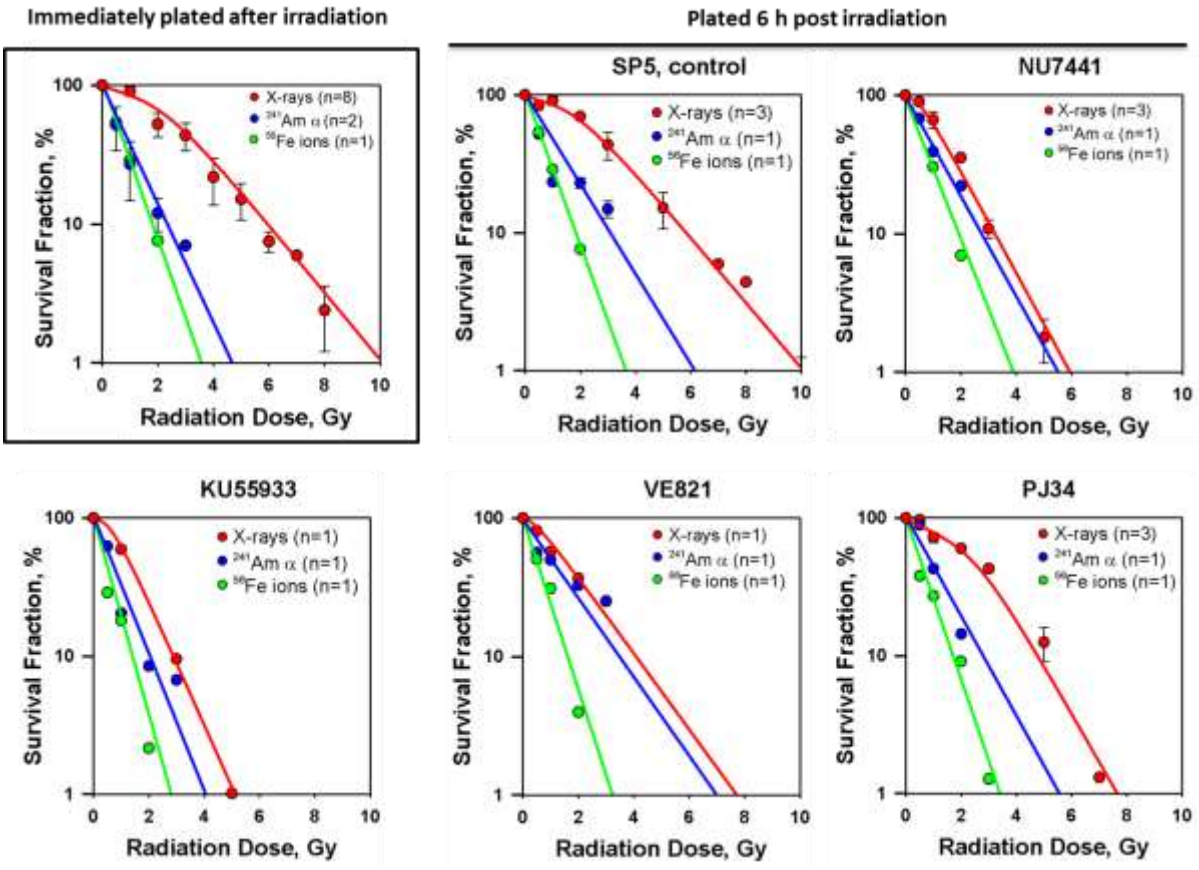

Overview about the clonogenic survival curves. Despite the indications in these figures the Fe ion exposed cells were plated 12 h post irradiation.

7.5 Reversion frequency data obtained with SP5 cells

Mitomycin C	Rev. frequency (Rev./10^5 cells)
0 nM	2.99
100 nM	8.05
250 nM	12.57
500 nM	6.66

#gRNA	Rev. frequency (Rev./10^5 cells)
Mock	8.1±0.37
#8	9.34±2.76
#10	7.11±1.89
#2	571.27±95.45
#9	2248±207.52
#2+9	247.7

	X-rays				
Dose (Gy)	DMSO	NU7741	KU55933	VE821	PJ34
0	2.99±0.55	4.55±0.48	5.97	6.03	8.15±0.08
1	3.13±1.05	5.52±0.88	3.28	4.29	5.37±0.04
3	3.38±0.38	5.84±0.35	4.01	5.29	3.94±0.18
5	7.54±0.25	5.40±1.38	30		7.12±1.9

	^{241}Am α particles				
Dose (Gy)	DMSO	NU7741	KU55933	VE821	PJ34
0	2.58±2	2.36	4.55	4.15	4.55
0.5	3.97±3.12	3.25±0.56	3.05	3.83	4.06
1	5.84±3.25	4.44±1.42	2.16	4.77	6.62
2	10.59±20.53	3.92±1.04		3.22	6.73
3	11.25±10.15	3.99±0.34	2.87	2.96	

	^{56}Fe-ions				
Dose (Gy)	DMSO	NU7741	KU55933	VE821	PJ34
0	4.16	4.55	5.97	6.03	8.15
0.5	12.62	10.66	14.28	9.25	16.01
1	11.71	8.99	13.96	7.86	20.77
2	18.91	17.04	20.05	24.55	36.14

	Treatment				
#gRNA	DMSO	NU7741	KU55933	VE821	PJ34
Mock	9.24±1.52	11±1.22	10	9.56	13
#2	474±148.66	883±330.52	326.97	438.18	583
#9	1807±311.6	3406	824.79	2155.6	2474
#2+9	569±76.15	657	474.82	765.45	1343

7.6 Reversion frequency data obtained with V79 cells

#gRNA	Rev. frequency (Rev./10^5 cells)
Mock	2.67±0.77
#9	32±6.31
#2	152±10.77
#11	30±4.43
#13	176±20.36
#8	46±21.89
#12	38±9.87

#gRNA	Rev. frequency (Rev./10^5 cells)
Mock	2.67±0.77
#11+8	121.91±43.17
#12+8	165.17±5.62
#11+12	216.32±50.45
#11+13	181.83±118.23
#12+13	122.12±82.12
#9+2	92.31±65.95

	Treatment				
#gRNA	DMSO	NU7741	KU55933	VE821	PJ34
Mock	1.39±0.58	1.31±0.78	4.99	3.85	1.81
#8	31.78±16.45	57.61±17.29	5.01	6.42±4.29	31.94±31.96
#11	27.85±7.56	42.23±17.47	2.03	1.96	22.4±9.36
#11+8	95.32±13.31	447.22±58.23	89.43	32.72±14.79	308.25±157.85

7.7 Comparative IC_{50} values of inhibitors employed

ATM inhibitor (KU55933)	**IC_{50} ATM = 13 nM** IC_{50} ATR = 100 µM IC_{50} DNA PKcs = 2.5 µM
ATR inhibitor (VE821)	IC_{50} ATM = 8 µM **IC_{50} ATR = 26 nM** IC_{50} DNA PKcs = 4.4 µM
DNA PKcs inhibitor (NU7441)	IC_{50} ATR = >100 µM IC_{50} ATM = >100 µM **IC_{50} DNA PKcs = 13 nM**

7.8 Overview of plasmids used in the CRISPR/Cas9 system

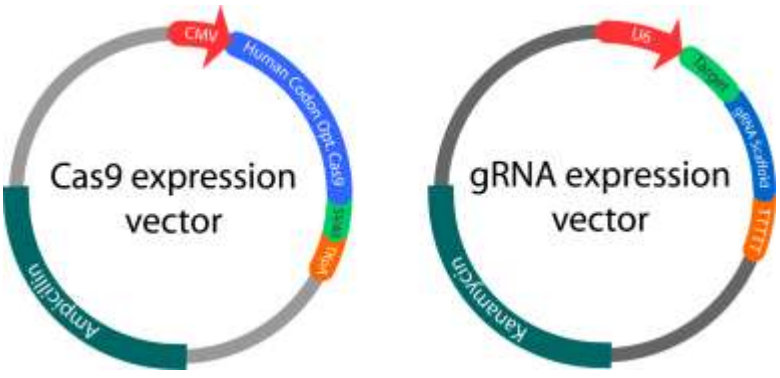

The used gRNA expression vectors in this thesis differed in the target sequence (here in green illustrated) only. The recognition sequence of each generated gRNA plasmid can be found in the material and method part. The Cas9 expression vector remained unchanged.

7.9 Calculation

The probability that a break is formed within the *hprt* gene after exposure to 1 Gy X-rays is approximately the following, when considered that 20 DSBs are formed and the DSBs are distributed equally:

The size of the Chinese hamster genome: $2{,}33\text{x}10^6$ kb

The size of the *hprt* gene: 36 kb

$$\frac{36kb}{2{,}33x10^6\text{kb}}\text{x}20 = 3{,}09\text{x}10^{-4}\text{or } 3{,}09 \text{ times in } 10.000$$

Acknowledgements

Die vorliegende Arbeit wurde durch das Projekt “Hoch-LET Strahlung induzierte DNA Läsionen: Beschaffenheit, chemische Entwicklung, Prozessierung und mögliche Rolle in der Karzinogenese” mit dem Förderkennzeichen ESA.50WB-1229-AO-10-IBER der Europäischen Weltraumorganisation (ESA) unterstützt.

An dieser Stelle möchte ich mich ganz besonders bei Prof. Dr. George Iliakis für seine kompetente und engagierte Betreuung bedanken. Seine Art wissenschaftliche Neugier zu wecken haben mich stets motiviert und inspiriert neue Ansätze auszuprobieren. Ebenfalls danke ich ihm für sein kritisches Lesen der Arbeit und die vielen Vorschläge.

Ein weiterer Dank geht an Prof. Dr. Shirley Knauer für die unkomplizierte Übernahme als Mentor und die unterstützende Betreuung bei meinem Projekt.

Ein ganz besonderer Dank geht an Dr. Emil Mladenov, der mir bei Schwierigkeiten durch seine vielen Ratschläge durchgehend helfend zur Seite stand und dadurch wesentlich zum Gelingen dieser Arbeit beigetragen hat.

Ich danke Burkhard Jakob für die Ermöglichung der Schwer-Ionen Experimente im GSI Helmholtzzentrum für Schwerionenforschung in Darmstadt.

Weiter bedanke ich mich bei allen Mitarbeitern des Instituts für Medizinische Strahlenbiologie für das freundliche miteinander im Labor, die angenehme Arbeitsatmosphäre sowie die Unterstützung und die vielen Tipps im Laboralltag.

Zuletzt geht mein Dank an meine Eltern Sibylle und Wolfgang, an meine Frau Yujing und Tochter Sophia Elisabeth, die mich in jeder Situation unterstützen.

Der Lebenslauf ist in der Onlineversion aus datenschutzrechtlichen Gründen nicht enthalten

Declaration

Erklärung:

Hiermit erkläre ich, gem. § 6 Abs. 2, g der Promotionsordnung der Fakultät für Biologie zur Erlangung der Dr. rer. nat., dass ich das Arbeitsgebiet, dem das Thema „The effect of high linear energy transfer ionizing radiation on mutation and reversion events at the hypoxanthin-guanin-phosphoribosyltransferase locus“ zuzuordnen ist, in Forschung und Lehre vertrete und den Antrag von Mathias Sebastian Kallies befürworte.

Essen, den _____ _____ _____

Name des wissenschaftl. Betreuers/Mitglieds der Universität Duisburg-Essen	Unterschrift d. wissenschaftl. Betreuers/Mitglieds der Universität Duisburg-Essen

Erklärung:

Hiermit erkläre ich, gem. § 7 Abs. 2, d und f der Promotionsordnung der Fakultät für Biologie zur Erlangung des Dr. rer. nat., dass ich die vorliegende Dissertation selbständig verfasst und mich keiner anderen als der angegebenen Hilfsmittel bedient habe und alle wörtlich oder inhaltlich übernommenen Stellen als solche gekennzeichnet habe.

Essen, den _____ _____

Unterschrift des/r Doktoranden/in

Erklärung:

Hiermit erkläre ich, gem. § 7 Abs. 2, e und g der Promotionsordnung der Fakultät für Biologie zur Erlangung des Dr. rer. nat., dass ich keine anderen Promotionen bzw. Promotionsversuche in der Vergangenheit durchgeführt habe, dass diese Arbeit von keiner anderen Fakultät abgelehnt worden ist, und dass ich die Dissertation nur in diesem Verfahren einreiche.

Essen, den _____ _____

Unterschrift des/r Doktoranden/in